Modélisation du cancer de la prostate par l'imagerie : détection, stratification, planning thérapeutique et suivi en 3D d'une thérapie focale basés sur le recalage-fusion d'image en multi modalité

Clément Orczyk

Normandie Université

THESE

Pour obtenir le diplôme de doctorat

Spécialité Recherche Clinique, innovation technologique, santé publique

Préparée au sein de l'Université de Caen Normandie

Modélisation du cancer de la prostate par l'imagerie : détection, stratification, planning thérapeutique et suivi en 3D d'une thérapie focale basés sur le recalage-fusion d'image en multi modalité.

Présentée et soutenue par
Clément ORCZYK

Thèse soutenue publiquement le 1er Juin 2017 devant le jury composé de		
Pr Pierre Mozer	PU-PH, Université Pierre et Marie Curie, Paris VI, Paris	Rapporteur
Pr Olivier Rouvière	PU-PH , Université de Claude Bernard Lyon 1	Rapporteur
Dr Myriam Bernaudin	DR, CNRS, Université de Caen Normandie, Caen	Examinateur
Dr Nicolas Barry Delongchamps	MCU-PH, Université Paris Descartes CPSC, Paris	Examinateur
Dr Samuel Valable	CR, CNRS, Université de Caen Normandie, Caen	Directeur de thèse
Pr Arnauld Villers	PU-PH, INSERM, Université de Lille 2, Lille	Codirecteur de thèse

Thèse dirigée par le Dr. Samuel VALABLE, UMR6301-ISTCT, Equipe CERVOxy,
et le Pr Arnauld VILLERS, Université de Lille 2- CHRU Lille- INSERM 1189 ONCO-THAI

UNICAEN UNIVERSITÉ CAEN NORMANDIE

EdNBISE

Ecole doctorale Normande

Biologie Intégrative, Santé, Environnement

CERVOxy

Table des matières

Introduction

Epidémiologie :

Dans le rapport à l'Organisation Mondiale de la Santé de 2015 pour 2012, le groupe GLOBOCAN(1) révèle une incidence de 758 700 nouveaux cas de cancer de prostate dans les pays les plus développés, cancer le plus incident chez l'homme et représentant 26,6% des cas de cancer chez l'homme. En revanche, il s'agit de la troisième cause de décès par cancer chez l'homme dans ces mêmes régions, avec 142 000 décès, soit 9,9% des décès par cancer. En 2012 en France, 53 000 nouveaux cas de cancer de la prostate ont été diagnostiqués selon les estimations de Binder-Foucard et al.(2), représentant presque le quart de l'ensemble nouveaux cas de cancer de l'homme. Ce cancer est ainsi le premier cancer incident chez l'homme. 8876 décès seraient imputables à cette maladie sur la même période, ce qui en fait le 3ème néoplasie en termes de nombre de décès en France.

Caractéristiques clinico-histologique de la prostate et du cancer :

Organe solide, glandulaire et déformable, la prostate participe des fonctions génito-urinaires en se situant à un véritable carrefour anatomique entre le sphincter urinaire, les bandelettes vasculo-nerveuses gouvernant à l'érection et reposant sur le rectum. Cette situation anatomique rend la prise en charge clinique exigeante. L'anatomie zonale est décrite par McNeal(3).

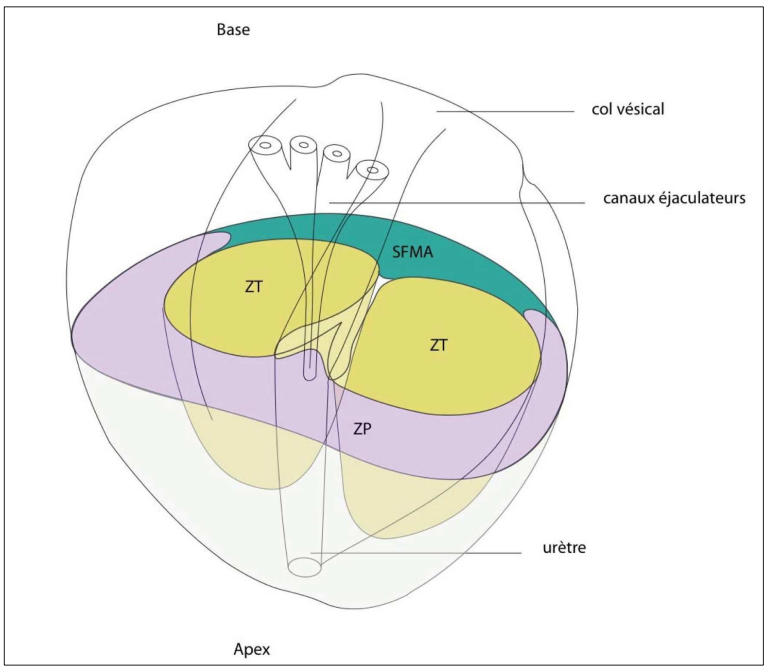

Figure 1: Anatomie Zonale de la prostate selon McNeal : ZP : zone périphérique, ZT zone de transition, SFMA : stroma fibro musculaire antérieur.

L'histoire naturelle du cancer de la prostate possède la particularité de présenter un temps de croissance relativement lent avec des manifestations cliniques pouvant s'étaler sur 20 ans(4).

Une des questions centrales dans la prise en charge du cancer de prostate reste la réduction de la mortalité du cancer de prostate, mais aussi l'évolution vers le stade métastatique et symptomatique, à balancer avec la qualité de vie. Les lésions cancéreuses évoluant potentiellement vers ces stades cliniques sont dites « lésions cliniquement significatives ». Deux définitions historiques basées sur le grade histologique et le volume font toujours référence(5,6).

Au début du spectre de l'agressivité des cancers prostatiques se trouvent les lésions dites indolentes. Dans « Latent carcinoma of the prostate », Franks (7)révélait déjà en 1954, la large incidence du cancer de prostate sur les séries autopsiques ainsi que la divergence avec le taux de mortalité due à la maladie. Il observait aussi la nature latente de certaines lésions avec des caractéristiques histologiques singulières.

Le score de Gleason(8) représente l'agressivité de la lésion au niveau histologique. Il s'agit d'un score histologique basé en microscopie optique sur l'évaluation de l'anaplasie nucléaire, les signes d'invasion tissulaire et les modifications d'organisation architecturale glandulaire. Ce score fait référence et un important prédicteur de récidive et d'évolution, récemment mis à jour(9).

Prise en charge du cancer et standard de soins :

Le stade de découverte de la maladie est devenu plus précoce(10) avec l'utilisation du PSA (*Prostate* Specific Antigen), biomarqueur sanguin et des biopsies de prostate échoguidées par voie transrectale introduites par Hodge(11) en 1989, concomitante de l'avènement de la prostatectomie totale moderne avec préservation nerveuse par Walsh(12) comme modalité chirurgicale de traitement du cancer de la prostate potentiellement préservant la fonction érectile. Actuellement, les traitements de référence pour le cancer localisé de prostate sont la chirurgie par prostatectomie totale ou la radiothérapie(13).

La diffusion du PSA couplé aux biopsies systématisées échoguidées a eu comme conséquence une plus large détection des lésions indolentes, c'est à dire ne menaçant pas à long terme la survie globale du patient.

Dépistage et problématique des essais cliniques à grande échelle :

Les résultats de larges essais de dépistage, basé sur le taux de PSA et le toucher rectal, prospectifs multicentriques européen (ERSPC(14)) et américain (PLCO (15) sont controversés. L'essai américain, négatif, a fait l'objet d'une contamination importante du groupe contrôle(16) par la réalisation du taux de PSA hors protocole avant ou après l'inclusion. L'essai européen montre dans sa dernière actualisation à 13 ans de suivi que le screening de 1000 patients prévient 1.28 décès(17), représentant une diminution relative du risque de décès de 27%. 27 patients devaient être à la fois diagnostiqués et traités pour prévenir un décès ; ceci au prix d'un important surdiagnostic de lésion non significative (43%) et de surtraitement(18). Ces résultats renforcent ceux de l'étude précédente Scandinavian randomized controlled trial (SPCG-4) qui comparait la chirurgie à la surveillance simple chez des patients avec le diagnostic de cancer localisé avant l'ère du dépistage basé sur le PSA

et qui montait une diminution du risque absolu de décès spécifique à 8 ans de seulement 5% (de 14% à 9%) et 6% à 15 ans dans le groupe à haut risque. Les résultats de l'étude « the Prostate Intervention Versus Observation Trial (PIVOT)(19) ont montré l'absence de bénéfice à la chirurgie radicale dans tous les groupes de patients même si un bénéfice modeste apparaît dans l'analyse en sous-groupe pour les patients de risque intermédiaire et haut. L'essai PROTECT(20) comprenant une phase de screening et une phase de randomisation entres trois attitudes thérapeutiques (chirurgie, radiothérapie et surveillance), ne montre pas de différence à 10 ans entre les trois choix de management du cancer de prostate en terme de survie, et ce sans effet de la stratification du risque.

Le surdiagnostic et le subséquent surtraitement inhérent aux schémas de soins du cancer de la prostate n'ont jamais été aussi débattu qu'actuellement. La US Preventive Services TAsk Force a attribué un grade D au dépistage utilisant le PSA en 2012, le mettant au rang de « certitude moyenne à forte que le service médical rendu n'est pas net ou que les dommages dépassent les bénéfices attendus » et avait déjà rendu une recommandation contre le dépistage après 75 ans dans leur précédent rapport en 2008. Une actualisation de ces recommandations est en cours, plaçant le screening au grade C(21), proposant un dépistage individualisé pour les 55-69 ans. Outre la mise à jour des résultats de l'ERSPC, cette reconsidération du screeining tient à la plus marge adoption par la communauté de la surveillance active (40% des nouveaux cas aux USA), réduisant ainsi les effets secodaires à un surdiagnsotic et surtraitement.

Depuis l'introduction du PSA, il est observé un glissement dans le profil de la maladie vers une augmentation de la détection d'une maladie de bas volume et bas risque(22). Par conséquent, le risque de sur traitement et différent effets secondaires lié au traitement est significatif. Même le bénéfice du traitement des patients à risque intermédiaire est équivoque, basé sur PIVOT. Cependant, les patients porteurs de cette catégorie de la maladie qui ont une espérance de vie supérieure à 10 ans se voient actuellement offrir un traitement radical, dans l'ambition d'une augmentation de leur survie.

Les connaissances sur quel patient bénéficiera de cette thérapie évoluent. C'est éminemment lié à la définition du cancer significatif qui requière un traitement et à partir de

quel seuil la maladie peut être surveillée. Un des problèmes à propos du choix actuel du traitement du cancer de prostate localisé est que les options thérapeutiques se situent à des extrêmes opposés. A un extrême se situe le traitement radical avec sa morbidité conséquente. Actuellement les patients peuvent s'attendre aux taux suivants d'effets secondaires des traitements radicaux : 30-90% de dysfonction érectile, 5-20% d'incontinence et 5-20% de toxicité rectale(23,24). Sur l'autre extrême se trouve la surveillance active. Celle-ci a démontré un excellent taux de survie à moyen terme(25,26). Cependant, les cliniciens et les patients ont soulevé des questions sur le suivi clinique, le dosage du PSA et les biopsies répétées (avec leurs complications) et le potentiel effet psychologique de vivre avec une maladie non traitée jusqu'à ce que le moment soit venu de l'extirper. L'évaluation préopératoire du cancer de la prostate reste un challenge et un quart à un tiers des patients en surveillance active nécessite un traitement dans les 2 à 5 années qui suivent le diagnostic en raison d'une sous-estimation initiale de la maladie ou d'une progression rapide(26,27)**.** De plus, 73% des patients éligibles à une surveillance active avaient un cancer significatif sur la pièce opératoire de prostatectomie totale dans une série contemporaine(28)**.** L'évaluation initiale était basée sur les biopsies transrectales et paramètres clinico-biologiques standard, la « progression » intervenait majoritairement dans les deux premières années de surveillance, pouvant suggérer une déficience de l'évaluation initiale basée sur les caractéristiques clinico-histologiques. Le retentissement psychosocial négatif de la surveillance active est également un élément à prendre en compte (28). Aussi, la stratégie actuelle de détection par biopsie systématisée a montré ces larges limitations(29–32). Typiquement, les lésions de la partie antérieure de la glande sont mal échantillonnées par les biopsies systématisées(33). L'accès au volume lésionnel, qui détermine en partie la significativité clinique d'une lésion(34), ne se faisait qu'à travers le prisme dépoli des longueurs de cancer sur les biopsies de prostate réalisées à l'aveugle.

Le concept de thérapie focale et bases histopathologiques:

L'ensemble de ces éléments a contribué à l'émergence du concept de thérapie focale. La méthode consiste à sélectionner des patients par des stratégies de biopsies et/ou d'imagerie par IRM(35), à appliquer un traitement focal limitée à la partie tumorale de la glande par ultrasons focalisés de haute intensité (HIFU), photothérapie dynamique (PDT), thermothérapie Laser interstitielle (LITT), chirurgie partielle, cryoablation ou radiofréquence(36) tout en préservant les structures nerveuses et sphinctériennes

nécessaires au maintien de la continence et des érections. Ces techniques sont en cours d'évaluation(37). La détection du cancer de la prostate repose sur ses caractéristiques histopathologiques, de volume et de distribution au sein de la glande afin d'améliorer les stratégies de biopsies et de valider les résultats de l'imagerie moderne qui sont nécessaires pour la planification du traitement focal. Aussi un traitement partiel de la glande de type thérapie focale doit s'appuyer sur les connaissances des caractéristiques de développement de la tumeur au sein de prostate(35). Des études morphométriques des cancers sur pièces de prostatectomies totales (38,39) et des cas incidentels sur cystoprostatectomies(40) précisent ces données volumétriques et d'extension dans les différentes zones de la prostate. Le volume de la tumeur apparaît comme un facteur reflétant l'extension de la tumeur dans la zone périphérique avec notamment un seuil de 2cc pour l'extension unilatérale. Mouraviev et al. (41) reprend dans une revue de la littérature les caractéristiques histologiques du cancer de prostate, concluant que la migration de la maladie vers un stade plus localisé permet d'envisager une thérapie focale.

Cependant, la multifocalité fréquente des cancers de la prostate qui représente environ 70% des cas(42,43) constitue une réserve au développement de cette modalité thérapeutique. Néanmoins, et malgré cette multifocalité, seules les lésions significatives (volume > 0,5 cc ou > 0,2 cc avec présence de grade de Gleason 4/5(5)) semblent à risque de progression métastatique dans les 5 à 10 ans et sont donc une indication de traitement qui peut être focal (6,35). Cette hypothèse a été confortée par une étude autopsique de patients décédés d'un cancer de prostate et qui suggère une origine monoclonale des cellules tumorales responsables des métastases(44). La possibilité de détecter et de quantifier les foyers tumoraux en préopératoire constitue donc un pré-requis indispensable au développement des modalités de thérapie focale.

<u>L'IRM de prostate, un examen multiparamétrique potentiellement répondant à des objectifs cliniques :</u>

Cela est désormais possible grâce aux progrès de l'imagerie moderne par IRM multiparamétrique couplée aux biopsies dirigées. L'ajout de séquences fonctionnelles, initialement la perfusion(45) puis de diffusion, aux séquences conventionnelles (séquences pondérées T1 et T2) a permis d'augmenter les performances du test d'imagerie par IRM, notamment pour la détection des lésions significatives décrites plus haut. L'apport de

l''imagerie moderne consiste notamment à la définition en 3D d'une cible biopsique, approche tranchant singulièrement avec les biopsies systématisées procédant à un échantillonnage à l'aveugle de la glande(46). Dans une récente revue de la littérature, Fütterer(47) et al. rapportent un taux de détection de 47 à 88% avec une valeur négative prédictive pour exclure une lésion significative s'échelonnant de 63 à 98%. Aussi l'IRM a également été validée pour la détection et la localisation des cancers antérieurs de la prostate inaccessibles aux biopsies systématisée réalisées par voie postérieure transrectale (48). Un essai randomisé comparant Panebianco et al. (49) ont aussi reporté l'avantage des biopsies ciblées combinées aux systématisées sur une approche uniquement systématique dans un essai randomisé.

Un consensus sur les modalités de réalisation de l'IRM dite multiparamétrique (IRMmp) de prostate et son interprétation(50) a été publié par Dickinson et al.(50) .Plusieurs études ont montré l'apport potentiel de l'IRMmp en situation prébiopsique (46,51), c'est-à-dire prédiagnostique, en permettant d'augmenter le taux de détection de lésion dite signifiante, et évitant le surdiagnostique de lésion indolente. Ceci a notamment abouti à l'adoption dans les recommandations française sur le diagnostic du cancer de la prostate à incorporer l'IRM dans la stratégie diagnostique en cas de première série négative et persistance de la suspicion clinique(13).

Toutefois, l'utilisation de l'IRMmp requiert une expertise à l'interprétation. Celle-ci tient en partie au fait que le résultat de l'IRMmp est rendu par le radiologue sous la forme d'un score visuel d'estimation (52)(Score de Likert ou score PiRADS 2(53)). La large dissémination de la technique n'a pas cependant pas encore eu lieu.

<u>De l'utilisation de paramètres quantitatifs d'imagerie et de l'analyse d'image « radiomique » :</u>

Ainsi, les paramètres quantitatifs de l'imagerie fonctionnelle pourraient apporter une reproductibilité inter et intra centre des résultats fournis par l'IRMmp. Une restriction du coefficient de diffusion apparent (ou ADC) calculé avec l'IRM de diffusion a déjà montré une corrélation avec la détection des foyers cancéreux mais aussi avec l'agressivité de la maladie**(54–57)**. Néanmoins, toutes les lésions ne sont pas détectées par cette cartographie ADC(58), reflétant ainsi l'hétérogénéité de la maladie. Il existe une zone grise de cette valeur quantitative pour déterminer le grade histologique(56). L'imagerie de la néoangiogenèse tumorale est en partie réalisée avec la séquence de perfusion (DCE-MRI) après injection d'un agent de contraste(59). L'estimation visuelle par la prise rapide de contraste et da

décroissance du signal permet déjà de détecter certaines lésions(60). Malgré cela, il existe des faux positifs en se basant sur cette estimation visuelle. Ainsi, l'anatomie zonale de la prostate montre différent type de tissu au sein de la glande(3) et la zone de transition, notamment lorsqu'elle est adénomateuse car elle peut présenter une prise de contraste très rapide(61). De plus, il a été montré que la détection du cancer de prostate par l'IRMmp dépend de l'histologie du cancer de prostate et de sa composition au niveau tissulaire(58), avec une variabilité quant aux séquences détectant le cancer. Ceci conforte l'approche multiparamétrique, basée sur les séquences anatomiques et fonctionnelles, pour la détection du cancer. Le score PIRADS 2 est basé sur cette approche multi séquentielle. C'est pourquoi, une approche visant à établir le profil quantitatif des lésion prostatiques en utilisant des modèles pharmacocinétiques connus dans d'autre organes (modèle de Toft, Toft modifié(62)) peut se révéler d'intérêt. Langer et Al.(63) ont ainsi montré une différence significative de Ktrans (constante de transfert de l'agent de contraste du compartiment vasculaire vers le parenchyme) entre les cancers de la zone périphérique et le tissu normal de cette même zone. Franiel et al.(64) ont étudié une modalité de perfusion en IRM montrant des différences modestes entre tissu cancéreux et tissu pathologique mais non cancéreux (prostatite). L'obtention de paramètres objectifs doit permettre la distinction entre les lésions cancéreuses et les lésions bénignes affichant des caractères similaires d'un point de vue visuel ou semi-quantitatifs. Ceci nécessite une corrélation fine entre l'imagerie et l'histologie en microscopie optique, pouvant être considérée comme une modalité d'imagerie.

L'analyse « radiomique » s'attache à extraire de nombreuses caractéristiques quantitatives de l'imagerie en utilisant des modèles et définitions mathématiques. Le maximum d'informations est alors tiré des examens d'imagerie de routine en utilisant l'analyse et le traitement d'image(65). Le but est d'augmenter la capacité de décision des modèles existant reposant sur l'imagerie. Il s'agit d'un domaine d'investigation complexe qui ouvre les possibilités d'identifier des caractéristiques de l'image, comme son hétérogénéité, reflétant un processus tissulaire voir génétique sous-jacent(66). Cette analyse radiomique, avec l'analyse de texture pourrait trouver son application à l'IRMmp de prostate tant les attentes des cliniciens de cet examen d'imagerie sont complexes : non seulement de la pure détection, mais aussi stratification, pronostique et même planning thérapeutique et suivi oncologique.

Dans ce domaine d'analyse d'image, Franiel et al. (67) ont initié une recherche sur l'échantillonnage d'une lésion pour en extraire les voxels montrant la prise de contraste, en le comparant à l'intégralité de la lésion. Aussi l'hétérogénéité du cancer par rapport au tissu bénin été montré en imagerie de diffusion par Rosenkrantz et al.(68) notamment en se focalisant sur l'entropie de l'ADC, analyse de texture d'ordre 1. Ce paramètre d'ordre 1 s'appliquant à une lésion complète n'a pas fait l'objet d'une évaluation en ce qui concerne la perfusion.

Les recherches entreprises ont conduit à une standardisation de la technique de l'IRM prostatique multiparamétrique définie par consensus comme nécessitant au minimum une image anatomique en séquence pondérée T2, une séquence en perfusion dynamique et des séquences de diffusion avec génération d'une carte de coefficient apparent de diffusion(50) suivi d'une interprétation visuelle pour la détection. Les performances de détection de l'IRMmp dans cette configuration ont été évaluée dans un essai multicentrique PROMIS récemment publié(69) contre le standard de soin, biopsie échoguidées systématisées avec un test de référence par biopsie transpérinéale en saturation. Les très bonnes performances, avec une valeur prédictive négative de 89% et une sensibilité de 93%, lors de cet essai constituent des preuves de niveau Ib de l'efficacité de l'IRMmp dans cette indication et pour une définition de cancer cliniquement significatif controversée(70) .
S'il s'agit là d'un haut niveau de preuve de confirmation de l'utilité clinique de l'IRMmp dans le diagnostic du cancer de prostate, des investigations complémentaires sont nécessaires pour extraire les informations attendues des cliniciens d'un test robuste d'imagerie. Il s'agit en particulier de l'utilisation d'un test d'imagerie pour stratifier la maladie, guider et planifier des interventions, d'une manière différente de la navigation. Les questions de précision diagnostique, planning thérapeutique ou encore du potentiel dans la suite de la prise en charge doivent être explorées.

Les attentes et défis cliniques nécessitent une approche méthodologique dont la technique par biopsies échoguidées d'échantillonnage à l'aveugle de la glande n'avait pas auparavant soulevé la nécessité pour le cancer de la prostate. Il s'agit, en plus d'indiquer la présence ou non de cancer, de dériver de l'imagerie l'agressivité du cancer, sa localisation de manière assez précise pour guider une geste chirurgical oncologique conservateur, la thérapie focale, ou encore effectuer un suivi soit dans un contexte post thérapeutique soit de surveillance

active. Ceci nécessite, en autre une corrélation précise de l'imagerie aux tests de référence histologique.

En parallèle à l'avènement de l'IRMmp, le champ du traitement et recalage d'image s'est trouvé d'intérêt dans la problématique prostatique (71)(72), porté par l'explosion des capacités de calcul des produits informatiques commerciaux. Cette discipline permet objectivité, contrôle des paramètres, évaluation de ses propres limitations mais aussi d'aller plus en profondeur dans ce que l'imagerie permet, notamment certaine modélisation quantitative(73).

De la nécessité oncologique d'établir une cible précise pour un traitement focal :

Dans la perspective d'un traitement chirurgical oncologique, la notion de marge chirurgicale de traitement est fondamentale(74) de même que leur aspect pronostique(75). La notion de marge indique une résection complète de la tumeur. La localisation et la caractérisation dans l'espace des lésions est un prérequis pour effectuer une thérapie focale efficiente(35,76). L'IRMmp ouvre la possibilité de détecter les lésions au sein de la prostate. La signature IRM d'un foyer cancéreux a été décrite comme différente en fonction des séquences dans les travaux initiaux sur l'IRM avec séquence fonctionnelle(45). Une comparaison entre l'aspect IRM d'une lésion et son extension en histologie apparaît alors essentiel pour envisager un planning thérapeutique basé sur cette modalité d'imagerie et permettre une couverture complète de la cible à détruire. Aussi, Il a été démontré historiquement une différence de volume entre l'état in vivo et l'examen histologique(77) pouvant atteindre 30%. Une corrélation entre l'histologie et l'IRMmp doit permettre de surmonter cet obstacle avec la précision nécessaire à l'application d'un traitement chirurgical guidé par l'imagerie, par définition dans un espace à trois dimensions.
Le développement de nouvelles méthodes d'évaluation est nécessaire pour permettre l'exploitation des capacités de l'IRMmp et de dépasser la problématique clinique de sur diagnostique et sur traitement.

L'objet de cette thèse se propose d'appliquer les outils et concepts de traitement d'image à l'IRM multiparamétrique de prostate pour participer à la réponse aux problématiques de détection, stratification, planning thérapeutique et suivi de la thérapie focale. La robustesse de l'IRMmp permet d'envisager une modélisation du cancer de la prostate dans cette optique.

Objectifs

La première étape de ce travail de modélisation par l'imagerie a été de développer une méthodologie de corrélation précise, automatisée, de l'IRM et ses différentes séquences avec l'histologie comme standard de référence. Une première méthodologie manuelle de recalage non rigide basée sur des points de repères entre l'histologie et l'imagerie anatomique en séquence pondérée T2 avait montré sa faisabilité(78) lors d'un travail à NYU de master 2 recherche. Des résultats initiaux(45) suggèrent en effet une différence de volume non seulement entre l'histologie et l'IRM mais aussi au sein même des différentes séquences. En parallèle de ce développement, une question s'est révélée de première importance quant à la capacité de l'IRM de capturer et quantifier les déformations post-chirurgicales de la prostate, ce qui s'avèrerait la pierre angulaire des travaux subséquents. Il s'agissait de revisiter les travaux fondateurs de Schmid et McNeal(77) sur l'approximation du volume prostatique in vivo après résection. En effet, l'accès à la troisième dimension, au volume, est un avantage de l'imagerie en coupe. L'analyse fine du processus histologique sous-jacent à la modification du signal IRM est aussi d'intérêt pour comprendre ce qui est détecté et les limites de l'examen. Aussi, le volume d'une lésion cancéreuse est à la base de la définition de la significativité d'une lésion, notamment avec les seuils de 0,2(79) et 0,5 cc(6) et donc de la stratification de la maladie. Les implications des capacités de prédiction de volume et des marges ont un effet direct sur la potentielle utilisation pour la thérapie focale dont les premiers résultats fonctionnels au sein d'un essai de phase I/II (80) par l'équipe de UCL venaient d'être disponibles en 2011 dans Journal of Urology.

La méthodologie de recalage de l'histologie à l'IRM s'est ensuite appliquée à une population de patient ayant eu une IRMmp avant une prostatectomie totale au New York University Medical Center. Ceci permet d'obtenir des résultats sur l'estimation du volume par l'IRM confrontée à l'histologie, remise à l'échelle in vivo avec un facteur de correction individualisé.

Les résultats de l'évaluation des paramètres quantitatifs pour les séquences de diffusion tel que le coefficient apparent de diffusion en corrélation avec le score de Gleason (54,56) mais aussi pour les séquences de perfusion en corrélation avec l'histologie (63) sont apparus d'importance. Ceux-ci encouragent l'initiation d'investigation de ces données, notamment de manière multiparamétrique en combinant les informations disponibles des différentes séquences et en appliquant une méthodologie fine de recalage. Aussi, l'utilisation des différents algorithmes de recalage, notamment de l'information mutuelle(81,82), a permis une compréhension de la nature discrète de l'imagerie médicale et les potentielles applications dérivées de l'analyse de l'histogramme. La collaboration avec NYU et l'équipe de modélisation de l'imagerie du Pr Rusinek combinée avec le savoir-faire de CERVOxy en imagerie de perfusion a permis d'envisager l'application d'analyse de texture d'ordre 1 et notamment de l'entropie à l'IRMmp en acquisition de routine. Le protocole de recherche clinique QDCEprost (annexe) a ainsi été déposé auprès du Comité de protection des personnes du Nord-Ouest. Il s'agissait d'étudier les performances des paramètres quantitatifs de l'IRMmp en situation de diagnostic et pour stratification initiale de la maladie. La taille de l'échantillon a été calculée pour obtenir une différence significative de Ktrans entre tissu sain et cancéreux comme minimum requis aux analyses subséquentes. Les performances de ces paramètres quantitatifs et d'analyse de texture ont été interrogés en situation de diagnostic et notamment pour la sélection des cibles IRM à biopsier dans cette étude préliminaire.

Enfin, les capacités des techniques de recalage et de fusion d'image ayant montré un intérêt dans la modélisation des déformations post prostatectomies, l'idée a émergé au contact de différentes techniques d'ablation focale (photothérapie dynamique et thermo ablation laser dans l'IRM) au sein d'essai clinique au NYUMC qu'une modélisation des déformations focales pouvait être explorées dans le but de définir une marge histologique biopsique à ces traitements émergents. L'objectif est double : permettre un suivi oncologique précis et l'évaluation des capacités d'ablation des technologies à moyen terme. Il s'agit alors d'une approche innovante de l'utilisation de l'IRM recalée pour un suivi objectif longitudinal oncologique après un traitement très localisé. Les travaux se sont focalisés sur la faisabilité, la méthodologie et le challenge de l'évaluation quand la cible à suivre est précisément ce qui a été détruit par un traitement physique.

Les travaux de cette thèse sont donc présentés de manière séquentielle autour des trois axes : modélisation du cancer et de la prostate par le recalage de l'imagerie en multimodalité, l'analyse de texture de l'IRMmp et proposition d'un score multiséquentiel pour la détection et la stratification du cancer prostatique et enfin le suivi longitudinal en 3D d'une thérapie focale du cancer de prostate basé sur le recalage-fusion d'image non rigide.

Matériels et Méthodes

Institutions :

Le présent travail est une collaboration entre la New York University, le New York University Medical Center (NYUMC) et l'équipe CERVoxy (Normandie Univ) et le CHU de Caen, dans le prolongement du travail initié en Master 2 Recherche.

Patients et protocoles :

Les données issues du NYUMC tombent sous l'accord du « Institutional Review Board » n° S13-00767 du NYUMC sous le numéro, ne nécessitant pas l'accord écrit des patients pour utilisation des données anonymisées de manières rétrospectives. Un droit de préemption sur les données spécifiques aux travaux a été cédé par le Pr Associé Andrew Rosenkrantz, Department of Radiology, New York University Medical Center, dans le cadre de la thèse.

L'utilisation des données du CHU de Caen ont fait l'objet d'un accord du Comité de Protection des Personnes du Nord Ouest III sous le n° A14-D66-VOL.23 ne nécessitant pas l'accord écrit des patients pour utilisation des données anonymisées de manières rétrospectives.

Propriété intellectuelle :

Une licence et un accord de support pour le logiciel Firevoxel (https://wp.nyu.edu/firevoxel/) a été cédé à l'équipe CERVOxy par la New York University, représentée par le Pr Henry Rusinek, Department of Mathematics, New York University, NY, Etats-Unis, pour la durée de la thèse.

Partie 1 : Modélisation du cancer et de la prostate par le recalage de l'imagerie en multimodalité : méthodes et implications pour la détection et le planning thérapeutique basé sur l'IRMmp

Etude des déformations prostatiques post chirurgicale : comparaison IRM in vivo et ex vivo du spécimen frais

Une des premières étapes a été d'utiliser l'excellente résolution de l'IRM pour revisiter les travaux initiaux de McNeal et de l'équipe de Stanford concernant la corrélation volumétrique entre la pièce de prostatectomie totale, référence histologique, et l'organe in vivo(83,84). Ainsi, nous avons étudié les différences de forme et de volume entre la prostate in vivo et ex vivo, post chirurgie, en utilisant l'IRM 3T comme outils de mesure par l'utilisation d'une plateforme logicielle. Nous montrons ainsi une importante variation de volume de moins -19.5% en moyenne entre les états in vivo et ex vivo. Cette variation volumétrique s'accompagne aussi de déformations significatives de forme de la prostate prédominantes sur les coupes axiales avec une variation de 12,2% du ratio entre les distances droite-gauche/ antéro-postérieures. Ceci correspondant à une forme plus sphérique de la prostate ex vivo par rapport à 'état plutôt pyramidal in vivo. Il existe une forte variabilité inter individuelle en fonction du volume prostatique. Ces résultats ont des implications pour une analyse en 3 dimensions qui viserait à établir une corrélation fine entre l'analyse histologique et l'imagerie pour optimiser l'utilisation de celle-ci en termes de stratification ou de planning thérapeutique, chirurgical, par définition tridimensionnel.

Se référant à :

« Assessment of change in prostate volume and shape following surgical resection through co-registration of in-vivo MRI and fresh specimen ex-vivo MRI. »

Clinical Radiology. 2014 Oct;69(10):e398–403

Orczyk C, Taneja SS, Rusinek H, Rosenkrantz AB.

Clinical Radiology 69 (2014) e398–e403

Contents lists available at ScienceDirect

Clinical Radiology

journal homepage: www.clinicalradiologyonline.net

Assessment of change in prostate volume and shape following surgical resection through co-registration of *in-vivo* MRI and fresh specimen *ex-vivo* MRI

C. Orczyk [a,c,d,e,f,g,*], S.S. Taneja [a,b], H. Rusinek [a,b], A.B. Rosenkrantz [b]

[a] *Division of Urologic Oncology, Department of Urology, New York University Langone Medical Center, New York, NY, USA*
[b] *Department of Radiology, New York University Langone Medical Center, New York, NY, USA*
[c] *Department of Urology, Côte de Nacre University Hospital, Caen, France*
[d] *CNRS, UMR 6301 ISTCT, CERVOxy. GIP CYCERON, F-14074 Caen, France*
[e] *CEA, DSV/I2BM, UMR 6301 ISTCT, F-14074 Caen, France*
[f] *UNICAEN, UMR 6301 ISTCT, F-14074 Caen, France*
[g] *Normandie Univ, France*

ARTICLE INFORMATION

Article history:
Received 8 January 2014
Received in revised form
27 May 2014
Accepted 12 June 2014

AIM: To compare the size and shape of the prostate between *in-vivo* and fresh *ex-vivo* magnetic resonance imaging (MRI), in order to quantify alterations in the prostate resulting from surgical resection.

MATERIAL AND METHOD: Ten patients who had undergone 3 T prostate MRI using a phased-array coil and who were scheduled for prostatectomy were included in this prospective study. The *ex-vivo* specimen underwent MRI prior to formalin fixation or any other histopathological processing. Prostate volume *in vivo* and *ex vivo* was assessed using planimetry. Prostate shape was assessed by calculating ratios between the diameters of the prostate in all three dimensions.

RESULTS: Mean prostate volume was significantly smaller *ex vivo* than *in vivo* (39.7 ± 18.6 versus 50.8 ± 26.8 cm^3; $p = 0.008$), with an average change in volume of -19.5%. The right-to-left (RL)/anteroposterior (AP) ratio of the prostate, representing the shape of the prostate within its axial plane, was significantly larger *ex vivo* than *in vivo* (1.33 ± 0.14 versus 1.21 ± 0.12; $p = 0.015$), with an average percent change in RL/AP ratio of the prostate of $+12.2\%$. There was no significant difference between *in-vivo* and *ex-vivo* acquisitions in terms of craniocaudal (CC)/AP ($p = 0.963$, median change $= -2.1\%$) or RL/CC ($p = 0.265$, median change $= +1.3\%$) ratios.

CONCLUSION: The observed volume and shape change following resection has not previously been assessed by comparison of *in-vivo* and fresh *ex-vivo* MRI and likely represents loss of vascularity and of connective tissue attachments in the *ex-vivo* state. These findings have implications for co-registration platforms under development to facilitate improved understanding of the accuracy of MRI in spatial localization of prostate tumours.

* Guarantor and correspondent: C. Orczyk, Department Of Urology, Côte de Nacre University Hospital, Caen, France. Tel.: +33 6 22 48 26 44; fax: +33 2 31 06 49 47.
E-mail addresses: clementorczyk@yahoo.fr, clement.orczyk@nyumc.org (C. Orczyk).

http://dx.doi.org/10.1016/j.crad.2014.06.012
0009-9260/

Introduction

Multiparametric magnetic resonance imaging (MRI) (mpMRI) of the prostate is increasingly being used for a broad array of clinical applications, including tumour detection and localization,[1,2] planning of targeted biopsies,[3] treatment selection,[4] pre-operative planning,[4] and monitoring of active surveillance.[5] These applications rely upon accurate spatial localization of tumour on mpMRI. An understanding of the accuracy of such localization is important for proper incorporation of imaging findings on mpMRI into clinical practice. Such validation has been attempted in a large volume of previous studies via attempted correlation of *in-vivo* MRI images with histopathological findings observed following radical prostatectomy.[6] However, past studies have generally not considered or accounted for the potential impact of the surgical procedure itself upon the size and shape of the prostate. It is possible that alterations in prostate vascularity and elasticity resulting simply from the prostatectomy may significantly change prostate morphology,[7] thereby impairing the ability to reliably assess the accuracy of tumour localization at *in-vivo* MRI via correlation with histopathological slides, and adjustments to correct for such changes would be warranted in future research. Thus, in the present study, the size and shape of the prostate between *in-vivo* and *ex-vivo* prostate MRI images were compared, in an effort to quantify changes resulting from surgical resection. The *ex-vivo* prostate was imaged fresh, prior to formalin fixation or any other processing.

Materials and methods

Patients

This prospective study was HIPAA-compliant and approved by the institutional review board. All patients signed written informed consent prior to participation. Ten patients (mean age 65 ± 5.94 years) with biopsy-proven prostate cancer scheduled to undergo radical prostatectomy were included. Mean preoperative prostate-specific antigen (PSA) level 6.17 ± 0.43 ng/ml (median 6.2ng/ml). All patients had undergone a preoperative 3 T mpMRI of the prostate, which is routinely performed following a positive prostate biopsy at New York University Langone Medical Center. In addition, the fresh *ex-vivo* prostate specimen underwent MRI, as described below. No patient received therapy between MRI and surgery. Mean delay between MRI and surgery was 45.4 ± 54 days (median 33 days). Final histopathological stages were: pT2c ($n = 3$), pT3a ($n = 6$), and pT3b ($n = 1$). Final Gleason scores were 6 (3 + 3) in one case, 7 (3 + 4) in five cases, 7 (4 + 3) in four cases.

In-vivo MRI acquisition

Patients underwent preoperative MRI of the prostate using a 3 T system (Magnetom Trio, Siemens Healthcare, Erlangen, Germany) using a pelvic phased-array coil. The protocol included an axial turbo-spin echo (TSE) T2-weighted imaging (T2WI) sequence of the prostate and seminal vesicle [3600 ms repetition time (TR)/123 ms echo time (TE); 3 mm section thickness; 160 × 160 mm field of view (FOV); 256 × 256 matrix; parallel imaging factor of 2; three signals averaged]. Dynamic contrast-enhanced (DCE) imaging and diffusion-weighted imaging (DWI) were also performed, but not assessed as part of this study.

Surgical resection and ex-vivo MRI

All 10 patients underwent robotic-assisted radical prostatectomy, performed by a single surgeon with 15 years of experience (SST). The fresh surgical specimen was prepared by sewing a segment of urethral catheter into the prostatic urethra for preservation of urethral elongation. Within 12 h of resection and prior to formalin fixation, sectioning, or any other histopathological processing, the fresh specimen underwent *ex-vivo* MRI using the same 3 T system as for *in-vivo* imaging and comprising T2WI with sequence parameters matching *in-vivo* MRI aside from use of a rectangular FOV of 40% given the lack of surrounding pelvic tissues. During this delay, the specimen was maintained at 4°C to minimize tissue changes.

Assessment of prostate volume and shape

Analysis of the images was performed by a research fellow (C.O.), under supervision of a fellowship-trained abdominal radiologist (A.B.R.), with 5 years of experience in prostate MRI interpretation. The image analysis was performed using locally-developed in-house software (Firevoxel), which has previously been used to assess volume of other tissues.[8]

Volume measurements of the *in-vivo* and *ex-vivo* prostate was achieved via planimetry, which has been previously shown to be an accurate method for this purpose.[9] First, the prostate was manually delineated on *in-vivo* and *ex-vivo* T2WI, excluding of surrounding peri-prostatic fat, the neurovascular bundles (if present *ex vivo*), the bladder neck, and the seminal vesicles. Subsequently, volume was computed on a voxel basis.

The shape of the prostate was assessed by initially measuring the largest diameter of the prostate in the anteroposterior (AP), right-to-left (RL), and craniocaudal (CC) dimensions. Then, the AP/RL, AP/CC, and RL/CC ratios were calculated *in vivo* and *ex vivo*.

Statistical assessment

Paired *t*-tests were used to compare prostate volume, the three linear dimensions of the prostate, and the three ratios between these linear dimensions representing prostate shape, between *in-vivo* and *ex-vivo* images for each case. The mean, standard deviation, and median percent changes in volume and in terms of the three ratios were computed between the *in-vivo* and *ex-vivo* images. All *p*-values are two-sided and considered statistically significant at $p < 0.05$. Statistical analysis was performed using software

(R, version 2.14.0, CRAN, Vienna, Austria) and Excel (version 2011, Microsoft, Redmond, WA, USA).

Results

In-vivo and *ex-vivo* MRI acquisitions, as well as the described volume and shape measurements, were successfully performed in all 10 patients. The obtained volume and shape measurements are summarized in Table 1. Mean prostate volume was significantly smaller *ex vivo* than *in vivo* (39.7 ± 18.6 versus 50.8 ± 26.8 cm^3, respectively; $p = 0.008$), with an average percent change in size of the prostate of −19.5%, equivalent to a 23% greater volume of the prostate on *in-vivo*, compared with *ex-vivo*, MRI (Fig 1). In addition, there was a decrease in size of the prostate in all three dimensions between *ex-vivo* and *in-vivo* scans: RL dimension, 4.82 ± 0.77 cm versus 5.05 ± 0.92 cm, $p = 0.015$; AP dimension, 3.62 ± 0.56 cm versus 4.01 ± 0.78 cm, $p = 0.002$; CC dimension, 3.9 ± 0.82 cm versus 4.09 ± 1.40 cm, $p = 0.087$.

The ratios between the three linear dimensions of the prostate were compared to assess for a tendency for the shape of the prostate to change between *in-vivo* and *ex-vivo* scans in a particular orientation (Fig 2). The RL/AP ratio of the prostate, thus representing the shape of the prostate within its axial plane, was significantly larger *ex vivo* than *in vivo* (1.33 ± 0.14 versus 1.21 ± 0.12, respectively; $p = 0.015$), with an average percent change in RL/AP ratio of the prostate of +11.3%. There was no significant difference between scans in terms of CC/AP ratio ($p = 0.963$, average percent change = −2.1%) or RL/CC ratio ($p = 0.265$, average percent change = +1.3%). Images from a representative case are shown in Fig 3.

Table 1
Comparison of volume and shape assessments between *in vivo* and *ex vivo* MRI.

	In-vivo MRI		*Ex-vivo* MRI
Volume			
Mean ± SD (cc)	50.8 ± 26.8		39.7 ± 18.6
p-Value[a]		**0.008**	
Average percent change[b]		−19.5	
Median percent change[b]		−22.3%	
RL/AP ratio			
Mean ± SD	1.21 ± 0.12		1.33 ± 0.14
p-Value[a]		**0.015**	
Average percent change[b]		12.2%	
Median percent change[b]		11.3%	
CC/AP ratio			
Mean ± SD	1.09 ± 0.22		1.10 ± 0.18
p-Value[a]		0.963	
Average percent change[b]		0.34%	
Median percent change[b]		−2.1%	
RL/CC ratio			
Mean ± SD	1.15 ± 0.29		1.24 ± 0.22
p-Value[a]		0.265	
Average percent change[b]		8.8%	
Median percent change[b]		1.3%	

RL/AP ratio, right-to-left/anteroposterior ratio; CC/AP ratio, craniocaudal/anteroposterior ratio; RL/CC ratio, right-to-left/craniocaudal ratio.
[a] Listed in bold when statistically significant at $p < 0.05$.
[b] Change from *in-vivo* to *ex-vivo* measurements.

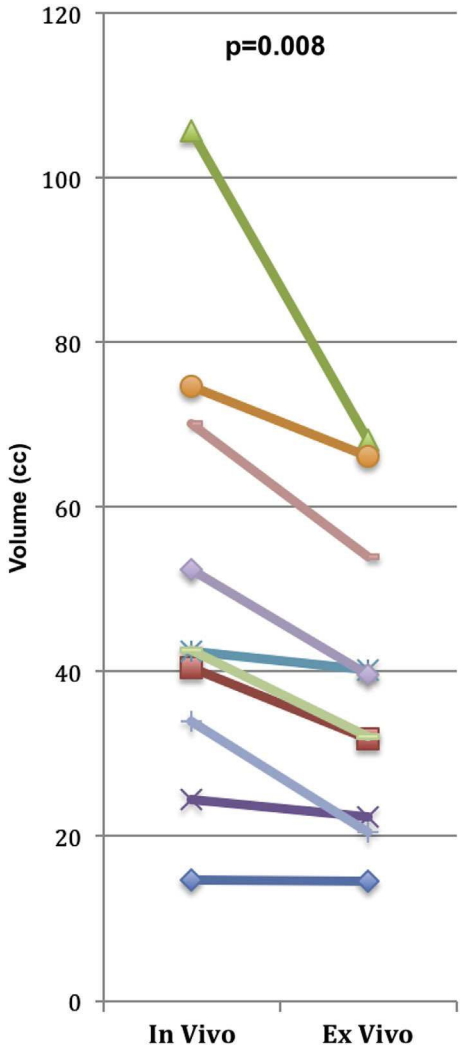

Figure 1 Comparison of *in-vivo* and *ex-vivo* prostate volumes in 10 patients. *p*-Value represents result of paired *t*-test comparing the two sets of data.

Discussion

In the present study, a significant difference was observed in volume of the prostate following surgical resection, with an average loss of 19.5% of the gland's volume. To the authors' knowledge, this finding has not been previously assessed by comparison of *in-vivo* and *ex-vivo* prostate MRI. The use of MRI for this purpose facilitated the determination of prostate dimensions and volume. Furthermore, via careful evaluation of *ex-vivo* T2WI, it was possible to include within the *ex-vivo* volume measurement only the prostate gland itself, while excluding all surrounding tissues. This is important because the resected prostate is intimately associated with surrounding tissue such as fat, pelvic fascia, or the neurovascular bundles, depending of the operative technique. These adjacent structures can confound accurate specimen measurements

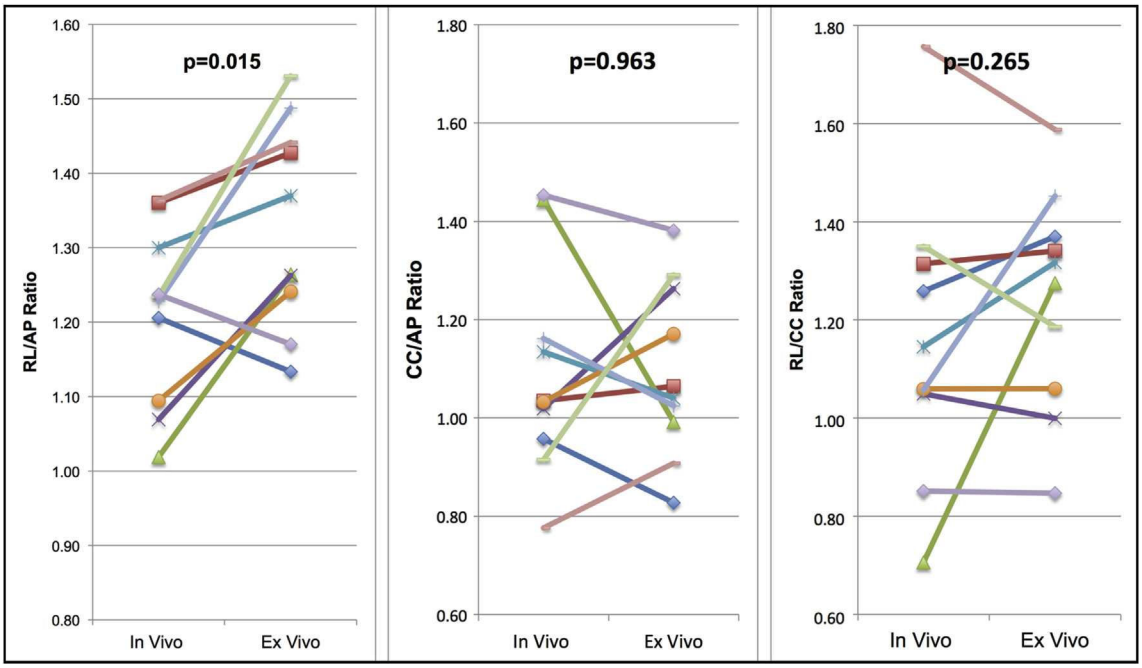

Figure 2 Comparison of *in-vivo* and *ex-vivo* ratios of linear prostate dimensions in 10 patients. *p*-Value represents result of paired *t*-test comparing the two sets of data.

of the specimen, but cannot be removed physically; doing so may negatively impact evaluation of the surgical margin status[10] and lead to improper staging. Thus, the present approach to evaluating the *ex-vivo* prostate via MRI allowed for accurate measurements after image-based exclusion of peri-prostatic structures, while preserving the integrity of the specimen for further histopathological evaluation.

An additional key aspect of the present method was that the *in-vivo* MRI was performed without use of an endorectal coil, which potentially could compress and deform the prostate, thereby confounding the comparison with the *ex-vivo* prostate. For instance, Heijmink et al.[11] reported an approximately 18% difference in volume of the prostate evaluated by MRI between examinations performed with and without an endorectal coil. Thus, in the present study, the only difference between the two acquisitions was the interval surgical procedure itself.

This finding in terms of volume reduction is important given the role of correlative studies between multi-parametric and histology, which have often used radical prostatectomy specimens as the reference standard, in influencing the clinical integration of mpMRI.[12,13] Numerous past studies have accounted for shrinkage of the prostate attributed to the process of histopathological processing.[14–16] This step accounts for change in volume due to tissue dehydration that results from formalin fixation and paraffin embedding, but does not correct for the loss of volume due to the surgery procedure, as per the current report. It is possible that a greater degree of volume correction may be needed than in past studies given the additional observed contribution of the surgical procedure to volume changes.

Although the decrease in volume of the *ex-vivo* prostate was due to a reduction in size in all dimensions, this size reduction was not homogeneous between the three dimensions, as indicated by the significant difference in the AP/RL ratio between the two acquisitions. Thus, the surgical procedure is associated with a change in the shape of the prostate in the axial plane. This spatial deformation may relate to a loss of connective tissue attachments, for instance to the dorsal venous complex or lateral pelvic fascia,[17] that maintain the shape of the *in-vivo* prostate, thereby releasing the prostate in the *ex-vivo* state and resulting in a change in shape given the prostate's visco-elastic properties.[18] Therefore, magnification alone of histopathological images, in order to account for the volume reduction, is not likely to be sufficient to achieve optimal co-registration of *in-vivo* prostate MRI and histopathological images; rather, as correlation of lesions is predominantly performed within the axial plane, measures are needed to correct for the deformation within this plane resulting from the surgery.

Numerous reports describe co-registration platforms currently in development from a variety of centres.[19,20,21] The present findings support the need for such platforms to employ a three-dimensional deformable approach in order to achieve optimal correlation. The resulting improved compensation for changes in volume and shape will be of much value when performing co-localization of small tumours between MRI and histology.

Limitations of the present study include the small sample size, lack of assessment of reproducibility of the volume metrics, and lack of confirmation of suggested reasons for the change in prostate volume following prostatectomy.

In conclusion, via performance of MRI of fresh *ex-vivo* prostatectomy specimens, a significant decrease of approximately 19% was demonstrated in the volume of the prostate resulting from this surgical procedure. In addition,

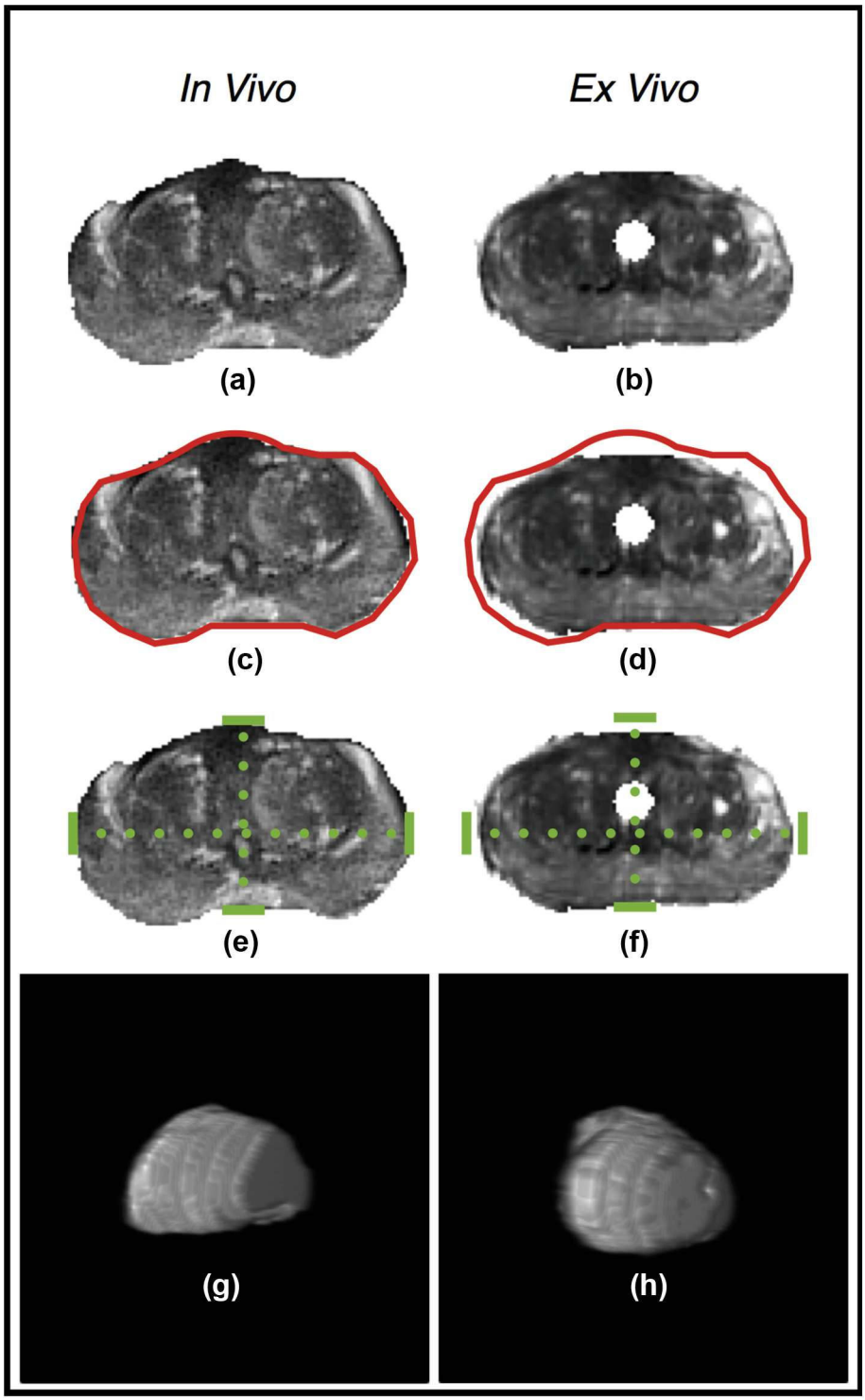

Figure 3 Change in volume and shape between *in-vivo* and *ex-vivo* MRI. Axial T2WI images at the level of the verumontanum are shown for (a) *in-vivo* and (b) *ex-vivo* acquisitions for a single patient. (c–d) Images depict an identical red contour reflecting the external contour of the (c) *in-vivo* prostate, although superimposed on the prostate in both images and demonstrating the smaller size of the (d) *ex-vivo* prostate. (e–f) Images depict identical dotted green lines reflecting the RL and AP dimensions of the (e) *in-vivo* prostate, although superimposed on the prostate in both images and demonstrating the change in relation between these lines in the (f) *ex-vivo* prostate. (g–h) Images depict a three-dimensional, rendered, shaded surface display of the (g) *in-vivo* and (h) *ex-vivo* prostate, generated from the two sets of T2WI images, demonstrating a difference in prostate shape between the two scans; the prostate exhibits its typical pyramidal shape in the *in-vivo* scan and a relatively spherical shape in the *ex-vivo* scan. (For interpretation of the references to color in this figure legend, the reader is referred to the web version of this article.)

the surgery resulted in a significant change in shape of the prostate in the axial plane. It is, therefore, advised that co-registration platforms employ three-dimensional deformable transformation to compensate for this volume loss and change in orientation in the axial plane, in order to achieve reasonable accuracy in correlation. More accurate co-registration incorporating the present findings will facilitate improved understanding of the accuracy of mpMRI in the spatial localization of tumours within the prostate.

Acknowledgements

The authors acknowledge The Joseph and Diane Steinberg Charitable Trust and the Grant UL1 RR029893 from NIH (National Center for Research Resources is part of National Institutes of Health) for support. C.O., H.R. and A.B.R. have nothing to disclose. S.S.T. is consultant for Eigen, consultant and scientific investigator for GTX, scientific investigator for Steba Biotech, speaker for Janssen, has royalties from Elsevier. No direct financial conflict of interest is identified.

References

1. Dickinson L, Ahmed HU, Allen C, et al. Magnetic resonance imaging for the detection, localisation, and characterisation of prostate cancer: recommendations from a European consensus meeting. *Eur Urol* 2011;**59**:477–94.
2. Rosenkrantz AB, Deng F-M, Kim S, et al. Prostate cancer: multiparametric MRI for index lesion localization—a multiple-reader study. *AJR Am J Roentgenol* 2012;**199**:830–7.
3. Rosenkrantz AB, Taneja SS. Targeted prostate biopsy: opportunities and challenges in the era of multiparametric prostate magnetic resonance imaging. *J Urol* 2012;**188**:1072–3.
4. Rosenkrantz AB, Scionti SM, Mendrinos S, et al. Role of MRI in minimally invasive focal ablative therapy for prostate cancer. *AJR Am J Roentgenol* 2011;**197**:W90–6.
5. Villers A, Lemaitre L, Haffner J, et al. Current status of MRI for the diagnosis, staging and prognosis of prostate cancer: implications for focal therapy and active surveillance. *Curr Opin Urol* 2009;**19**:274–82.
6. Villers A, Puech P, Mouton D, et al. Dynamic contrast enhanced, pelvic phased array magnetic resonance imaging of localized prostate cancer for predicting tumor volume: correlation with radical prostatectomy findings. *J Urol* 2006;**176**:2432–7.
7. Terris MK, Stamey TA. Determination of prostate volume by transrectal ultrasound. *J Urol* 1991;**145**:984–7.
8. Ko JP, Berman EJ, Kaur M, et al. Pulmonary Nodules: growth rate assessment in patients by using serial CT and three-dimensional volumetry. *Radiology* 2012;**262**:662–71.
9. Matthews GJ, Motta J, Fracchia J. The accuracy of transrectal ultrasound prostate volume estimation: clinical correlations. *J Clin Ultrasound* 1996;**24**:501–5.
10. Berney DM, Wheeler TM, Grignon DJ, et al. International Society of Urological Pathology (ISUP) consensus conference on handling and staging of radical prostatectomy specimens. Working group 4: seminal vesicles and lymph nodes. *Mod Pathol* 2011;**24**:39–47.
11. Heijmink SWTPJ, Scheenen TWJ, van Lin ENJT, et al. Changes in prostate shape and volume and their implications for radiotherapy after introduction of endorectal balloon as determined by MRI at 3T. *Int J Radiat Oncol Biol Phys* 2009;**73**:1446–53.
12. Turkbey B, Mani H, Aras O, et al. Correlation of magnetic resonance imaging tumor volume with histopathology. *J Urol* 2012;**188**:1157–63.
13. Mazaheri Y, Hricak H, Fine SW, et al. Prostate tumor volume measurement with combined T2-weighted imaging and diffusion-weighted MR: correlation with pathologic tumor volume. *Radiology* 2009;**252**:449–57.
14. Schned AR, Wheeler KJ, Hodorowski CA, et al. Tissue-shrinkage correction factor in the calculation of prostate cancer volume. *Am J Surg Pathol* 1996;**20**:1501–6.
15. Schmid HP, McNeal JE. An abbreviated standard procedure for accurate tumor volume estimation in prostate cancer. *Am J Surg Pathol* 1992;**16**:184–91.
16. Jonmarker S, Valdman A, Lindberg A, et al. Tissue shrinkage after fixation with formalin injection of prostatectomy specimens. *Virchows Arch* 2006;**449**:297–301.
17. Lepor H. A review of surgical techniques for radical prostatectomy. *Rev Urol* 2005;**7**:S11–7.
18. Zhang M, Nigwekar P, Castaneda B, et al. Quantitative characterization of viscoelastic properties of human prostate correlated with histology. *Ultrasound Med Biol* 2008;**34**:1033–42.
19. Orczyk C, Rusinek H, Rosenkrantz AB, et al. Preliminary experience with a novel method of three-dimensional co-registration of prostate cancer digital histology and *in vivo* multiparametric MRI. *Clin Radiol* 2013;**68**:e652–8.
20. Ward AD, Crukley C, McKenzie CA, et al. Prostate: registration of digital histopathologic images to *in vivo* MR images acquired by using endorectal receive coil. *Radiology* 2012;**263**:856–64.
21. Mazaheri Y, Bokacheva L, Kroon D-J, et al. Semi-automatic deformable registration of prostate MR images to pathological slices. *J Magn Reson Imaging* 2010;**32**:1149–57.

Méthodologie et évaluation du recalage déformable 3D de l'IRMmp et de l'histologie du spécimen chirurgical

Une méthode 3D de corrélation déformable a été développée pour permettre une étude fine de la localisation spatiale d'une lésion basée sur l'IRMmp. Le développement et l'évaluation de la méthode s'est faite autour de la même plateforme logicielle développée avec NYU permettant un recalage multimodal par méthodes géométriques et iconiques automatisées. La méthode s'appuie sur une reconstruction digitale 3D du spécimen chirurgical frais coupé, comme pont entre la modalité histologique 2D digitalisée et l'IRM multiparamétrique. Les différentes séquences IRM (pondérée T2-perfusion DCE WI - Diffusion et la carte du Coefficient de Diffusion) sont recalées dans l'espace de la séquence pondérée T2 en utilisant une méthode automatisée iconique basée sur l'information mutuelle. Le recalage non-rigide permet une meilleure précision du recalage de l'histologie à l'IRM et ses séquences fonctionnelles, avec une erreur de moyenne de 1,6 mm basée sur une mesure du RMSE (*Root Mean Square Error*) correspondant à une amélioration de 32% (p=0,003) par rapport à un recalage rigide. L'évaluation volumétrique par l'index de Dice montre un recouvrement satisfaisant entre les séquences variant de 0,81 à 0,89 en moyenne. La méthode iconique automatisée ne présente pas de différence significative avec la méthode manuelle basée sur points de repères dérivés de l'anatomie zonale de la prostate avec des index de Dice respectivement de 0,89 et 0,86 (p=0.48). De plus la corrélation déformable donne accès à un volume histologique compensé des déformations et perte de volume inhérents à la chirurgie et au processus histologique. La précision de la méthodologie permet d'envisager son utilisation pour définir une cible pour la thérapie focale du cancer de prostate avec une précision cliniquement pertinente par rapport à la taille de l'organe et l'exécution des différentes énergies disponibles.

Se référant à :

« Preliminary experience with a novel method of three-dimensional co-registration of prostate cancer digital histology and in vivo multiparametric MRI. »

Clinical Radiology. 2013 Dec;68(12):e652–8.

Orczyk C, Rusinek H, Rosenkrantz AB, Mikheev A, Deng F-M, Melamed J, Taneja SS.

Clinical Radiology 68 (2013) e652–e658

Contents lists available at SciVerse ScienceDirect

Clinical Radiology

journal homepage: www.clinicalradiologyonline.net

Preliminary experience with a novel method of three-dimensional co-registration of prostate cancer digital histology and *in vivo* multiparametric MRI

C. Orczyk [a,b,c,d,e,f,*], H. Rusinek [g], A.B. Rosenkrantz [g], A. Mikheev [g], F.-M. Deng [h], J. Melamed [h], S.S. Taneja [a,g]

[a] *Division of Urologic Oncology, New York University Langone Medical Center, New York, NY, USA*
[b] *Department of Urology and Renal Transplantation, Côte de Nacre University Hospital, Caen, France*
[c] *CNRS, UMR 6301 ISTCT, CERVOxy Group, GIP CYCERON, France*
[d] *CEA, DSV/I2BM, UMR 6301 ISTCT, France*
[e] *UNICAEN, UMR 6301 ISTCT, F-14074 Caen, France*
[f] *Normandie University, France*
[g] *Department of Radiology, New York University Langone Medical Center, New York, NY, USA*
[h] *Department of Pathology, New York University Langone Medical Center, New York, NY, USA*

ARTICLE INFORMATION

Article history:
Received 9 April 2013
Received in revised form
8 July 2013
Accepted 18 July 2013

AIM: To assess a novel method of three-dimensional (3D) co-registration of prostate cancer digital histology and *in-vivo* multiparametric magnetic resonance imaging (mpMRI) image sets for clinical usefulness.

MATERIAL AND METHODS: A software platform was developed to achieve 3D co-registration. This software was prospectively applied to three patients who underwent radical prostatectomy. Data comprised *in-vivo* mpMRI [T2-weighted, dynamic contrast-enhanced weighted images (DCE); apparent diffusion coefficient (ADC)], *ex-vivo* T2-weighted imaging, 3D-rebuilt pathological specimen, and digital histology. Internal landmarks from zonal anatomy served as reference points for assessing co-registration accuracy and precision.

RESULTS: Applying a method of deformable transformation based on 22 internal landmarks, a 1.6 mm accuracy was reached to align T2-weighted images and the 3D-rebuilt pathological specimen, an improvement over rigid transformation of 32% ($p = 0.003$). The 22 zonal anatomy landmarks were more accurately mapped using deformable transformation than rigid transformation ($p = 0.0008$). An automatic method based on mutual information, enabled automation of the process and to include perfusion and diffusion MRI images. Evaluation of co-registration accuracy using the volume overlap index (Dice index) met clinically relevant requirements, ranging from 0.81–0.96 for sequences tested. *Ex-vivo* images of the specimen did not significantly improve co-registration accuracy.

* Guarantor and correspondent: C. Orczyk, Department of Urology and Renal Transplantation, Côte de Nacre University Hospital, Avenue de la côte de Nacre, Caen, Lower Normandy, 14033 Cedex, France. Tel.: +33 6 22 48 26 44; fax: +33 2 31 06 49 57.
E-mail address: clementorczyk@yahoo.fr (C. Orczyk).

http://dx.doi.org/10.1016/j.crad.2013.07.010

CONCLUSION: This preliminary analysis suggests that deformable transformation based on zonal anatomy landmarks is accurate in the co-registration of mpMRI and histology. Including diffusion and perfusion sequences in the same 3D space as histology is essential further clinical information. The ability to localize cancer in 3D space may improve targeting for image-guided biopsy, focal therapy, and disease quantification in surveillance protocols.

Introduction

Contemporary methods of multiparametric magnetic resonance imaging (mpMRI) of the prostate have greatly improved the ability of urologists to localize prostate cancer for detection and targeting.[1,2] In evaluating the accuracy of mpMRI in disease localization, simple, reproducible methods for correlating imaging findings with histology are lacking. Such co-registration methods aim to map different image sets within the same "space." Therefore, a geometrical transformation must be computed for optimal image alignment. These computational methods may be based on geometrical features of the image, incorporating various anatomical landmarks internal or external to the prostate, or be based on image intensity values that are generally assessed via an automated process. In addition, the transformation used to achieve image alignment can be attained using a rigid or deformable approach. The more commonly applied rigid transformation performs alignment of objects without their modification, whereas the more advanced deformable approach allows and compensates for changes in object size and/or shape. In view of these various, and possibly complex, methods available for achieving co-registration, the present pilot study was undertaken to assess a novel image-based method of automatically co-registering mpMRI with three-dimensional (3D) reconstructed prostate histology data sets.

Materials and methods

Three patients (57–73 years old) with a diagnosis of localized prostate cancer were prospectively enrolled according to an ethics committee-approved protocol. The patients' prostate-specific antigen (PSA) values ranged from 5.1–7.7 ng/ml. Informed consent was obtained for each study subject.

In-vivo and ex-vivo mpMRI acquisition

The patients underwent a previously described protocol of mpMRI[3] using a 3 T system (Magnetom Trio, Siemens Healthcare, Erlangen, Germany) equipped with a pelvic phased-array coil. MRI sequences included T2-weighted imaging (T2WI; 3 mm section thickness), dynamic contrast-enhanced (DCE) imaging, and diffusion-weighted images (DWI) acquired at 3 mm section thickness (b-values 0 and 1000 s/mm^2), with in-line generation of apparent diffusion coefficient (ADC) maps.

All three patients underwent robotic-assisted prostatectomy at NYU Medical Center. Within 12 h of radical prostatectomy and prior to sectioning, *ex-vivo* MRI of the fresh specimen was performed, before any fixation or histopathology process.

Pathology processing

Pathology processing follows a standard institutional protocol. Fresh gross specimens were sliced perpendicular to rectal wall at regular intervals. All slices were then digitally photographed with a linear scale indication. A digital 3D surgical specimen was then rebuilt (Fig 1) using assembled digital photographs of the gross specimen slices, leading to a 3D dataset compatible for registration to MRI. The rebuilding process was fully independent of the MRI findings, with the aim of reproducing the slicing process of the specimen, which is perpendicular to the posterior capsule and distal urethral axis. The images of the gross specimen slices were assembled in a digital 3D model (Fig 1) using five steps: (1) photographs of fresh slices of the specimen were taken with a ruler included in the field of view; (2) each slice was saved as a separate digital image and loaded in Adobe Photoshop in a prefixed numeric matrix. The pixel size was based on ruler marks; (3) the slices were segmented from the background using global thresholding. Images were then rotated in two-dimensions so that the posterior capsule becomes the horizontal axis, and the urethra matches the prefixed vertical axis. Images were rotated and translated using Adobe Photoshop; (4) the aligned slices were saved in TIFF format and then imported in Image J software (V 1.44e, NIH). The slices were assigned original thickness and the entire 3D volume was exported from image J in Analyze 7.5 format; (5) to verify the continuity of the urethra, images were reconstructed in mid-sagittal view after importation in the dedicated platform to enable co-registration.

The 3D surgical specimen offers access to volumetry with detailed zonal anatomy of the gland. Following fixing and staining, all histopathology slides were digitized using a whole-slide scanner (Leica SCN 400, Leica Microsystems, Germany), allowing virtual whole-mount sections (Fig 2). Digital histopathology was performed using high-resolution square pixels of 25 $\times$ 25 μm, sufficient for diagnosis. The reassembled histology cross-sections [see Fig 2] were saved in Analyze 7.5 format.

Co-registration method

Co-registration of the MRI and histology images was carried out using a software platform with in-house code. Two methods of co-registration were tested: (1) a manually

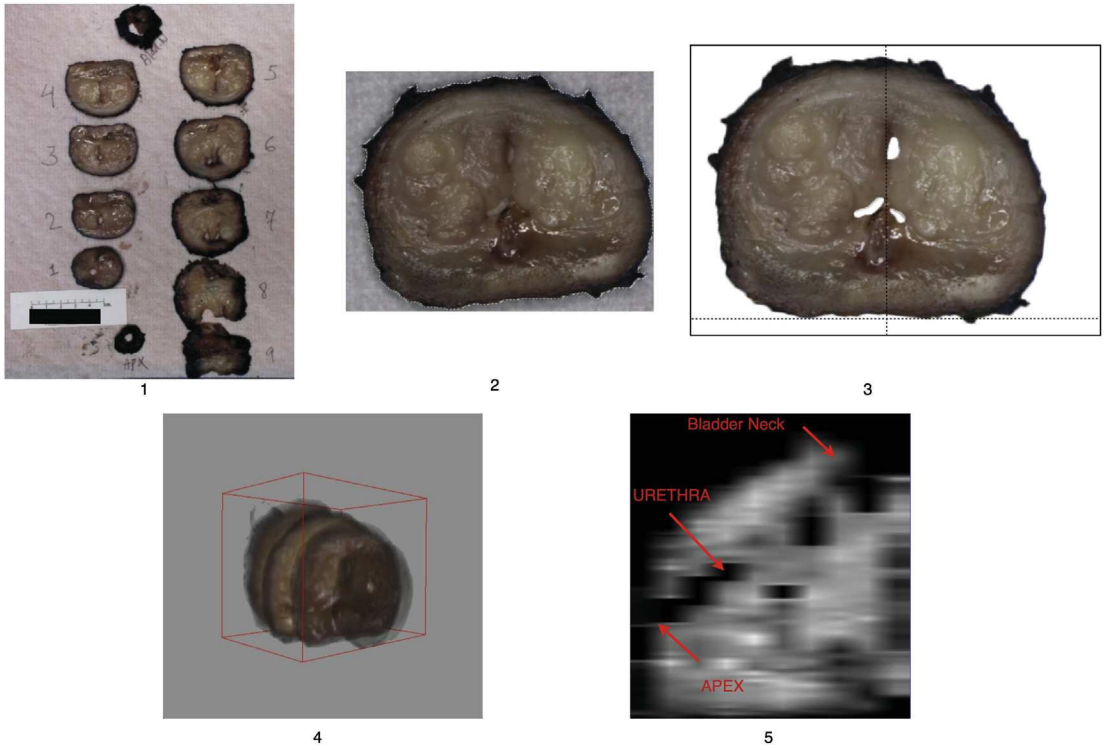

Figure 1 Rebuilding of 3D fresh gross specimen after cutting in contiguous parallel slices, perpendicular to the posterior capsule. See text for detailed description of the five steps illustrated in the figure.

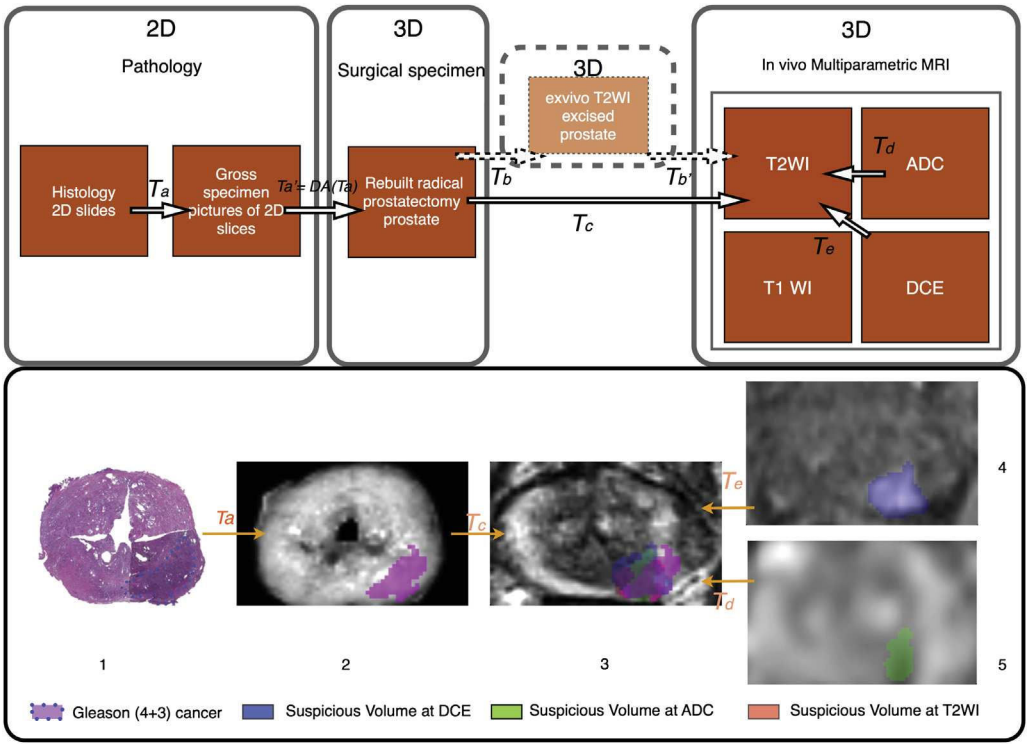

Figure 2 Co-registration workflow applied to cancer focus. *1st row.* Workflow for pathology–mpMRI co-registration in a surgical 3D space. *2nd row.* 3D deformable co-registration of virtual whole-mount histology (1), fresh specimen (2), T2WI (3), perfusion (4), and diffusion (5) sequences (ADC) applied to prostate cancer Gleason score 7 (4 + 3). The T2WI is the common space. Data extracted from the 3D volume (2,3,4,5). mpMRI, multiparametric magnetic resonance imaging; T2WI, T2-weighted imaging; ADC, apparent diffusion coefficient; T1WI, T1-weighted imaging; DCE, dynamic contrast-enhanced weighted images; 2D, two-dimensional 3D, three-dimensional; T(x), transformation x.

directed landmark-based method,[4] and (2) an automatic, voxel-based, mutual information[5,6] (MI)-based method. Each method was tested by performing rigid transformation, which aligns without volume modification, and affine transformation (computed with 12 degrees of freedom), which compensates for changes in volume and shape.

For the landmark-based method, the operator indicated a set of identical internal points of interest within each technique to be co-registered (e.g., Fig 3). Observation of prostate zonal anatomy enables detection of identical landmarks in mpMRI and the 3D rebuilt specimen. The co-registration is carried out to achieve alignment of the defined landmarks within the same space, thus realizing co-registration of the whole image. The MI-based automated method enabled co-registration in 3D between the *in-vivo* T2WI and the 3D rebuilt specimen based upon individual voxels of each image. The MI-based automated method performed iterative adjustment of the transformation parameters to maximize the similarity between the mpMRI and rebuilt pathology datasets in 3D. Initially, the *in-vivo* T2W MRI was co-registered with the 3D rebuilt specimen. Subsequently, the functional MRI sequences (ADC maps and DCE-MRI) were co-registered with the T2WI. The automatic MI-based method was employed for the functional sequences; landmark-based co-registration was not implemented owing to less precise definition of anatomical landmarks on these images. Thus, T2WI provided the final 3D space for analysis of all techniques and sequences.

The software enabled the operator to analyse the consistency of each transformation by overlaying the source and the target data and modifying each in real-time. The processes required to reach optimal alignment and deformation compensation are presented in Fig 2. Anatomical techniques provided the link between *ex-vivo* and *in-vivo* prostate images.

Data analysis

For the landmark-matching method, the residual error was computed as the 3D distance between the transformed

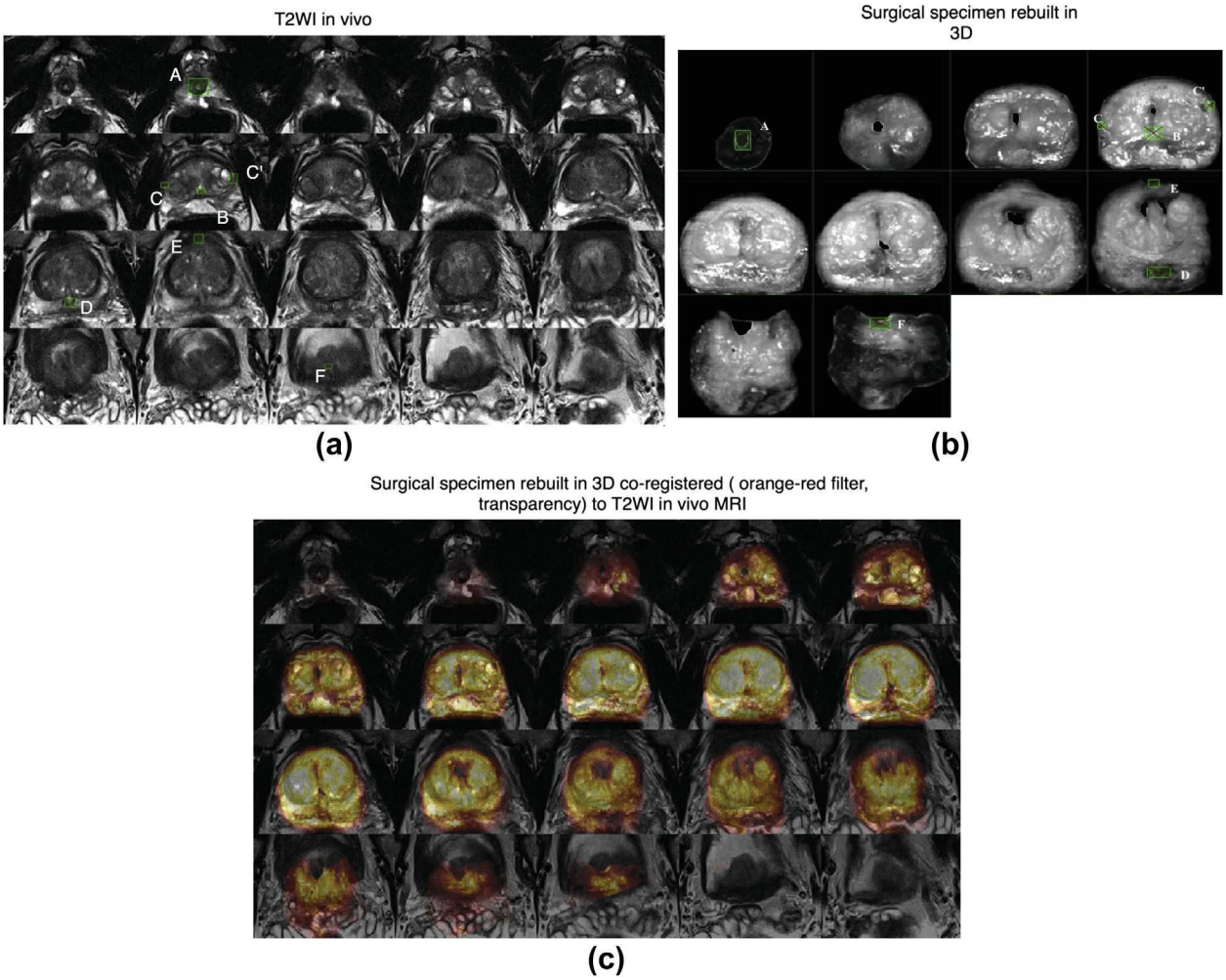

Figure 3 Zonal anatomy landmarks and examples of landmark-based co-registration in 3D. 3D landmarks are in green boxes plotted by an operator and used for transformation computation. The landmarks were A: distal point of urethra at apex; B: veru montanum; C & C′: anterior-most point of the right and left peripheral zone horn; D: ejaculatory duct; E: anterior-most point of the gland overall; F: proximal end of urethra at the prostate base, adjacent to the bladder. MRI, magnetic resonance imaging; T2WI, T2-weighted images; 3D, three dimensional. (For interpretation of the references to colour in this figure legend, the reader is referred to the web version of this article.)

source and the target zonal anatomy landmarks. The residual error was computed for each zonal anatomy landmark, which was recorded for both rigid and affine transformation. This produced a set of 22 paired data points for comparison. The overall residual root mean square (RMS) distance was computed and recorded by the software. RMS was considered to represent a good measure of utility of the technique because the zonal anatomy landmarks were clinically relevant, for example, in biopsy targeting,[7] and they were derived from the whole gland, thus avoiding sampling error.

The automatic method was evaluated by the overlap between the prostate volume, delineated within the software, in each technique after alignment using rigid or affine transformation. The overlap across techniques for each method was computed as a volume overlap index (Dice index).[8] Dice index is the ratio between twice the volume of gland overlap across two methods and the sum of the gland volume for those two methods. It is a similarity index that reflects volume overlap. This provides an additional measure for evaluating the success of the co-registration method, in addition to linear displacement as measured by RMS.

The two co-registration methods (MI-based and landmark-based) were evaluated to transform the 3D rebuilt specimen to T2WI with Dice index. This enabled comparison of the automatic and manual methods. Internal consistency of the automatic framework and evaluation process was tested using a phantom test. T2WI was co-registered to itself rotated by 5° in the *y*-axis to test rigid registration. Similarly, the ability of affine transformation to co-register T2WI to itself rotated by 5° in the *y*-axis was tested after a 20% size reduction in the *x*, *y*, and *z* directions. Paired *t*-tests were used to compare residual error for rigid and affine 3D transformation for each of the 22 zonal anatomy landmarks; the overall RMS for landmark-based transformation (either rigid or affine) as a measure of linear displacement error; and Dice index calculated for manual and automatic methods of volume overlap. The method was also tested both with and without the use of the fresh *ex-vivo* specimen MRI images, in order to evaluate the value of incorporating the *ex-vivo* imaging in the workflow as a method of improving co-registration accuracy. All *p*-values are two-sided and considered statistically significant at $p < 0.05$. Shapiro–Wilk's test was used to check normality of the variable if required. Statistical analysis was performed using R software (R, version 2.14.0, CRAN, Vienne, Austria).

Results

Final histopathology revealed pT3aR0 stage in two cases and pT2cR0 stage in the remaining case. Specimen Gleason's scores were 7 (3 + 4) in two cases and 7 (4 + 3) in one case. Prostate volumes at T2WI were 13.89, 41.39, and 73.17 cm^3. In all three cases, MRI-detected cancer was observed on all sequences. For each case, all techniques were transformed to a common 3D space, as illustrated in Fig 2.

Twenty-two landmarks extracted from the zonal anatomy were used to co-register the rebuilt surgical specimen with the *in-vivo* T2WI. Anatomical landmarks were more precisely mapped using affine transformation than rigid transformation. In mapping the surgical specimen to T2WI, the mean residual error for zonal anatomy landmarks was significantly lower for affine than for rigid transformation [1.47 mm (range 0.59–2.88) versus 2.18 mm (range 0.55–3.64), respectively $p = 0.0008$, mean difference (MD) between methods of 0.71 mm, 95% confidence interval: −1.0877 to −0.329], improving precision by a median of 38%.

An average RMS error of 1.6 mm (range 1.51–1.85 mm) was observed when mapping *in-vivo* MRI to the surgical specimen using affine landmark-based transformation, which represented an improvement in RMS error compared with the rigid method of 2.35 mm (range 2.17–2.58 mm; $p = 0.003$, MD −0.73, 95% CI: −0.9039 to −0.5561), and corresponded to a 32% improvement.

Table 1 displays the results for each transformation (Ta, Tb', Tc; referring to Fig 2), modelled by incorporating volume changes. For these transformations, the affine method performed better than the rigid method in the prostate workflow, with respective *p*-values of 0.01 (MD −1.2, 95% CI: −1.6303 to −0.7697), 0.03 (MD −0.56, 95% CI: −1.0362 to −0.0905) and 0.003 (MD −0.73, 95% CI: −0.9039 to −0.5561). The automatic framework (MI-based method) achieved the same performance for overlap (Dice index) as the landmark-based method (Table 1). Dice index D measurements were D = 0.89 versus D = 0.86 ($p = 0.48$).

The inter-sequence MRI registration showed good co-registration accuracy, with a Dice index of 0.81 for the ADC map and 0.89 for DCE (Table 1). This indicates that the automatic framework achieved alignment in the same 3D

Table 1
Results for each transformation.

	Landmark-based registration		Mutual information-based registration			
	Ta	Tc		Td	Te	Test
	Specimen–pathology	3D specimen–T2WI *in vivo*		ADC–T2WI *in vivo*	DCE–T2WI *in vivo*	T2WI–phantom T2WI
Best transformation type	Affine	Affine	Affine	Affine/rigid	Rigid	Rigid/affine
Mean RMS (range)	0.9mm (0.7–1.2)	1.61mm (1.51–1.85)				
Mean similarity Dice index (range)		0.86 (0.83–0.88)	0.89 (0.84–0.97)	0.81 (0.71–0.91)	0.86 (0.74–0.94)	0.96 (0.95–0.98)

T2WI, T2-weighted imaging; DCE, dynamic contrast enhanced weighted images; ADC, apparent diffusion coefficient; 3D, three-dimensional; RMS, root mean square distance.

space as the functional and anatomical sequences with enough similarity to be useful.

The internal consistency of the automatic framework and evaluation process was excellent and able to reach D = 0.96 and D = 0.95, respectively, for the rigid and affine phantom studies.

The use of *ex-vivo* acquired MRI images for co-registration to histology was found to yield a 3.5 mm RMS error, suggesting inferior accuracy as compared to co-registration using the *in-vivo* mpMRI. Moreover, adding the *ex-vivo* step did not further decrease the error in the observed alignment between the *ex-vivo* and *in-vivo* MRI.

Discussion

In-vivo mpMRI has evolved as the most promising non-invasive method of visualizing prostate anatomy and for detecting tumours.[1] Modern mpMRI, incorporating ADC and DCE, has been shown to have a significant role in localizing dominant[3] tumours and potentially excluding clinically significant disease.[1] In addition, ADC values obtained from DWI correlate with the Gleason score.[1,9]

Regarding the validation of MRI accuracy in predicting the location of cancer, no simple method for correlating MRI to the histological sections has been devised, and localization in 3D space remains a problem. This also limits the ability to implement focal therapy strategies in which it has been shown repeatedly that localization of suspicious lesions in 3D surgical space is essential.[10] Adequate therapeutic targeting requires the ability to delineate the target volume in 3D, which is difficult with two-dimensional (2D) assessment alone. Moreover, working in two-dimensions assumes that each slice of the prostate will exactly match an axial MRI section. Good accuracy was demonstrated for an automated system of 3D co-registration using transformation of internal landmarks seen within each image. Although the method was applied between mpMRI sequences and histology, the technique could be easily applied to any image sequences used in diagnosis or treatment of prostate cancer.

The prostate undergoes shape changes after surgical removal and during histology processing. Specimen formalin fixation and paraffin embedding induces variable tissue shrinkage.[11] Various authors have used either 2D image transformation[8] or prostate moulds[12] created before sectioning the specimen to overcome deformation. To overcome discordance between the MRI acquisition plane[13] and the plane used in cutting the surgical specimen, *ex-vivo* MRI-based cutting devices[13] and software for recognition of injected landmarks[14] have been developed. Although these methods result in accurate transformation as measured by Dice index, prostate moulds and customized cutting devices are labour intensive, costly, and do not fully compensate for tissue deformation.

Chappelow et al.[15] describe a method based on mutual information that co-registers T2WI, DCE, and ADC. However, this method is based on 2D histology and requires considerable expertise to determine the correspondence between histology and 3D MRI volume. As such, wide implementation of this method may have variable outcomes.

To the authors' knowledge, the present co-registration method is the first to create a 3D counterpart within the same reference space between histology and both anatomical and functional sequences provided by prostate mpMRI. The method enables a true, deformable transformation and provides 1–2 mm accuracy. This is less than twice the thickness of an 18 G prostate biopsy needle and matches the diameter of laser fibres already used in focal therapy trials.[16] The observed 3D Dice index (0.89) enables adequate accuracy for targeting cancers >0.18 cm^3, suggesting it would enable detection of those cancers typically defined as clinically significant.[1] Moreover, Ven et al.[17] concluded that co-registration accuracy between another technique and MRI had to reach 1.9 mm in linear displacement to correctly co-register the smallest volume of interest detected by the ADC map, in order to achieve clinical utility. The present method fulfils this objective.

Both manual landmark-based and automatic methods for alignment of T2WI and the 3D rebuilt specimen were tested, using Dice index to measure similarity. The automatic method achieved the same performance as the manual method and is independent of the user experience in either pathology or image interpretation. This is critical to achieve objective correlation between pathology and MRI.

The proposed method is not subject to limitations relating to slicing location and cut angle variation, because the rigid transformation corrects for the orientation of the prostate specimen in 3D. Affine transformation furthermore compensates for any change in volume, slice thickness, and shape between MRI and histology. By adding only one step in the clinical workflow—taking pictures of the sliced specimen—this image-based method is widely transferable.

Internal consistency was excellent with a mean Dice index of 0.95–0.96 for the phantom tests. This indicates that variation in Dice index relies on differences in the image sequence, for instance, between T2WI and the ADC map. However, mpMRI with ADC and DCE still requires further standardization across institutions. This may affect the reliability of the presented technique in other centres. The presented workflow is nonetheless attractive because there is no need for an intermediate image representing an *ex-vivo* MRI, an elaborate and time-consuming process. The anatomical landmarks, extracted from McNeal zonal anatomy, achieved a bridge between *in-vivo* and *ex-vivo* techniques. These were highly discernible at T2WI. Accuracy for the distinguishing parts of the gland are essential owing to their central role in procedural guidance.[7] Although the method was tested with very different prostate volumes and for numerous anatomical landmarks, more cases are needed for clinical validation.

The inter-sequence registration of MRI is decisive for quantitative assessment of functional aspects in 3D. The aim of this part of the protocol is to allow the conjunction of all relevant sequences in the same 3D space. Therefore, it is essential to be able to co-register both ADC and DCE, as these each represent different tissue properties.[18] The co-registration method is critical considering prostate

motion,[19] especially related to rectal peristalsis. Good accuracy was achieved in this domain, with a Dice index of 0.81 for ADC and 0.89 for DCE. Rigid registration was sufficient to correct motion and, therefore, affine transformation was not required (Table 1). Functional sequences were then correctly mapped to anatomical sequences in the same 3D space, allowing objective comparison between these. As shown previously,[20] co-registration of different sequences can improve cancer detection. As some tumours are primarily detected on functional sequences without clear anatomical correlation at T2WI, greater accuracy in targeting can be achieved through simultaneous registration of sequences in 3D.

An immediate clinical use of the present method could be to facilitate achieving efficient, yet accurate, correlation between MRI and pathological findings, which is critical for quality assurance in any prostate MRI program and may assist in the education of radiologists and clinicians involved in MRI interpretation. For instance, the present technique may be used to more reliably investigate discrepancies, in terms of both false-positive and false-negative interpretations, between MRI and pathology. In addition, the present preliminary work suggests that any anatomical changes to the prostate induced by the prostatectomy procedure itself may be compensated and fit to the MRI images by deformable transformation. Also, further studies may explore a potential role of the described algorithm in performing co-registration of prostate images obtained before and after ablative therapies, which can cause gross anatomical deformation of the prostate; the present co-registration method may impact the reliability of follow-up imaging. Finally, a natural extrapolation of the work will be the co-registration of diagnostic sequences in 3D for procedure guidance. The technique requires limited preprocessing, making it widely transferable to a number of therapeutic strategies.

In conclusion, the present workflow for 3D co-registration between preoperative prostate MRI and pathology produced clinically acceptable accuracy in terms of zonal anatomy. The system is able to account for changes in the *ex-vivo* specimen using non-rigid (affine) transformation. The use of an accurate 3D automatic method could offer greater accuracy and reproducibility than existing 2D methods, suggesting the potential for wide implementation. The present findings will be validated in larger datasets and implemented into clinical diagnostic and therapeutic research workflows.

Acknowledgements

The authors acknowledge the support of The Joseph and Diane Steinberg Charitable Trust and the Grant 1UL1RR029893 from the National Center for Research Resources, National Institutes of Health. C.O., H.R., A.M., F.M.D., J.M., and A.B.R. have nothing to disclose. S.S.T. is a consultant for Eigen, consultant and scientific investigator for GTX, scientific investigator for Steba Biotech, speaker for Janssen, and receives royalties from Elsevier. No direct financial conflict of interest is identified.

References

1. Dickinson L, Ahmed HU, Allen C, et al. Magnetic resonance imaging for the detection, localisation, and characterisation of prostate cancer: recommendations from a European consensus meeting. *Eur Urol* 2011;**59**:477–94.
2. Hoeks CMA, Barentsz JO, Hambrock T, et al. Prostate cancer: multiparametric MR imaging for detection, localization, and staging. *Radiology* 2011;**261**:46–66.
3. Rosenkrantz AB, Deng F-M, Kim S, et al. Prostate cancer: multiparametric MRI for index lesion localization—a multiple-reader study. *AJR Am J Roentgenol* 2012;**199**:830–7.
4. Fitzpatrick JM, West JB, Maurer Jr CR. Predicting error in rigid-body point-based registration. *IEEE Trans Med Imaging* 1998;**17**:694–702.
5. Wells 3rd WM, Viola P, Atsumi H, et al. Multi-modal volume registration by maximization of mutual information. *Med Image Anal* 1996; **1**:35–51.
6. Maes F, Collignon A, Vandermeulen D, et al. Multimodality image registration by maximization of mutual information. *IEEE Trans Med Imaging* 1997;**16**:187–98.
7. Ouzzane A, Puech P, Lemaitre L, et al. Combined multiparametric MRI and targeted biopsies improve anterior prostate cancer detection, staging, and grading. *Urology* 2011;**78**:1356–62.
8. Mazaheri Y, Bokacheva L, Kroon D-J, et al. Semi-automatic deformable registration of prostate MR images to pathological slices. *J Magn Reson Imaging* 2010;**32**:1149–57.
9. Hambrock T, Somford DM, Huisman HJ, et al. Relationship between apparent diffusion coefficients at 3.0-T MR imaging and Gleason grade in peripheral zone prostate cancer. *Radiology* 2011;**259**:453–61.
10. Ukimura O, Gill IS. Reply from authors re: Mark Emberton. Tissue preservation may offer a harm-reduction strategy for men with early prostate cancer. *Eur Urol* 2012;**62**:64–6. *Eur Urol* 2012; **62**: 66–67.
11. Schned AR, Wheeler KJ, Hodorowski CA, et al. Tissue-shrinkage correction factor in the calculation of prostate cancer volume. *Am J Surg Pathol* 1996;**20**:1501–6.
12. Trivedi H, Turkbey B, Rastinehad AR, et al. Use of patient-specific MRI-based prostate mold for validation of multiparametric MRI in localization of prostate cancer. *Urology* 2012;**79**:233–9.
13. Kimm SY, Tarin TV, Lee JH, et al. Methods for registration of magnetic resonance images of *ex vivo* prostate specimens with histology. *J Magn Reson Imaging* 2012;**36**:206–12.
14. Ward AD, Crukley C, McKenzie CA, et al. Prostate: registration of digital histopathologic images to *in vivo* MR images acquired by using endorectal receive coil. *Radiology* 2012;**263**:856–64.
15. Chappelow J, Bloch BN, Rofsky N, et al. Elastic registration of multimodal prostate MRI and histology via multiattribute combined mutual information. *Med Phys* 2011;**38**:2005.
16. Rosenkrantz AB, Scionti SM, Mendrinos S, et al. Role of MRI in minimally invasive focal ablative therapy for prostate cancer. *AJR Am J Roentgenol* 2011;**197**:W90–6.
17. Ven WJM, Hulsbergen-van de Kaa CA, Hambrock T, et al. Simulated required accuracy of image registration tools for targeting high-grade cancer components with prostate biopsies. *Eur Radiol* 2013;**23**: 1401–7.
18. Rosenkrantz AB, Mendrinos S, Babb JS, et al. Prostate cancer foci detected on multiparametric magnetic resonance imaging are histologically distinct from those not detected. *J Urol* 2012;**187**:2032–8.
19. Van Herk M, Bruce A, Kroes AP, et al. Quantification of organ motion during conformal radiotherapy of the prostate by three dimensional image registration. *Int J Radiat Oncol Biol Phys* 1995;**33**:1311–20.
20. Rosenkrantz AB, Mannelli L, Kong X, et al. Prostate cancer: utility of fusion of T2-weighted and high b-value diffusion-weighted images for peripheral zone tumor detection and localization. *J Magn Reson Imaging* 2011;**34**:95–100.

Application du recalage déformable: Comparaison entre volume tumoral histologique et IRM

Cette méthode de recalage multi modalité déformable a été utilisée sur les données d'une série de 37 patients consécutifs ayant eu une IRMmp à 3 Tesla avant une prostatectomie totale. Les résultats de cette étude ont permis de montrer une sous-estimation significative du volume cancéreux, remis à l'échelle in vivo de manière individualisée, par l'imagerie en pondération T2 WI et la cartographie ADC. Cette sous-estimation atteint en moyenne respectivement – 32% et – 47% sur les 50 tumeurs étudiées. La sous-estimation apparaît plus marquée pour la cartographie ADC (différence moyenne -57% à -16%) que pour la séquence T2 WI (-45% - +2%). La sous-estimation semble être plus marquée pour les tumeurs de score de Gleason ≥7 ou de score 4-5. Cette dernière observation souligne l'hétérogénéité du cancer de la prostate et signale la potentialité de l'IRMmp dans la stratification de la maladie en situation de pré diagnostique ainsi que la sélection des patients pour les différents traitements.

Se référant à :

« Prostate tumour volumes: evaluation of the agreement between magnetic resonance imaging and histology using novel co-registration software: Prostate tumour volume: co-registration between MRI and pathology. »

British Journal of Urology International. 2014 Dec;114(6b):E105–12.

Le Nobin J, Orczyk C, Deng F-M, Melamed J, Rusinek H, Taneja SS, Rosenkrantz AB.

BJUI
BJU International

Prostate tumour volumes: evaluation of the agreement between magnetic resonance imaging and histology using novel co-registration software

Julien Le Nobin*†, Clément Orczyk*‡, Fang-Ming Deng§, Jonathan Melamed§, Henry Rusinek¶, Samir S. Taneja* and Andrew B. Rosenkrantz¶

*Department of Urology, Division of Urological Oncology and §Departments of Pathology and ¶Radiology, New York University Langone Medical Center, New York, NY, USA, †Department of Urology, University Hospital of Lille, Lille and ‡Department of Urology and Renal Transplantation/UMR 6301-Cervoxy Group, University Hospital of Caen, Caen, France

Objective

To evaluate the agreement between prostate tumour volume determined using multiparametric magnetic resonance imaging (MRI) and that determined by histological assessment, using detailed software-assisted co-registration.

Materials and Methods

A total of 37 patients who underwent 3T multiparametric MRI (T2-weighted imaging [T2WI], diffusion-weighted imaging [DWI]/apparent diffusion coefficient [ADC], dynamic contrast-enhanced [DCE] imaging) were included. A radiologist traced the borders of suspicious lesions on T2WI and ADC and assigned a suspicion score of between 2 and 5, while a uropathologist traced the borders of tumours on histopathological photographs. Software was used to co-register MRI and three-dimensional digital reconstructions of radical prostatectomy specimens and to compute imaging and histopathological volumes. Agreement in volumes between MRI and histology was assessed using Bland–Altman plots and stratified by tumour characteristics.

Results

Among 50 tumours, the mean differences (95% limits of agreement) in MRI relative to histology were −32% (−128 to +65%) on T2WI and −47% (−143 to +49%) on ADC. For all tumour subsets, volume underestimation was more marked on ADC maps (mean difference ranging from −57 to −16%) than on T2WI (mean difference ranging from −45 to +2%). The 95% limits of agreement were wide for all comparisons, with the lower 95% limit ranging between −77 and −143% across assessments. Volume underestimation was more marked for tumours with a Gleason score ≥7 or a MRI suspicion score 4 or 5.

Conclusion

Volume estimates of prostate cancer using MRI tended to substantially underestimate histopathological volumes, with a wide variability in extent of underestimation across cases. These findings have implications for efforts to use MRI to guide risk assessment.

Keywords

prostate cancer, diffusion-weighted MRI, histology, tumour volume, image processing, computer-assisted

Introduction

There is a growing range of options for the treatment of prostate cancer (PCa), including radical prostatectomy, radiation therapy, active surveillance and investigational focal ablative therapy. MRI provides the most widely used imaging test for depicting focal prostate lesions, and the ability to precisely define the volume of identified lesions using MRI would be of immense value for candidate selection, for guiding therapy and for monitoring both surveillance and treatment. A number of previous studies have suggested that MRI has limited value in predicting the volume of PCa [1–6], but the results of such studies may be difficult to apply to contemporary PCa management, given their use of older technology, lack of focus on index lesions and statistical methods that mainly explore volume correlations between imaging and histopathology [1–6]. While positive correlations may be useful for establishing the role of MRI in guiding

 | doi:10.1111/bju.12750
Published by John Wiley & Sons Ltd. www.bjui.org

prognosis and risk estimates, strong correlations do not guarantee a high level of consistency in predicting actual volumes, thereby limiting the impact of these results in risk assessment. While a more recent study did improve on earlier work by exploring the associations between volumes of PCa index lesions determined using multiparametric MRI at 3T and histopathology [7], that study also mainly used correlative statistics. Furthermore, histopathological tumour volumes in that study were determined using the ellipsoid formula, which is prone to error [8]. We have previously developed and validated a novel software tool that can determine the volume of three-dimensional (3D) digitally rebuilt histological specimens as well as perform accurate automated 3D deformable transformation and co-registration of such specimens with MRI [9]. This tool can correct for shrinkage and deformation of the prostate caused by the myriad of steps involved in the surgical procedure itself and by subsequent histological processing. The tool may be useful for more reliably estimating the performance of MRI in predicting actual tumour volumes and thereby determining the clinical impact of MRI in guiding candidate selection and treatment. The aim of the present study was to evaluate the level of agreement in volumes of PCa index lesions between histopathology and MRI, using novel co-registration software. We also assess the impact of various features, such as the MRI sequence and tumour grade, location and imaging appearance, on this level of agreement.

Materials and Methods

Study Population

This retrospective single-institution study was compliant with the *Health Insurance Portability and Accountability Act* and approved by our institutional review board with a waiver for informed consent. A total of 66 patients who underwent radical prostatectomy for PCa between November 2012 and July 2013 were identified. A number of patients were then excluded for the following reasons: they had not undergone preoperative MRI at our centre ($n = 11$); a full set of pathological images was unavailable ($n = 11$); no dominant tumour was identified on histological assessment ($n = 2$); an index lesion was not identified on preoperative MRI ($n = 4$); or there was no tumour on pathological examination (pT0 disease) [10] ($n = 1$). Patients with no visible tumour lesion on MRI were excluded because such patients would not be candidates MRI-guided focal lesion ablation. After these exclusions, the final cohort included 37 patients (mean age 60 ± 9 years) with a median (range) preoperative PSA 5.0 (0.32–98) ng/mL.

MRI Data Acquisition

All patients underwent multiparametric MRI using a 3T system (MAGNETOM Trio, Siemens Healthcare, Erlangen, Germany) and a pelvic phased-array coil. Examinations included non-enhanced multiplanar turbo spin-echo T2-weighted imaging (T2WI; slice thickness 3 mm, no interslice gap; field of view 180 × 180 mm; matrix 256 × 256), axial turbo spin-echo T1-weighted imaging (slice thickness 3 mm, no interslice gap; field of view 180 × 180 mm; matrix 192 × 192), axial diffusion-weighted imaging (DWI) (b-values between 50 and 1000 s/mm^2) with inline reconstruction of the apparent diffusion coefficient (ADC) map (slice thickness 3 mm, no interslice gap; field of view 200 × 200 mm; matrix 100 × 100), as well as dynamic contrast-enhanced (DCE) imaging of the prostate using 0.1 mmol/kg of gadolinium chelate (partition thickness 3 mm; field of view 240 × 240 mm; matrix 128 × 128). Contrast was injected using a power injector (Spectris; Medrad, Warrendale, PA, USA).

Histopathological Analysis

Prostatectomy specimens were processed according to standard institutional protocol. Specimens underwent fixation for 24 h after immediate fine-needle injection with formalin. The specimen was then cut at regular 5-mm intervals perpendicular to the posterior capsule, and intact slices were photographed using a digital camera at 210 pixels per cm and with a 1024 × 1366 matrix, thereby allowing appreciation of zonal anatomy on the photographs. Slices were then cut into quadrants, embedded in paraffin on 3–4-micron slides and stained with haematoxylin and eosin; four very large prostates were cut into sextants. The stained histology slides were digitalised in high resolution (400× magnification) using a Leica scanner SN 400 (Leica Microsystems, Wetzlar, Germany). These images were then rebuilt into a whole-mount image by border alignment and comparison with the previous photographs of the intact slices using Photoshop CS5 (Adobe Systems Inc, San Jose, CA, USA). A single uropathologist traced the border of all tumours on each slice and assigned a Gleason score based on the previously published consensus criteria. Lesions measuring <0.1 mL were excluded ($n = 2$).

MRI Assessment

A single genito-urinary radiologist was given a description of the approximate location of each tumour for each patient (left vs right, anterior vs posterior, base, middle or apex) but no other information regarding lesion size, location or grade. The radiologist then identified a corresponding abnormality in that region most likely to represent the tumour, based upon joint review of T2WI, DWI and DCE. This approach was used to simulate the clinical and investigational paradigms by which targeted biopsy and treatment are currently performed, directed to a lesion identifiable on MRI [11]. Then, the radiologist traced the margins of the lesion on each slice on which it was visible on both the axial T2WI and the ADC

map. This radiologist also assigned a suspicion score to each lesion using a 1–5 Likert scale to indicate the probability of the lesion representing a significant cancer, generally based on previously published criteria [12]. These scores were then combined into a binary classification with scores 2–3 indicating low suspicion and scores 4–5 indicating high suspicion. Given that all included lesions were visible on MRI and that a score of 1 is used at our institution to indicate a negative MRI, all lesions received a suspicion score of at least 2. This binary division was based on previous work from our institution showing a substantial increase in cancer yield and grade among lesions with a score of 4 or 5, compared with lesions with a lower score [13].

Co-registration between MRI and Histopathology

Co-registration was performed using a previously validated method. Digital 3D representations of the surgical specimens were assembled using the digital photographs of the intact slices using computer software (ImageJ® and Photoshop; Adobe), providing 3D datasets for co-registration with MRI. This co-registration between MRI and the 3D digital gross specimens was performed using in-house software (FireVoxel); that uses both a manually directed landmark-based component and an automatic Mutual Information process. For the landmark-based component, the operator indicates a set of identical internal points of interest within each of the two image sets. For this purpose, corresponding landmarks relating to prostate zonal anatomy were selected on T2WI and the 3D rebuilt specimen. A combination of eight landmarks was extracted based on the zonal anatomy: distal urethra at the level of the apex; proximal urethra at the level of the base; verumontanum; anterior-most aspect of the anterolateral horn of the peripheral zone; anterior-most margin of the prostate; posterior junction of peripheral and transition zones; and left and right ejaculatory ducts. Co-registration was then performed to attain alignment of these landmarks within a mutually defined space, thus achieving co-registration of the whole image. The software allows the operator to analyse the consistency of each transformation by overlaying the source and target data and modifying each of these in real-time.

For each case, to first assess the accuracy of co-registration, the margins of the entire prostate were traced on axial T2WI and the 3D specimen, and the volume of the prostate on each of these image sets was determined after co-registration. Then, the ADC map was registered to the axial T2WI using the software's Mutual Information process. Subsequently, for each tumour, three regions of interest were generated: one representing the lesion defined on T2WI, one representing the lesion defined on ADC following co-registration to T2WI, and one representing the lesion defined on 3D histology with co-registration to T2WI, which was referred to as the registered histology (ReH) lesion (Figs 1, 2). The software was then used to obtain the volume of each of these regions of interest for each tumour in the co-registered 3D space.

Statistical Analysis

Agreement between volumes determined using ReH and MRI was assessed using Bland–Altman analyses. This approach provides both the mean difference between the measurements (taking into account both the direction and magnitude of any difference) and the 95% limits of agreement (representing the mean difference ±1.96 SD of the difference, thereby indicating the expected range of variability between MRI and ReH measurements for the large majority of cases). The comparison was performed between volumes of the entire prostate determined on T2WI and 3D histology as well as between volumes of tumours determined on ReH and on T2WI and the ADC maps. Given a positive association between lesion volume and difference in volume between the techniques, the Bland–Altman analysis of tumour volumes was conducted in terms of percent differences. In addition, these assessments were performed for tumours stratified by various imaging and histological characteristics (Gleason score [6 vs ≥7], zone [peripheral vs transition] and MRI suspicion score [1–3 vs 4–5]). A *post hoc* analysis was performed comparing those lesions larger on T2WI than on ReH with the remaining lesions; these tumours were compared in terms of volume on ReH using the unpaired *t*-test and in terms of MRI suspicion score using the Mann–Whitney *U*-test. Statistical analysis was performed using MedCalc for Windows, version 12.7 (MedCalc Software, Ostend, Belgium).

Results

Comparison of Entire Prostate Volumes

The entire prostate in the 37 included patients had a mean volume on registered histopathology of 46.6 ± 16.3 mL and on T2WI of 46.9 ± 16.2 mL. The mean difference in prostate volumes between T2WI and registered histopathology was 0.37 mL, with 95% limits of agreement of −6.97 to +7.72 mL.

Lesion Characteristics

A total of 50 tumours were identified in the 37 prostatectomy specimens. Of these, 80.0% (40/50) were in the peripheral zone and 20.0% (10/50) were in the transition zone. The distribution of Gleason scores was as follows: 22.0% (11/50) Gleason 6; 76.0% (38/50) Gleason 7; 0% (0/50) Gleason 8; and 2.0% (1/50) Gleason 9. In all, 28.0% of tumours (14/50) had a low MRI suspicion score and 72.0% (36/50) had a high MRI suspicion score. The characteristics of patients and lesions are summarized in Table 1and Fig 3.

Assessment of Lesion Volumes

The 50 tumours had a mean volume on ReH of 1.38 ± 1.20 mL, on T2WI of 0.93 ± 0.79 mL, and on ADC of 0.86 ±

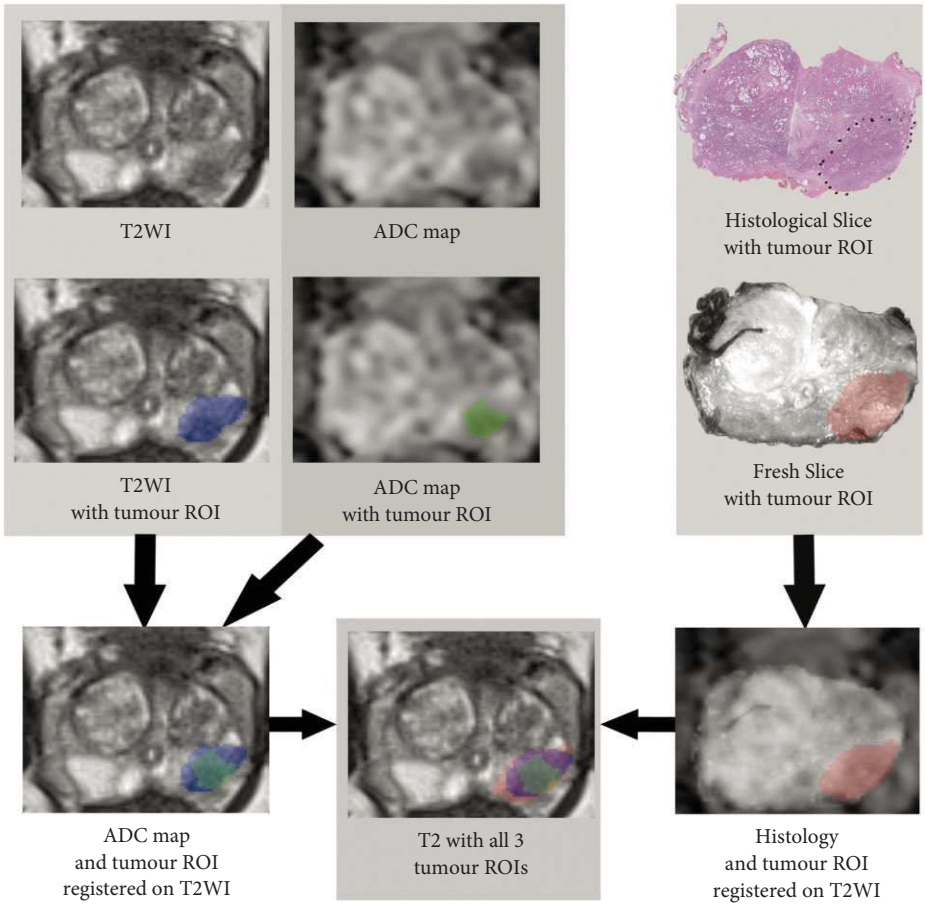

Fig. 1 Demonstration of co-registration methodology in one case. Tumour is marked in blue, green and red on T2-weighted imaging (T2WI), apparent diffusion coefficient (ADC) and histology, respectively. ROI, region of interest.

Table 1 Characteristics of patients and lesions.

Variable	Mean ± SD	Median	Min	Max
Patients (n = 37)				
Age, years	60.3 ± 5.5	62	48	77
PSA, ng/mL	9.5 ± 7.6	5	0.3	98.0
Prostate volume on registered histology, mL	46.6 ± 16.3	42.0	18.0	99.8
Prostate volume on T2-weighted imaging, mL	46.9 ± 16.2	40.1	20.9	106.0
Tumours (n = 50)				
Gleason score	–	7	6	9
MRI suspicion score	–	4	2	5
Tumour volume on registered histology, mL	1.38 ± 1.20	0.73	0.11	10.1
Tumour volume on T2-weighted imaging, mL	0.93 ± 0.79	0.45	0.08	6.77
Tumour volume on apparent diffusion coefficient map, mL	0.86 ± 0.78	0.34	0.06	7.69

0.78 mL. Table 2 summarizes the results of the Bland–Altman assessments. Overall, MRI substantially underestimated lesion volumes, and had wide 95% limits of agreement. The mean difference and associated 95% limits of agreement on MRI relative to ReH were −32% (−128 to +65%) on T2WI and −47% (−143 to +49%) on ADC.

Table 2 also presents results for tumours stratified into various subsets. For all subsets, there was a more marked underestimation of volumes on the ADC maps (mean difference ranging from −57 to −16%) than on T2WI (mean difference ranging from −45 to +2%). Nonetheless, 95% limits of agreement were wide for all comparisons, with the lower 95% limit ranging between −77 and −143% across all assessments. There was more marked underestimation of volumes for tumours with Gleason score ≥7 or with an MRI suspicion score of 4 or 5. Transition zone tumours showed slightly more pronounced underestimation of lesion volumes on T2WI, although similar underestimation on ADC, compared with peripheral zone tumours. For both T2WI

Fig. 2 Co-registration of tumours between T2-weighted imaging (T2WI) MRI and histology, showing examples of (**A**) larger volume on histology in tumour with Gleason score 7 and MRI suspicion score 5/5, and (**B**) larger volume on MRI in tumour with Gleason score 6 and MRI suspicion score 2/5. ROI, region of interest.

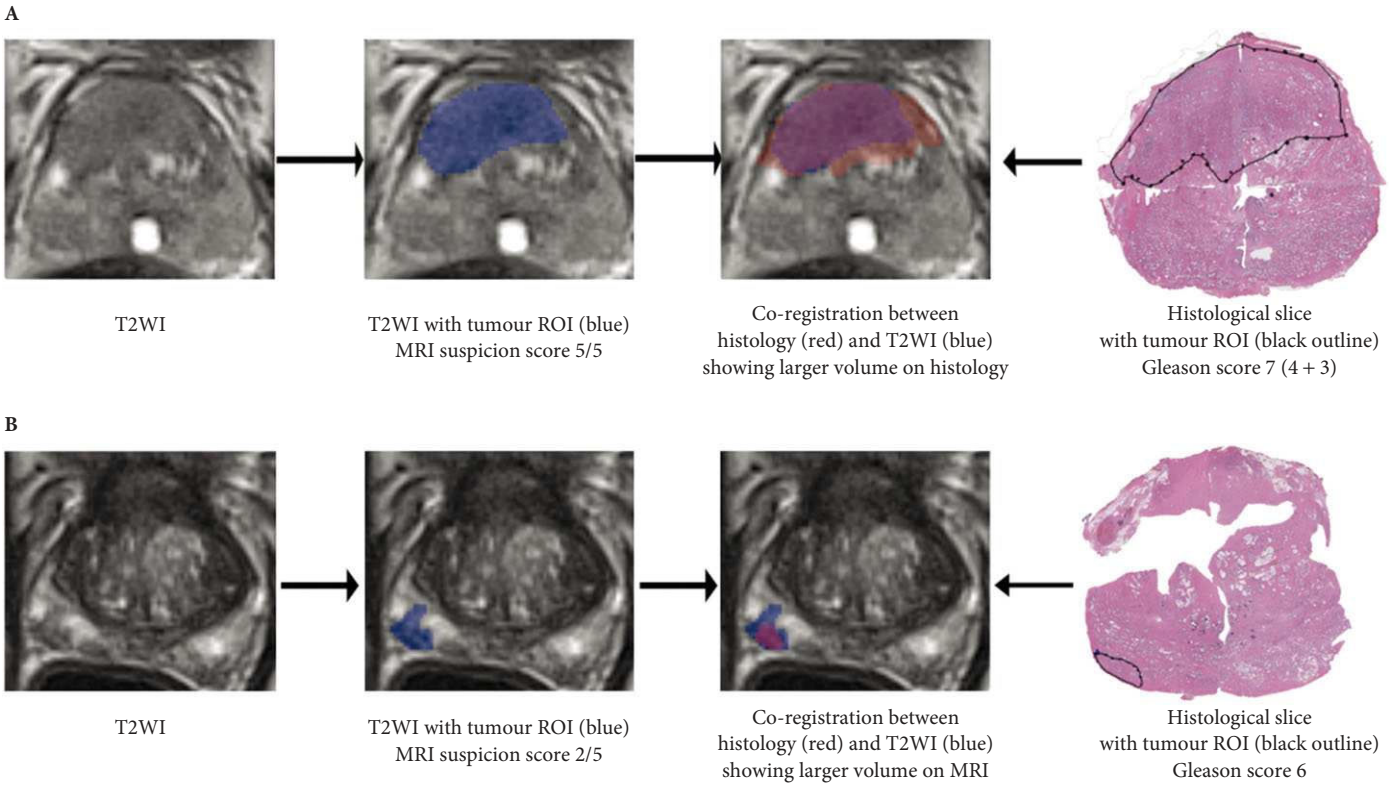

Table 2 Results of Bland–Altman analyses comparing tumour volumes between MRI sequences and registered histology (ReH).

Sample	T2WI		ADC	
	Mean difference, %	95% limits of agreement, %	Mean difference, %	95% limits of agreement, %
All tumours (n = 50)	−32	−128 to +65	−47	−143 to +49
MRI suspicion score 2/3 (n = 14)	+2	−107 to +111	−25	−122 to +72
MRI suspicion score 4/5 (n = 36)	−45	−97 to +7	−57	−124 to +10
Gleason 6 (11)	−5	−96 to +87	−16	−94 to +63
Gleason ≥7 (n = 39)	−39	−104 to +26	−57	−129 to +14
Transition zone (n = 10)	−42	−77 to −6	−48	−112 to +16
Peripheral zone (n = 40)	−29	−110 to +52	−48	−129 to +33
Histological tumour volume <1 mL (n = 31)	−24	−133 to +85	−46	−152 to +60
Histological tumour volume >1 mL (n = 19)	−44	−112 to +24	−48	−128 to +31

and ADC, the limits of agreement were slightly wider for smaller tumours. The extent of volume underestimation was somewhat less for smaller lesions on T2WI, although essentially identical between smaller and larger lesions for ADC.

A *post hoc* analysis of the 10 tumours larger on T2WI than on ReH was performed. In comparison with the other 40 lesions, these lesions had a lower median MRI suspicion score (3 vs 4; P = 0.003) and tended to be smaller on ReH (0.49 vs 1.60 mL; P = 0.08).

Discussion

Previous studies have explored the associations between PCa volumes determined using MRI and those determined through histolopathological assessment [1–6]. These studies have obtained varying results and are limited in a number of respects, including the use of outdated MRI technology (such as lack of modern multiparametric sequences), imprecise estimates of pathological volume as the reference standard, suboptimal techniques for achieving co-registration of MRI and pathological images, and the use of correlative

Fig. 3 Bland–Altman plots comparing volumes of all tumours between registered histology (ReH) and T2-weighted imaging (**A**) and apparent diffusion coefficient (**B**) from preoperative MRI.

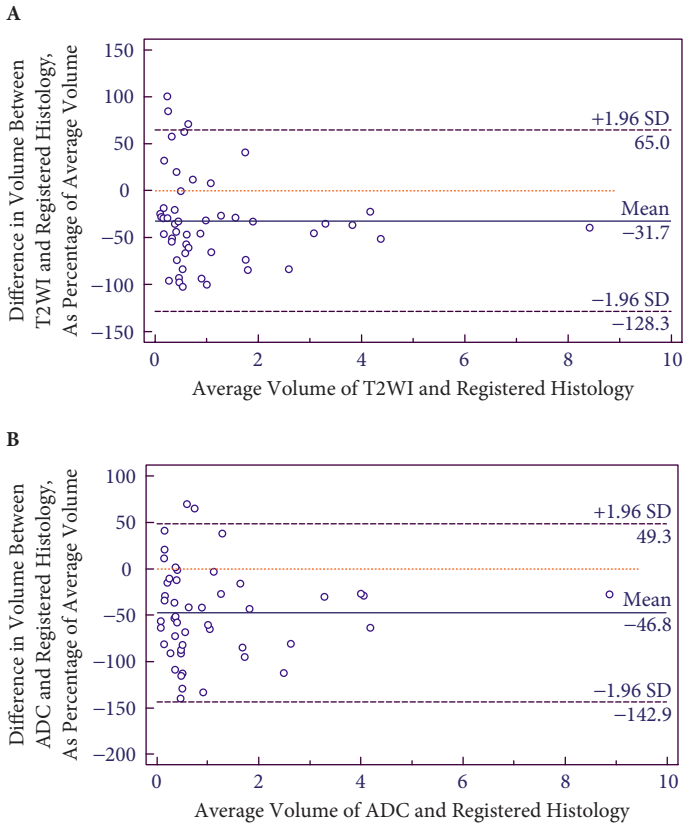

statistical methods (such as the Pearson correlation coefficient) that do not evaluate true agreement in volume estimations between MRI and pathology. In the present study, we attempted to address these issues by investigating the accuracy of volume estimates from 3T multiparametric MRI using novel co-registration software for comparing the two techniques [9], in addition to the use of software for determining pathological tumour volumes and the Bland–Altman method for assessing true agreement in terms of these volumes.

Through this approach, we obtained different results from those previously obtained in the literature. Overall, MRI substantially underestimated tumour volumes in comparison with histopathology. This underestimation of tumour volume may relate to the findings of Langer et al. [14]. These authors observed that prostate tumours contain regions of sparse tumour comprising mostly benign glands and stroma intermixed with the malignant epithelium. These regions were characterised as inherently invisible on MRI and posing limits on the ability to estimate full tumour volume with MRI. Two subsequent studies confirmed the impact of the histological architecture of prostate tumours in their detection using MRI, with both of these further studies also noting tumours with certain histological characteristics to be predisposed to be undetected [15,16]. One of these studies described the presence of solid tumour growth as a key contributor to tumour detection on MRI that was present in only 57.5% of tumours [15]. It would be anticipated, therefore, that tumour volumes measured with MRI would underestimate true volume given the presence of such regions within the volume of a tumour. Future studies could perform a more targeted evaluation of those portions of tumour volumes not appreciated on MRI in order to assess the accuracy of this possible explanation.

An unexpected finding was that the degree of underestimation of tumour volumes was more pronounced using the ADC map than using T2WI as well as for tumours with a higher Gleason score or higher MRI suspicion score. Indeed, based on extensive previous literature showing associations between both ADC value and MRI detection with Gleason score [17–20], MRI would have been expected to be more reliable in estimating volume for more aggressive tumours and when recording volume on the ADC map. We note, however, that the previously mentioned studies demonstrating the impact of tumour histological architecture on MRI characteristics focused mainly on the impact on tumour detection rather than on volume estimation [15,16], and it is possible that improved detection of the more aggressive lesions does not directly translate to more accurate volume prediction. In particular, the ADC map was shown to be exquisitely sensitive to the presence of areas of solid tumour growth, with this histological feature more frequently present in higher grade tumours, having a very high odds ratio for lesion detection of 37.6 [15]. We speculate that in more aggressive tumours, these areas of solid tumour formation within the overall tumour margins manifest as clear dark regions on the ADC map, to which the radiologist's attention was directed when estimating lesion volume. This process inherently excluded from volume estimation on MRI any surrounding non-solid lower grade regions, which would be less conspicuous on imaging. Conversely, lower grade lesions, having a smaller component of solid tumour growth, will not have such a conspicuous intra-tumoural abnormality on the ADC map, leading to placement of a broader region of interest in the region of the tumour and resulting in larger volume estimate. This concept could be further explored by direct comparison of MRI findings and pathological characteristics in intra-tumoural sub-regions exhibiting distinct histological features. It is also possible that the sensitivity of T2WI to various benign processes such as inflammation and post-inflammatory atrophy contributed to the apparently larger volumes obtained for T2WI than for ADC.

It is interesting to note that there was a small subset of patients in our cohort in whom the volume predicted on MRI was larger than that obtained from histopathology. These were

mainly small tumours with a low MRI suspicion score. Our earlier discussion suggests that these may have included tumours lacking solid tumour growth that confounded reliable volume prediction on MRI; thus, it remains possible that such small low-suspicion lesions can be adequately treated without inclusion of a much larger treatment zone compared with the MRI finding. If validated, this observation could be useful for avoiding unnecessary increases in the duration and complexity of ablation procedures.

The present study has a number of limitations. It was a retrospective study with a relatively small number of patients. In addition, while we provide estimates of the degree of underestimation of tumour volumes using MRI, it is important to note that these tumours are frequently not spherical in shape, such that the extent of underestimation is likely to vary between different directions. Although DCE imaging was viewed when approximating lesion locations, contours were not placed on DCE imaging, given this sequence's lower spatial resolution and relative lack of technical standardization between centres in terms of acquisition and post-processing. In addition, in our experience, tumour sizes are generally measured on T2WI or DWI in clinical practice [3]. Lastly, variability in estimates of tumour volume between radiologists was not assessed.

In conclusion, estimates of the volume of known prostate tumours using MRI tended to substantially underestimate actual tumour volumes, with wide variability in terms of the extent of this underestimation across individual cases. The underestimation was more pronounced on the ADC map than on T2WI, as well as for tumours with a higher Gleason score and higher MRI suspicion score. These findings have implications for efforts to use MRI to guide risk assessment in candidate selection and choice of treatment of PCa. Future studies may explore the utility of our findings to define a volume surrounding the MRI-based lesion to be covered by targeted therapy.

Acknowledgments

We would like to acknowledge Artem Mikheev for his work on the co-registration process. Funding was received from the Joseph and Diane Steinberg Charitable Trust, an Association Française d'Urologie grant (bourse de l'AFU 2012) and grant 1UL1RR029893 from the National Center for Research Resources, National Institutes of Health.

Conflict of Interest

J.L.N, C.O., H.R., F.-M.D., J. M. and A.B.R. have nothing to disclose. S.S.T. is a consultant for GTX, Healthtronics and Bayer, speaker for Janssen, and has royalties from Elsevier, but has no direct financial conflict of interest.

References

1 **Jager GJ, Ruijter ET, van de Kaa CA et al.** Local staging of prostate cancer with endorectal MR imaging: correlation with histopathology. *AJR Am J Roentgenol* 1996; 166: 845–52

2 **Villers A, Puech P, Mouton D, Leroy X, Ballereau C, Lemaitre L.** Dynamic contrast enhanced, pelvic phased array magnetic resonance imaging of localized prostate cancer for predicting tumor volume: correlation with radical prostatectomy findings. *J Urol* 2006; 176 (6 Pt 1): 2432–7

3 **Mazaheri Y, Hricak H, Fine SW et al.** Prostate tumor volume measurement with combined T2-weighted imaging and diffusion-weighted MR: correlation with pathologic tumor volume. *Radiology* 2009; 252: 449–57

4 **Ponchietti R, Di Loro F, Fanfani A, Amorosi A.** Estimation of prostate cancer volume by endorectal coil magnetic resonance imaging vs. pathologic volume. *Eur Urol* 1999; 35: 32–5

5 **Coakley FV, Kurhanewicz J, Lu Y et al.** Prostate cancer tumor volume: measurement with endorectal MR and MR spectroscopic imaging. *Radiology* 2002; 223: 91–7

6 **Nakashima J, Tanimoto A, Imai Y et al.** Endorectal MRI for prediction of tumor site, tumor size, and local extension of prostate cancer. *Urology* 2004; 64: 101–5

7 **Turkbey B, Mani H, Aras O et al.** Correlation of magnetic resonance imaging tumor volume with histopathology. *J Urol* 2012; 188: 1157–63

8 **Sosna J, Rofsky NM, Gaston SM, DeWolf WC, Lenkinski RE.** Determinations of prostate volume at 3-Tesla using an external phased array coil: comparison to pathologic specimens. *Acad Radiol* 2003; 10: 846–53

9 **Orczyk C, Rusinek H, Rosenkrantz AB et al.** Preliminary experience with a novel method of three-dimensional co-registration of prostate cancer digital histology and in vivo multiparametric MRI. *Clin Radiol* 2013; 68: e652–8

10 **Hammerer P.** pT0 after radical prostatectomy: overtreatment for insignificant prostate cancer? *Eur Urol* 2004; 45: 35

11 **Oto A, Sethi I, Karczmar G et al.** MR imaging-guided focal laser ablation for prostate cancer: phase I trial. *Radiology* 2013; 267: 932–40

12 **Barentsz JO, Richenberg J, Clements R et al.** ESUR prostate MR guidelines 2012. *Eur Radiol* 2012; 22: 746–57

13 **Wysock JS, Rosenkrantz AB, Huang WC et al.** A prospective, blinded comparison of magnetic resonance (MR) imaging-ultrasound fusion and visual estimation in the performance of MR-targeted prostate biopsy: the PROFUS trial. *Eur Urol* 2013 (in press)

14 **Langer DL, van der Kwast TH, Evans AJ et al.** Intermixed normal tissue within prostate cancer: effect on MR imaging measurements of apparent diffusion coefficient and T2–sparse versus dense cancers. *Radiology* 2008; 249: 900–8

15 **Rosenkrantz AB, Mendrinos S, Babb JS, Taneja SS.** Prostate cancer foci detected on multiparametric magnetic resonance imaging are histologically distinct from those not detected. *J Urol* 2012; 187: 2032–8

16 **Bratan F, Niaf E, Melodelima C et al.** Influence of imaging and histological factors on prostate cancer detection and localisation on multiparametric MRI: a prospective study. *Eur Radiol* 2013; 23: 2019–29

17 **Verma S, Rajesh A, Morales H et al.** Assessment of aggressiveness of prostate cancer: correlation of apparent diffusion coefficient with histologic grade after radical prostatectomy. *AJR Am J Roentgenol* 2011; 196: 374–81

18 **Woodfield CA, Tung GA, Grand DJ, Pezzullo JA, Machan JT, Renzulli JF 2nd.** Diffusion-weighted MRI of peripheral zone prostate cancer: comparison of tumor apparent diffusion coefficient with Gleason score and percentage of tumor on core biopsy. *AJR Am J Roentgenol* 2010; 194: W316–322

19 **Turkbey B, Shah VP, Pang Y et al.** Is apparent diffusion coefficient associated with clinical risk scores for prostate cancers that are visible on 3-T MR images? *Radiology* 2011; 258: 488–95

20 **Hambrock T, Somford DM, Huisman HJ et al.** Relationship between apparent diffusion coefficients at 3.0-T MR imaging and Gleason grade in peripheral zone prostate cancer. *Radiology* 2011; 259: 453–61

Correspondence: Julien Le Nobin, Department of Urology, Hôpital Claude Huriez, CHRU de Lille, 1, place de Verdin, 59037 Lille cedex, France.

e-mail: julien.lenobin@gmail.com

Abbreviations: PCa, prostate cancer; T2WI, T2-weighted imaging; DWI, diffusion-weighted imaging; ADC, apparent diffusion coefficient; DCE, dynamic contrast-enhanced; 3D, three-dimensional; ReH, registered histology.

Partie 2 : Analyse de texture, proposition d'un score d'entropie multiparamétrique : détection et stratification du cancer de la prostate par l'IRMmp en situation prédiagnostique

L'analyse visuelle des différentes séquences de l'IRMmp en situation de prédiagnostique oriente vers la définition spatiale d'une cible biopsique. Les paramètres quantitatifs, l'ADC et les dérivés de la perfusion par modélisation pharmacocinétique, ont montré, pris séparément, un intérêt relatif pour la stratification de la maladie. L'analyse de la texture d'image(65), plus précisément d'un volume, permet entre autres d'explorer de manière quantitative des aspects complexes, non perceptibles à l'œil, d'une image discrète de manière indépendante de la nature de l'image, et donc de la séquence IRM. Ces aspects complexes peuvent potentiellement révéler des caractéristiques tissulaires sous-jacentes comme l'hétérogénéité d'une tumeur, de sa vascularisation(85). L'entropie de Shanon, dérivée de la théorie de l'information, se propose d'examiner de manière mathématique l'occurrence d'un événement, comme la fréquence de la valeur d'un voxel. Une entropie élevée traduit un état désorganisé et hétérogène. Les méthodes précédemment étudiées de recalage inter séquences couplées à une analyse de texture par l'entropie de lésion en 3 dimensions ont permis d'envisager un score quantitatif objectif potentiellement reflétant les caractéristiques tissulaires explorées par les séquences IRM et dérivés.

Après accord du comité local d'éthique (comité de protection des personnes nord-ouest III (ref : A14-D66-VOL.23), un total de 134 volumes d'intérêt (VOIs) ont été générés rétrospectivement à partir des données IRM de 20 patients consécutifs au moment des biopsies. Tous les patients ont eu une IRM à 1,5 T selon le protocole de routine (séquences pondérée T2, Diffusion avec génération de cartographie ADC-b50-b1000, Séquence dynamique pondérée T1 avec injection de contraste). Les VOIs comprenaient l'anatomie zonale segmentée, les zones périphériques et transitionnelles normales, les cibles biopsiques et les cancers. Le test de référence est la combinaison de biopsie systématisée en saturation avec des biopsies ciblées. L'entropie (E), comme analyse de texture d'ordre 1, est calculée et compilée comme un score multiparamétrique, Score d'Entropie SE définit comme SE= E ADC+ E Ktrans+ E Ve+ E T2WI. Les aires sous la courbe (AUC) sont obtenues pour la performance de détection de cancer significatifs (score de Gleason>6 et/ ou plus de 3mm de cancer sur une biopsie). Des modèles de régression logistiques sont effectués et comparés aux performances du SE. La corrélation au score de Gleason et à la longueur maximale de cancer (LMC) sont calculées respectivement avec les coefficients de corrélation de Spearman et Pearson.

Douze patients avec un PSA médian de 8,22ng/ml ont montrés du cancer. Le SE réalise des AUC respectives de 0,89 et 0,88 pour la détection de cancers significatifs parmi 34 Vois repésentant les cibles biopsiques et tous les Vois segmentés. Sous le meilleur seuil pour le SE de 16,61 NAT, la sensibilité est de 100% avec une valeur négative prédictive de 100%. Sous cette hypothèse, 52% des cibles de score 3 n'aurait pas été biopsiées. L'AUC du SE tend à être supérieure à chacun de ses composants pris séparément. Les modèles de régression logistiques n'améliorent pas significativement ces performances. Le cancer significatif (SE=17,96 ±0,72 NAT; IC

95%) est significativement plus élevé que le non-significatif (SE=15,33 ±0,76 NAT; IC 95%). Le SE corrèle positivement avec le score de Gleason (r_s =0,5683, p=0,033) et la LMC (ρ = 0,781; p=0,0009).

L'analyse de texture avec le Score d'Entropie présente dans cette étude pilote de hautes performances pour la détection et la stratification du cancer de prostate avec des implications potentielles pour sélectionner précisément les cibles biopsiques dérivées de l'IRM. Le suivi longitudinal de patient sous surveillance active est une application potentielle pour déterminer la progression de la maladie.

Se référant à :

"Prostate cancer heterogeneity: texture analysis of multiple MRI sequences for detection and stratification at time of biopsy"

Manuscrit soumis– Radiology

Clement Orczyk, Arnauld Villers, Henry Rusinek, Audrey Fohlen, Vincent Lepennec, Celine Bazille, Artem Mikheev, Myriam Bernaudin, Samuel Valable

Et

Annexe 1 : Protocole de recherche clinique enregistré au CPP Nord –Ouest A14-D66-VOL.23

Prostate cancer heterogeneity: texture analysis of multiple MRI sequences for detection and stratification at time of biopsy

Journal:	*Radiology*
Manuscript ID	Draft
Manuscript Type:	Original Research
Manuscript Categorization Terms:	Prostate < 5. STRUCTURES, Image Postprocessing < 2. MODALITIES/TECHNIQUES, MR-Imaging < 2. MODALITIES/TECHNIQUES, Biopsy/Needle Aspiration < 3. PROCEDURES, Adults < 1. SUBJECT MATTER, Urinary < 4. AREAS/SYSTEMS, Computer Applications-Detection/Diagnosis < 6. TOPICS, Tissue Characterization < 6. TOPICS

Prostate cancer heterogeneity: texture analysis of multiple mpMRI sequences for detection and stratification at time of biopsy

Purpose: To develop and test in a biopsy population a texture analysis score, entropy score, based on analysis of multiple MRI sequences and derivatives for detection and stratification of prostate cancer in view of selection of MRI targets for biopsy.

Material and methods:
Under ethical approval, 134 Volume of Interest (VOIs) were retrospectively generated from 20 consecutive patients who underwent a clinical 1.5T mpMRI (T2WI, DWI with ADC map and DCE WI) at time of biopsy. VOIs comprised zonal anatomy segmentation, biopsy targets and cancer. Reference standard for correlation was cognitive targeted biopsy and systematic saturation biopsy. As Order 1 texture analysis, calibrated Entropy (E) for each imaging feature was computed and plotted as a multiparametric score defined as Entropy Score (ES)= E ADC+ E Ktrans + E Ve+ E T2WI. Area Under the Curve (AUC) calculations were performed for significant cancer (pattern 4 and/or more than 3 mm of cancer). Correlation to Gleason Score (GS) and Maximum Cancer Length (MCL) were calculated using Pearson and Spearman correlation coefficient.

Results: Cancer (GS 6- 8) was found in 12 of the 20 patients with a median PSA of 8.22ng/ml. ES performed respectively an AUC of 0.89 and 0.88 for detection of significant cancer among the 34 VOIs for targets and cancer and all segmented VOIs. Best estimated threshold for the ES of 16.61 NAT led to a sensitivity (Se) of 100% and negative predictive value (NPV) of 100%. 52% of score 3 targets wouldn't have been selected for sampling. Significant cancer (ES=17.96 ±0.72 NAT; CI 95%) showed a significant higher ES than non-significant cancer (ES=15.33 ±0.76 NAT; CI 95%)). ES correlated with Gleason Score (r_s =0.5683, p=0.033) and MCL (ρ = 0.781; p=0.0009).

Conclusion: Texture analysis with ES performed high performances for detection and stratification of significant prostate cancer in this pilot biopsy population with potential to select accurately MRI targets for biopsy.

1. Introduction:

Prostate cancer is a heterogeneous challenging disease. While current diagnostic strategy based on PSA dosage and random sampling of the gland using transrectal ultra sound (TRUS) biopsy is known to lead to over diagnosis and subsequent overtreatment(1), it remains the second cause of death of cancer in Western countries(2). Therefore, newer diagnostic strategies focuses in detecting so called "clinically significant disease"(3,4).

Modern imaging with multiparametric MRI (mpMRI)(5) demonstrated its ability to detect significant prostate cancer and rule out significant disease as presented in the report of the prospective multicentric PROMIS trial recently published (6). Potential application implies in using mpMRI as a triage test to trigger further biopsy, which can be targeted on a specific area(7–9). Selecting patient for a biopsy needs robust and reproducible high negative predictive value of a test, without compromising sensitivity. Interpretation of prostate mpMRI requires expertise and some standardization in reporting aims to overcome the inter observer variability. Performances are highly variable among the different value of the visual score either using Lickert or PIRADS 2 scale(10). Large proportion of the MRI lesion are reported as indeterminate (3/5), up to more than half of the lesion(11). Quantitative parameters potentially offer alternative to visual scoring and even showed some correlation with aggressiveness of the disease. Specifically, Diffusion Weighted Imaging (DWI) through Apparent Coefficient of Diffusion (ADC) showed some correlation with Gleason Score(12–14) and cellularity. Recent report (15) remind the significant value of parameters for DCE, specifically the Time to Peak, aside analysis of the ADC map. Pharmacokinetic (PK) models which link contrast agent concentration to time-curve, like the Toft model(16), permit elaboration of PK quantitative parameters and their visualization through 3D parametric maps. PK parameters, like the transfert constant (Ktrans) are reported to be higher in prostate carcinoma(17,18), linked to micro vascularity (19)(20). However, those parameters are limited by substantial variability in absolute values even in the same data set using different computing methods(18). Therefore, threshold to predict nature and aggressiveness is even more challenging to establish among different institutions and imagers.
Radionomics is a process which intends to extract numbers of quantitative features and then maximal information from standard of care images(21) using image processing. Purpose is to increase power of decision making models. Prostate mpMRI is a model where Radionomics can find some application because of the complexity of clinical answer awaited from the scan: not only purely detection of cancer but also stratification, prognosis and even treatment planning. We propose in this work to apply texture analysis(22,23), specifically Entropy, as a component of Radionomics, to routine 1.5T mpMRI realised at time of biopsy. Entropy, from Shannon's definition(24), is an order 1 texture analysis(21,23) reflecting heterogeneity of some signal. A higher entropy will denote a higher frequency of different signal values, representing the unpredictability of the intensity of the metric within the tissue. Entropy already shown some potential use applied to some component of mpMRI for prostate cancer detection(25,26), stratification(27) and prognosis(28).

Aside quantitative mpMRI parameters, we propose to develop and investigate whole lesion 3D entropy as a new multiparametric approach to build some tool for decision making in selection of mpMRI lesion to biopsy and stratification of the disease.

2. Material and Methods:

a. Population

Under local ethic committee approval, we analysed the data of 21 consecutive patients referred for suspicion of prostate cancer to a single urologist in 2014. The sample size was calibrated to demonstrate significant difference in the value of Ktrans between cancer foci and benign tissue. Patients underwent mpMRI prior biopsy except those with suspicious of high risk disease. All patient underwent multiparametric MRI (T2WI, DWI with generation of ADC map and DCE WI) of the prostate at 1.5T using a pelvic phase array and a whole body clinical system (Siemens Magnetom Avanto), details of sequences acquisition are in Table 1.

b. MRI reporting and generation of biopsy targets:

Two radiologists with 6 and 3 years experiences in prostate mpMRI interpretation reported the scans according to a Likert scale(29) from 2 to 5 as PIRADS 2 was not available at the start of the study. All sequences were used to allocate the score, without appreciation of quantitative value for ADC. After review of images with the senior urologist performing the biopsy, a map of 36 ROIs (30) was issued before the procedure. Areas found to be suspicious lesions and in the trajectory of systematic sampling were not sampled twice, but identified as MRI target. Systematic Saturation biopsy and targeted biopsy were the reference standard.

c. Transrectal ultrasound guided biopsy

All patients underwent subsequent transrectal ultrasound guided biopsy as per local protocol which implied a saturation TRUS biopsy for PSA under 15ng/ml with a 22 cores template, as posterior sampling with 4, 4 and 3 cores from base to apex for each lobe. In case of suspicious lesion at mpMRI prior biopsy, targeted biopsies were performed under cognitive registration by a senior urologist trained to this technique. Each core was labelled and inked in a different pot. Targeted biopsy followed the same process and were performed prior systematic sampling. A senior uro-pathologist reported the biopsy. A drawing reporting location and numbering of the cores was issued for each patient and sent to pathology. Systematic biopsy TRUS biopsy combined with targeted biopsy corresponds to the reference standard.

d. Biopsy-mpMRI correlation:

Biopsy and MRI maps were compared in consensus to establish concordance leading to true positive, false positive, false negative and true negative MRI regions. To be considered as true positive the MRI lesion had to be in the same sextant as positive biopsy for cancer. A positive histology for cancer from a target core conferred a positive status to the whole lesion.

e. Image processing:

Image processing is illustrated in figure 1.

i. Modelling DCE using pharmacokinetic Toft model:

We used an in house developed software (Firevoxel, New York University, https://wp.nyu.edu/firevoxel), already used in other organs to compute pharmacokinetic models from 4D imaging (31,32), to generate maps derived from the Toft model. The two parameters were the Transfert Constant (Ktrans in ml/min) and Fraction of extracellular extravascular space (Ve, no unit). The input function, Arterial Input Function (AIF), was patient specific and contrast media concentration was approximated (see Appendix 1 for processing PK model).
Prior to computation of the pharmacokinetic model, the DCE sequence was registered in 4D to avoid motion artefacts in the resulting quantitative maps using the built-in algorithm of the software platform(33).

ii. Inter sequence image registration and delineation of volume of interest (VOI):

In order to investigate the same volume of prostate across the different sequences, we registered ADC map and DCE-derived maps (Ktrans and Ve) to the T2WI space, using a validated method for prostate(34) based on Mutual Information. As a result, all quantitative maps were aligned in the anatomical reference space (T2WI). This allowed direct comparison of the parameters without bias due to delineation.

Volume of interest (VOI) were manually segmented within the platform by an individual trained across datasets of prostate mpMRI-histology correlation and performing image guided procedure base on mpMRI. The different VOIs extracted from the zonal anatomy were the prostate (excluding seminal vesicle), the peripheral zone (PZ), the transition zone & anterior fibromuscular stroma (TZ). Patient related VOIs were the biopsy targets. According correlation of the biopsy results with MRI, normal peripheral zone (nPZ) and benign prostate hyperplasia nodule (BPHn) were also delineated. To be considered as BPHn, part of the nodule had to be at the distance inferior to 17mm from posterior capsule at mpMRI, representing the field of the systematic TRUS sampling.

As a results a set of VOIs at MRI was generated for: prostate, PZ, TZ, nPZ, BPHn, target (if any) and cancer (if present).

iii. *Texture analysis*:

Texture analysis was computed from the VOIs as a 3D assessment using a statistical analysis of the histogram(22,23,26), known as order 1 analysis.

We firstly verified interpatient consistency of histograms for each quantitative parameter using direct visualization of normalized histogram (see appendix 2 for methods and results).

Order 1 analysis comprised the computation of the entropy which is the variation in the

distribution of the voxel value. Increased entropy indicates a higher unpredictability of the value of the parameter. This reflects the heterogeneity of the signal. This was directly computed for the whole lesion in 3D by the in-house software according the following equation based on Shannon's theory of information(24) :

$$Entropy = -\sum(\frac{h[i]}{\mathrm{N}} \times \log \frac{h[i]}{\mathrm{N}})$$

where $h[i]$is the bin width of the histogram and N the number of voxels included in the analysis.

The computation entropy has been calibrated to sample the relevant information from a 0.2cc lesion, as considered as the minimum volume of significant disease(3) when Gleason pattern 4 is identified. Methods of calibration is detailed in Appendix 3.

This allowed to analyse the information with the same accuracy across the different sequences independently of the absolute value of voxels for a given sequence.

It has to be noted that the entropy unit is NATural unit of information (NAT). The entropy for each parameter is expressed with the same unit. This allows mathematical operation like addition of the entropy value between parameters.

We propose to investigate further an Entropy Score (ES) to represent quantitatively characteristics of a volume in the same manner the PiRADS 2 score is built on a multiparametric approach.

ES for a volume v is define in the present work as

$$ES(v) = E^{ADC}(v) + E^{Ktrans}(v) + E^{Ve}(v) + E^{T2WI}(v)$$

Texture analysis of Order 1 of was completed by the mean, median, standard deviation and interquartile range and computation of Kurtosis (K) and Skewness(Sk) (see appendix 4 for details of computation).

f. Statistical analysis:

Statistical analysis was performed by using R software *(http://cran.r-project. org).*

i. <u>Descriptive analysis:</u>

For each category of VOIs, descriptive statistics are calculated for each parameter either quantitative (ADC, Ktrans, Ve) or derived from the histogram analysis (E, Sk, K) for the same MRI parameters with addition of T2WI.

ii. Intra patient analysis:

The quantitative parameters and derivative metrics were first tested for normality using the Shapiro-Wilk normality test. In case of normality, a Student-T test for paired data was performed to compare the values of cancer VOIs to the matching normal tissue (either nPZ or BPHn depending of the zone of origin of the tumour). In case of non-normal distribution, non parametric Wilcoxon test was performed.

iii. Inter patient analysis:

We used a variance analysis test of Friedman for paired data to assess if the tested parameters were independent for a given type of VOI.

Performances were assessed at two levels of analysis. First (A) considered all VOIs except the whole prostate, whole PZ and whole TZ. The second (B) considered only Targets and Cancer VOIS.

For continuous data and Entropy score at the two aforementioned level of analysis, ROC curves were generated and AUC calculated (*pROC* package) in view of detection of significant prostate cancer defined as the presence of Gleason pattern 4 at histology and/or more than 3mm cancer on a single core(3). Comparison of the AUC of ES was carried out against each ES component taken individually.

Logistic regression (LR) modelling was performed for both A and B analysis including each single entropy parameter and promising raw quantitative value for Ktrans, Ve and ADC. Performances of the model were assessed using ROC curves for both A and B analysis. The AUC of the models and ES were compared.

Sensibility, specificity, positive and negative predictive values are also calculated for the LR models and the ES for both level of analysis using best calculated threshold from the ROC.

Correlation of ES with Gleason score was performed using the Spearman coefficient. Correlation of ES with the Maximum Core Length was assessed using the Pearson coefficient.

All statistical tests were conducted at the two-sided 5% significance.

1. Results:

a. Patients:

From the 21 patients enrolled, one patient found to be ineligible due to DCE WI issues.

From the 20 remaining patients, prostate cancer was detected among 12 patients following those biopsies either form systematic or targeted cores. Patient characteristics are shown in Table 2. Median time between MRI and biopsy was 35 days. The total number of targets was 28 of which 7 were positive for cancer. Targets were score 2, 3, 4 and 5 in respectively 1, 19, 5 and 3 cases. Detection rate of any cancer was 0%, 2/19 (10,5%), 2/5 (40%) and 3/3 (100%)

for the same range of score. All targets from MRI were outlined in the post processing software.

b. Segmentation of VOIs after MRI-histology correlation:

After correlation with histology findings, 15 cancer foci were delineated on MRI after fusion of the sequences and maps in the T2WI space. Prostate, PZ, TZ were segmented in all cases. Two patients did not present either normal PZ or TZ either at biopsy or MRI findings according our definition. Therefore 19 nPZ and 19 BPHn VOIs were generated.

c. Image processing:

In all cases, the computation of both Ktrans and Ve maps were possible using patient specific AIF. The registration of functional maps to the T2 WI was effective in all 20 cases. Histogram generation and analysis were available for all the 134 VOIs.

d. ***Results of Intra patient comparison****:*

i. *Descriptive results of the MRI parameters across zonal anatomy and VOIs*

The descriptive results of quantitative parameters and derived metrics are plotted in table 3. This summarizes the value parameters for different zones of the prostate anatomy as well as the generated VOIS.

ii. *Cancer vs normal prostate tissue for a single parameter:*

There was significance difference in median ADC value between cancer VOIs and normal paired tissue (p=0.005), which was not found for the entropy of ADC (p=0.56).

There was a significant difference for both median Ktrans and Ve values between cancerous (0.74 ml/min; 0.53) VOIs and normal paired tissue (0.32ml/min; 0.45) (p=0.007; p=0.009).

Significant difference was also found E Ktrans and E Ve for the same paired volume (p=0.0005; p=0.05).

Nor SK or K for those three quantitative data were significantly different for the same VOIs.

e. ***Entropy Score assessment in zonal anatomy****:*

Table 4. shows the different values taken by the Entropy Score for different VOIs. The whole prostate showed the highest Entropy Score with a mean value of 18.31 NAT. Both whole PZ and whole TZ showed the same mean ES value of 17.96 NAT. This finding contrasts with the significant difference between normal PZ and BPH nodule (15.58 vs 16.26, p=0.04).

f. Entropy for targeted VOIs:

i. Entropy per parameter:

None of E ADC, E Ktrans, E Ve, E T2WI individually reached significant difference between positive and negative targets for significant cancer. There was a trend for Entropy of positive targets to be higher than negative as shown in box plot in figure 2.

ii. Independence of Entropy values across the different MRI parameters:

The Friedman test was conducted for paired data within the target VOIs, comprising E ADC, E Ktrans, E T2WI, E Ve. It reached significance with p=0.0005, reflecting that each set of entropy value for one parameter formed an independent population. This further allows a meaningful entropy score as the entropy of each parameter is not related to others for the targeted VOIs.

g. Detection of significant cancer

i. First level Analysis (A): all VOIS (nPZ, nBPH, Targets, Cancer):

Among those VOIs, there was a significant difference (p=0.0009) in ES between positive VOIs for significant cancer (mean 17.96± 0.72 NAT; CI 95%) and those negative (mean 16.06 ± 0.31 NAT; CI 95%).

Receiver Operating Curves (ROC) were built for the ES, entropy and mean value of each individual MRI parameter for detection of significant cancer as previously defined. ROC curves were generated and AUC calculated from a total of 70 VOIS from targeted, cancer and normal tissue (figure 3). AUC Results and comparison are summarized in table 5.

ES achieved an AUC of 0.88 (0.76, 0.97; 95% CI) and was higher than any other single parameter. ES AUC was significantly higher than E T2WI AUC and mean Ktrans AUC. AUC for mean ADC was higher than the one of E ADC without reaching significance (0.87 vs 0.76 p=0.34) considering that selected normal tissue has been included at this level of analysis. Best threshold for ES was 16.69 NAT with Sensitivity 100% (95% CI 63.06 – 100) of and Specificity of 69.35% (95% CI 56.35 - 80.44) . The diagnostic accuracy was 72.86 (95% CI 60.9 - 82.8). The Youden's index was 0.69 (95% CI 0.19 - 0.80)

The logistic regression model using E Ktrans, E Ve, E T2WI, E ADC, mean ADC and volume reached an AUC of 0.93 (0.84-0.99), with no significant difference to the AUC of ES (p=0.15). Diagnostic accuracy and Youden index of the model were respectively 88.57% (95% CI 78.72 - 94.93) and 0.76 (95% CI 0.25 - 0.95).

ii. Second level Analysis (B): Target and Cancer VOIs:

There was a significant difference (p=0.001) in ES between VOIs positive for significant cancer (mean 17.96± 0.72 NAT; CI 95%) and those negative (mean 16.12 ± 0.44 NAT; CI 95%).

The same ROC curves (figure 4) were built for the 33 VOIs representing only targets (score 3 and above) and cancer. The AUC for the ES and detection of significant cancer was 0.89 (0.76, 0.99; 95% CI), with a trend to be higher than other E or quantitative value for any other parameter. Significant difference was observed with the mean Ve. Oppositely to analysis A, AUC for E ADC was higher than the AUC for mean ADC (0.81 vs 0.78); non-significant, when considering only cancer and targets. Results are summarized in table 5.

Best threshold was found for 16.61 NAT, with sensitivity of 100% and specificity of 72%.

Using this threshold of 16.61 NAT for detection of significant prostate cancer, we calculated a negative predictive value (NPV) of 100%, Positive Predictive Value (PPV) of 53.3%. 18 targets over the 33 were under this threshold, none of them harbouring significant prostate cancer. An estimated detection rate for score 3,4 and 5 targets would have been respectively 52%, 100% and 100% and resulting in avoiding to sample 54% of the VOIs. The diagnostic accuracy was 78.79 % (95% CI 61.09 - 91.02). Youden index of ES was 0.72 (95% CI 0.14 - 0.88).

The logistic model using E Ktrans, E VE, E T2WI, mean ADC reached an AUC of 0.93 (0.80-1), with no significant difference to the AUC of ES (p=0.4). Diagnostic accuracy and Youden index of the model were respectively 63.64% (95% CI 47.77 - 77.59) and 0.46 (95% CI 0.12 - 0.74).

Table 6 summarize diagnostic performances for ES and regression model for both A and B analysis.

h. Stratification of prostate cancer

Significant cancer (ES=17.96 ±0.72 NAT; CI 95%) showed a significant higher Entropy Score than non-significant cancer (ES=15.33 ±0.76 NAT; CI 95%)).

The Pearson's correlation coefficient of the ES of cancerous VOIs with the maximum cancer core length found to be positive with $\rho = 0.781$ (p=0.0009).

The Spearman's correlation coefficient of the ES of cancerous VOIs with matching biopsy Gleason score was also positive with $r_s = 0.5683$ and p=0.033.

Discussion:

In this pilot study, the results showed that the ES, as a combined texture analysis of multiple MRI sequences, could accurately select biopsy targets established on mpMRI reading for detection of significant cancer at time of biopsy in the context of a routine set up of an MRI scanner. ES presented potential in stratification of the disease by positively correlating with Gleason Score.

There is a growing interest in the use of radionomics to mine the amount of information that medical imaging presents(21,35) to increase precision in diagnostic, especially in oncology. Our report illustrates the potential of radionomics by the use of standard of care images to analyse a whole lesion in 3D.

This study presents original aspects in the chosen biopsy population and the unified analysis of texture of three different sequences, incorporating DCE WI, within one score in the purpose of selection of MRI lesion for biopsy.

Our choice of a biopsy population permits to avoid the bias of selection of patient undergoing radical prostatectomy, and inclusion of patient potentially eligible for active surveillance and without the diagnosis of prostate cancer. This authorizes to test our model in a situation that face clinicians.

The compilation of entropy among the different sequences was permitted by a combination of technical aspects. Corner stone of ES, calibration of entropy for all sequences to a 0.2cc lesion corresponds in this study to a solution to the scaling problem in adequation to the texture model(22) for prostate MRI. The score is a simple addition of the entropy of different parameters. Even calibrated E from other imaging modality could possibly be added and extend performances.

The advantage for texture analysis was more prominent for the DCE derived PK parameters. E Ve and E Ktrans performed better than the mean Ve and mean Ktrans on match paired AUC comparison at the two levels analysis A and B, including all normal tissue or targets only. There was an increase of the AUC for both parameters, respectively 0.63 to 0.86 for Ve and 0.68 to 0.80 for Ktrans. As a hypothesis, entropy might capture chaotic neoangiogeneis and underlying genetics process among the whole lesion, not revealed by the raw quantitative value. Also, microvessel density has been described to be linked with prognosis(36).

ADC did not follow the same trend. AUC for mean ADC was higher when considering all category of tissue (0.87) than in targets and cancer (0.78). This was reverse for the E ADC (0.76 vs 0.81). This illustrates the high capability of ADC map to direct visual detection of suspicious lesion as the main driver of the PIRADS 2 scoring system. However, mean ADC performances decrease for selection of lesion with significant cancer among other lesions as previously described(11).

The entropy score yield very good performances for detection of significant cancer among targets with an AUC of 0.89. The optimal threshold of 16.61 NAT achieved a sensitivity of 100% and a NPV of 100%. The ES presented higher performances than the multiple regression model we computed based on the same data sets when considering those two parameters. The AUC between ES and the regression model were in the same range and not significantly different, even if the models reached an high AUC of 0.93 in A and B analysis. This is an internal validation of the ES. ES also has the advantage to be a standard addition of quantitative values with the same unit, providing a potential user friendly feature in the radiologist workflow and being independent of the population used to train the model.

Previous studies investigated the potential role of texture analysis in detection of significant cancer but in the purpose to differentiate grade of tumor, not selecting targets. Most of

them used radical prostatectomy specimen as reference standard which may have induced bias related to the population.

Comforting the potential value of radionomics, Vignati et al.(37) found excellent AUC of 0.96 for a texture parameter based on T2WI alone for differentiating Gleason 6 and >6 in a radical prostatectomy cohort. Those parameters were not tested for detection of clinically significant large volume Gleason 6 lesion or confronted to non-cancerous VOIs. This limit translation of those results into a pre diagnosis setting.

In a recent report, Ginsburg et al.(38) trained a model based on numerous radionomics features in multi-institution data for detection of cancer on a voxel basis. Their maximal AUC of 0.71 was lower than our results and based on a single sequence analysis. We need also to recall that all lesion are not detected in all sequences because of some different histology features(39), potentially altering mono sequential approach. Even if different from a computer assisted diagnosis system, ES could be incorporated into such automated analysis.

Rosenktrantz et al.(11) applied different features of Order 1 to discriminate lesion with Gleason >6 to others among Likert 3 lesions. Entropy of ADC alone failed to discriminate those.

Using visual scoring, Tan et al(40) described an AUC of 0.82 for detection of significant disease by mpMRI in a meta-analysis.

Fütterer et al. reported in a meta-analysis a variability of NPV form significant disease from 63% to 98%, depending of the definition of significance disease and MRI score considered.

Advantage of targeting biopsy based on mpMRI has been reported several times(7,41). Panebianco et al. (42)already reported the advantage of targeted biopsy combined to random sampling over a solely systematic approach in an randomized control trial.

The PROMIS trial reported a NPV of 72% and sensitivity of 87% for detection at transperineal mapping biopsy of cancer according UCL definition 2 (≥ Gleason (3+4) or Gleason 6 MCL > 4mm (43)), which is closer to the definition we used than UCL definition 1(43). Also, there was agreement of 80% (kappa statistic of 0.5) for detection of significant cancer between radiologists. Rosenkrantz et al. reported variability in the same range of PIRADS 2 scoring among 6 mpMRI expert radiologists(44). This variability might be overcome by using a quantitative score, like the ES. As per the definition of the Entropy, it is a little sensitive to volume delineation. The value of entropy is more sensitive to the occurrence of a voxel value rather than to the value of the voxel itself, which would affect the mean for example. However, the PROMIS trial reported the potential value of mpMRI to avoid biopsy in 27% of men in a primary diagnostic setting using visual scoring.

ES could further help in discriminating those patients. The potential value of the ES might consist in selecting the targets to be biopsied and therefore rule out patient from biopsy. The high negative predictive value would avoid to unnecessary sample some lesion without missing the clinically significant cancer with a high sensitivity. ES would fulfill in this matter the role of radionomics tools in decision making.

The significant correlation of the Entropy Score from all cancerous foci with the biopsy

Gleason Score was positive at r_s = 0.5683 (p= 0.03). This is stronger correlation than reported inverse correlation of ADC of r=– 0.376 by Oto et Al.(45) or r=– 0,39 by Verma et al.(46). The Gleason score and even more the presence of volume of pattern Gleason 4/5 is an important driver of the oncologic outcome after radical treatment as reported recently by Choy et al.(47) using the update grading system from ISUP in 2014(48). In this report, the correlation between the systematic biopsy Gleason score and the radical prostatectomy specimen was relatively weak (r^2=0.32). MRI targeted biopsy might offer the possibility to overcome this degree of uncertainty(49).Furthermore, entropy of ADC for a whole lesion was found to be an independent predictor of biochemical failure by Rosenkrantz et al(28). ES might have a role in the stratification of the disease, interrogating the whole lesion and limiting the bias of sampling.

Finally, longitudinal analysis of ES in an active surveillance population might be of interest to detect progression of cancer leading to change in management. There is already an increased interest in using mpMRI in this indication(50).

Our study has limitations. The number of subject is relatively small even if some statistical differences has been found either for quantitative values or ES. This is a mandatory to validate those preliminary findings in a larger cohort before translation into clinical trials and multi users setting. The ideal population would be patients referred for primary diagnosis who underwent mpMRI before a template mapping biopsy. A study across different scanners, institutions and users is also a necessary step in the validation process of radionomics findings as imaging biomarker(51) .
Also mpMRI did not include high b value sequence, DCE had a low temporal resolution and was acquired at 1.5T. Some refinements might increase the accuracy of ES. However, the very good performances with this recent MRI set up are encouraging for widespread the use of radionomics. As a limitation but also advantage, the potential work flow relies on radiologists to determine which lesion to interrogate. Variability could be observed in this matter but also it permits radiologist to adapt their report to clinical situations.

To conclude, we firstly report an objective quantitative score based on texture analysis of three different MRI sequences. The entropy score offers the potential of high performances to select lesion to be targeted and stratification of prostate cancer before any biopsy. Those findings must be confirmed in larger cohort.

Tables:

Table 1. Parameters of Multiparametric MRI Sequences:

Sequences	Field of view (mm)	Matrix	Slice thickness (mm)	Flip angle	TE/TR (ms)	NSA	Temporal resolution
T2-weighted TSE							
axial	260-260	448-358	4	150	121/5100	3	
sagittal	260-260	448-358	3.5	144	144/5010	2	
coronal	260-260	448-358	3.5	137	123/5010	2	
Functional							
DWI							
b50	200-200	126-126	4	90	104/4000	9	
b1000	200-200	126-126	4	90	104/4000	9	
T1 TSE	260-260	320-272	6	180	21/567	2	
DCE - T1 GRE VIBE FS	230-230	160-136	4	25	4.76/7.5	1	15s

Table 2. Included Patients characteristics

Number patients	20
Median age (range) years	65 (55-74)
Median PSA (range) ng/ml	8.22 (4.54-52.72)
Number of patients with positive biopsy	12
Number of patients under active surveillance	2
Number of biopsy naive patients	14
Number of patients with previous negative TRUS biopsy	4
Number of high risk patients	2
Number of patient mpMRI naive	20
Maximum Gleason score per patient	
Gleason 6 (3+3)	8
Gleason 7 (3+4)	3
Gleason 8 (4+4)	1
Median number of target per patient (range)	1.5 (0-3)
Median maximum target score per patient (range)	3 (3-5)
Number of positive targets for any cancer (n significant cancer)	
score 3/5	2/19 (0)
score 4/5	2/5 (2)
score 5/5	3/3 (3)
Mean Maximum core length (range) mm	5.5 (1-17)

Table 3. Descriptive results of MRI quantitative parameters and texture metrics by MRI feature and type of VOI

		Prostate	Peripheral zone	Transition zone	BPH	normal PZ	Cancer	Target
ADC	mean mm.s-2	1157	1179	1143	1271	1476	1096	1111
	median mm.s-2	1159	1208	1131	1271	1411	1115	1076
	SD	163	177	170	188	207	231	186
	mean Kurtosis (+/- SD)	0.50 (1.62)	0.52(0.92)	1.01 (1.44)	-0.2(0.53)	0.27 (1.48)	0.30 (1.19)	0.43 (1.12)
	Skewness (+/- SD)	-0.36 (0.47)	-0.54 (0.32)	-0.17 (0.44)	0.26 (0.37)	-0.45 (0.69)	-0.17 (0.70)	0 (0.04)
	mean Entropy (+/-SD)	4.99 (+/-0.11)	5.05 (+/- 0.19)	4.88 (+/- 0.1)	4.37 (+/- 0.22)	4.22 (0.32)	4.44 (0.38)	4.26 (0.30)

		prostate	peripheral zone	Transition zone	BPH	normal ZP	Cancer	Target
Ktrans	mean ml/min	0.67	0.61	0.66	1.17	0.61	1.04	0.92
	median ml/min	0.402	0.37	0.5	0.98	0.44	0.765	0.73
	SD	0.41	0.32	0.45	1.02	0.60	0.625	0.62
	Kurtosis	77 (113)	68 (99)	51.14 (37.59)	16.08 (2.58)	24 (44)	7.87 (15.80)	9.53 (18.84)
	Skewness	5.56 (3.04)	5.56 (3.79)	4.66 (2.25)	2.29 (2.58)	3.01 (3.33)	1.91 (1.87)	1.87 (2.08)
	Entropy	3.78 (0.55)	3.64 (0.50)	3.59 (0.58)	3.76 (0.71)	3.18 (0.60)	3.84 (0.70)	3.68 (0.60)

		prostate	peripheral zone	Transition zone	BPH	normal ZP	Cancer	Target
Ve	mean	0.52	0.46	0.52	0.51	0.44	0.55	0.51
	median	0.496	0.44	0.51	0.51	0.415	0.52	0.51
	SD	0.18	0.17	0.17	0.20	0.18	0.2	0.18
	Kurtosis	3.41 (4.23)	4.83 (4.16)	4.52 (5.94)	12.59 (22.05)	7.61 (12.61)	4.73 (9.68)	4.44 (9.68)
	Skewness	1.09 (0.87)	1.42 (0.74)	1.23 (1.05)	1.72 (2.09)	1.75 (1.42)	1.22 (1.29)	1.07 (1.19)
	Entropy	4.82 (0.70)	4.61 (0.79)	4.67 (0.84)	3.99 (0.84)	3.97 (0.78)	4.21 (0.81)	4.10 (0.70)

		prostate	peripheral zone	Transition zone	BPH	normal ZP	Cancer	Target
T2 WI	Kurtosis	0.80 (0.61)	0.06 (0.62)	1.27 (0.78)	0.69 (1.16)	0.13 (0.66)	1.40 (2.20)	0.81 (1.33)
	Skewness	0.68 (0.20)	0.34 (0.25)	0.72 (0.25)	0.64 (0.51)	-0.32 (0.47)	0.60 (0.69)	0.55 (0.50)
	Entropy	4.80 (0.24)	4.93 (0.19)	4.69 (0.19)	4.34 (0.32)	4.19 (0.20)	4.23 (0.26)	4.18 (0.23)

BPH : Benign Prostate Hyperplasia ; VOI Volume of Interest; ADC : Apparent Diffusion Coefficient; Ktrans: transfert constant; Ve: Fraction of extracellular extravascular space; T2 WI: T2 weighted imaging; SD standard deviation; PZ: peripheral zone

Table 4. Values of Entropy Score for different VOIS:

	Entropy Score			
Volume of interest (n)	mean	median	standard deviation	CI 95%
Prostate (20)	18.31	18.78	1.17	0.51
whole Peripheral Zone (20)	17.96	18.56	1.30	0.57
whole Transition Zone (20)	17.96	18.20	1.26	0.55
Normal Peripheral Zone (19)***	**15.58**	15.47	3.84	1.72
BPH nodule (18)***	**16.26**	16.38	5.30	2.45
Target (28)	16.31	16.31	1.22	0.45
Positive Target (5)*	**17.21**	16.87	1.00	0.42
Negative Target (23)*	**16.11**	15.88	1.19	0.50
Cancer (12)	16.93	16.81	1.59	0.90
Significant Cancer (8)**	**17.73**	17.40	1.23	0.85
Non-significant cancer (4)**	**15.33**	15.12	0.78	0.76

*p=0.035; **p=0.0025; ***p=0.04

BPH : Benign Prostate Hyperplasia ;

Table 5: AUC values and p value comparison for ES, E and raw quantitative value of each MRI features in A and B analysis (in bold significant difference):

ALL VOIS (A analysis)

	AUC (CI 95%)	p value to Entropy score AUC	p value AUC E vs mean
Entropy Score	0.88 (0.76, 0.97)	na	
Entropy Ve	0.86 (0.71, 0.98)	0.613	0.11674
Mean Ve	0.63 (0.40, 0.85)	0.071	
Entropy ADC	0.76 (0.55, 0.92)	0.093	0.3457
Mean ADC	0.87 (0.74, 0.97)	0.881	
Entropy Ktrans	0.80 (0.57, 0.94)	0.264	0.1394
Mean Ktrans	0.68 (0.46, 0.87)	0.045*	
Entropy T2 WI	0.64 (0.36, 0.87)	0.035*	
Age	0.59 (0.43, 0.73)	0.002*	
PSA	0.61 (0.33, 0.86)	0.030*	

Target and cancer (B analysis)

	AUC (CI 95%)	p value to Entropy score AUC	p value AUC E vs mean
Entropy Score	0.89 (0.76, 0.99)		
Entropy Ve	0.84 (0.67,0.98)	0.405	0.125
Mean Ve	0.59	0.052	
Entropy ADC	0.81 (0.60, 0.96)	0.241	0.831
Mean ADC	0.78 (0.59, 0.94)	0.308	
Entropy Ktrans	0.80 (0.55, 0.97)	0.288	0.435
Mean Ktrans	0.72 (0.47, 0.94)	0.138	
Entropy T2 WI	0.71 (0.43, 0.95)	0.132	
Age	0.59 (0.38, 0.78)	0.009	
PSA	0.62 (0.33, 0.90)	0.052	

ADC : Apparent Diffusion Coefficient; Ktrans: transfert constant; Ve: Fraction of extracellular extravascular space; T2 WI: T2 weighted imaging; E : Entropy; ES: Entropy Score; AUC: area under the curve; PSA : prostatic specific antigen; VOI: volume of interest

Table 6. Comparison of performances of the Entropy Score and Multi logistic regression models:

	A analysis All VOIs		B Analysis-Targets- Cancer	
	Entropy Score	Regression Model	Entropy Score	Regression Model
Sensitivity % (95% CI)	100 (63.06 - 100)	87.5 (47.35 - 99.68)	100 (63.06 - 100)	87.5 (47.35 - 99.68)
Specificity % (95% CI)	69.35 (56.35 - 80.44)	88.71 (78.11 - 95.34)	72 (50.61 - 87.93)	84.3 (63.92 - 95.46)
PPV % (95% CI)	29.63 (13.75 - 50.18)	50 (95% CI 23.04 - 76.96)	53.33 (26.59 - 78.73)	63.64 (30.79 - 89.07)
NPV % (95% CI)	100 (91.78 - 100)	98.21 (90.45 - 99.95)	100 (81.47 - 100)	95.45 (77.16 - 99.88)
Diagnostic Accuracy % (95% CI)	72.86 (60.9 - 82.8)	88.57 (78.72 - 94.93)	78.79 (61.09 - 91.02)	84.85 (68.1 - 94.89)
Youden index (95% CI)	0.69 (0.19 - 0.8)	0.76 (0.25 - 0.95)	0.72 (0.14 - 0.88)	0.72 (0.11 - 0.95)
AUC (95% CI)	0.88 (0.76, 0.97)	0.93 (0.84, 0.99)	0.89 (0.76, 0.99)	0.93 (0.82, 1.00)
p value for AUC comparison	0.16		0.32	

PPV: positive predictive value; NPV: negative predictive value; CI: confidence interval; AUC: area under the curve; VOI: volume of interest.

REFERENCES :

1. Andriole GL, Crawford ED, Grubb III RL, et al. Mortality results from a randomized prostate-cancer screening trial. New England Journal of Medicine. 2009;360(13):1310–1319.
2. Siegel RL, Miller KD, Jemal A. Cancer statistics, 2017. CA: A Cancer Journal for Clinicians. 2017;67(1):7–30.
3. Epstein JI, Walsh PC, Carmichael M, Brendler CB. Pathologic and Clinical Findings to Predict Tumor Extent of Nonpalpable (Stage T1 c) Prostate Cancer. JAMA: The Journal of the American Medical Association. 1994;271(5):368–374.
4. Stamey TA, Freiha FS, McNeal JE, Redwine EA, Whittemore AS, Schmid HP. Localized prostate cancer. Relationship of tumor volume to clinical significance for treatment of prostate cancer. Cancer. 1993;71(3 Suppl):933–938.
5. Dickinson L, Ahmed HU, Allen C, et al. Magnetic resonance imaging for the detection, localisation, and characterisation of prostate cancer: recommendations from a European consensus meeting. Eur Urol. 2011;59(4):477–494.
6. Ahmed HU, Bosaily AE-S, Brown LC, et al. Diagnostic accuracy of multi-parametric MRI and TRUS biopsy in prostate cancer (PROMIS): a paired validating confirmatory study. The Lancet. 2017;0(0)/journals/lancet/article/PIIS0140-6736(16)32401-1/abstract. Accessed January 20, 2017.
7. Haffner J, Lemaitre L, Puech P, et al. Role of magnetic resonance imaging before initial biopsy: comparison of magnetic resonance imaging-targeted and systematic biopsy for significant prostate cancer detection. BJU Int. 2011;http://www.ncbi.nlm.nih.gov/pubmed/21426475. Accessed March 24, 2011.
8. Kasivisvanathan V, Dufour R, Moore CM, et al. Transperineal magnetic resonance image targeted prostate biopsy versus transperineal template prostate biopsy in the detection of clinically significant prostate cancer. J Urol. 2013;189(3):860–866.
9. Wysock JS, Rosenkrantz AB, Huang WC, et al. A Prospective, Blinded Comparison of Magnetic Resonance (MR) Imaging–Ultrasound Fusion and Visual Estimation in the Performance of MR-targeted Prostate Biopsy: The PROFUS Trial. European Urology. 2014;66(2):343–351.
10. Weinreb JC, Barentsz JO, Choyke PL, et al. PI-RADS Prostate Imaging – Reporting and Data System: 2015, Version 2. European Urology. 2016;69(1):16–40.
11. Rosenkrantz AB, Meng X, Ream JM, et al. Likert score 3 prostate lesions: Association between whole-lesion ADC metrics and pathologic findings at MRI/ultrasound fusion targeted biopsy: Whole-Lesion ADC Metrics in Likert 3 Prostate Lesions. Journal of Magnetic Resonance Imaging. 2016;43(2):325–332.
12. Hambrock T, Somford DM, Huisman HJ, et al. Relationship between Apparent Diffusion Coefficients at 3.0-T MR Imaging and Gleason Grade in Peripheral Zone Prostate Cancer. Radiology. 2011;http://www.ncbi.nlm.nih.gov/pubmed/21406633. Accessed March 28, 2012.
13. Kobus T, Vos PC, Hambrock T, et al. Prostate cancer aggressiveness: in vivo assessment of MR spectroscopy and diffusion-weighted imaging at 3 T. Radiology.

2012;265(2):457–467.
14. Hoeks CMA, Vos EK, Bomers JGR, Barentsz JO, Hulsbergen-van de Kaa CA, Scheenen TW. Diffusion-weighted magnetic resonance imaging in the prostate transition zone: histopathological validation using magnetic resonance-guided biopsy specimens. Invest Radiol. 2013;48(10):693–701.
15. Hoang Dinh A, Melodelima C, Souchon R, et al. Quantitative Analysis of Prostate Multiparametric MR Images for Detection of Aggressive Prostate Cancer in the Peripheral Zone: A Multiple Imager Study. Radiology. 2016;151406.
16. Tofts PS, Brix G, Buckley DL, et al. Estimating kinetic parameters from dynamic contrast-enhanced T(1)-weighted MRI of a diffusable tracer: standardized quantities and symbols. J Magn Reson Imaging. 1999;10(3):223–232.
17. Langer DL, van der Kwast TH, Evans AJ, et al. Prostate tissue composition and MR measurements: investigating the relationships between ADC, T2, K(trans), v(e), and corresponding histologic features. Radiology. 2010;255(2):485–494.
18. Azahaf M, Haberley M, Betrouni N, et al. Impact of arterial input function selection on the accuracy of dynamic contrast-enhanced MRI quantitative analysis for the diagnosis of clinically significant prostate cancer: Impact of AIF on K^{trans} in PCa. Journal of Magnetic Resonance Imaging. 2015;n/a – n/a.
19. Oto A, Yang C, Kayhan A, et al. Diffusion-Weighted and Dynamic Contrast-Enhanced MRI of Prostate Cancer: Correlation of Quantitative MR Parameters With Gleason Score and Tumor Angiogenesis. American Journal of Roentgenology. 2011;197(6):1382–1390.
20. Ren J, Huan Y, Wang H, et al. Dynamic contrast-enhanced MRI of benign prostatic hyperplasia and prostatic carcinoma: correlation with angiogenesis. Clin Radiol. 2008;63(2):153–159.
21. Gillies RJ, Kinahan PE, Hricak H. Radiomics: Images Are More than Pictures, They Are Data. Radiology. 2015;278(2):563–577.
22. Depeursinge A, Foncubierta-Rodriguez A, Van De Ville D, Müller H. Three-dimensional solid texture analysis in biomedical imaging: Review and opportunities. Medical Image Analysis. 2014;18(1):176–196.
23. Castellano G, Bonilha L, Li LM, Cendes F. Texture analysis of medical images. Clinical Radiology. 2004;59(12):1061–1069.
24. Shannon C. A Mathematical Theory of Communication. 1948;27:379–423.
25. Wibmer A, Hricak H, Gondo T, et al. Haralick texture analysis of prostate MRI: utility for differentiating non-cancerous prostate from prostate cancer and differentiating prostate cancers with different Gleason scores. European Radiology. 2015;25(10):2840–2850.
26. Rosenkrantz AB, Triolo MJ, Melamed J, Rusinek H, Taneja SS, Deng F-M. Whole-lesion apparent diffusion coefficient metrics as a marker of percentage Gleason 4 component within Gleason 7 prostate cancer at radical prostatectomy. J Magn Reson Imaging. 2014;
27. Sidhu HS, Benigno S, Ganeshan B, et al. "Textural analysis of multiparametric MRI detects transition zone prostate cancer." Eur Radiol. 2016;1–11.
28. Rosenkrantz AB, Ream JM, Nolan P, Rusinek H, Deng F-M, Taneja SS. Prostate Cancer: Utility of Whole-Lesion Apparent Diffusion Coefficient Metrics for Prediction of Biochemical Recurrence After Radical Prostatectomy. American Journal of Roentgenology. 2015;205(6):1208–1214.
29. Rosenkrantz AB, Kim S, Lim RP, et al. Prostate Cancer Localization Using Multiparametric MR Imaging: Comparison of Prostate Imaging Reporting and Data System (PI-RADS) and Likert Scales. Radiology. 2013;
30. Barentsz J, Villers A, Schouten M. Reply to Letter to the Editor re: ESUR prostate MR guidelines. European Radiology. 2013;23(8):2322–2323.

31. Aronhime S, Calcagno C, Jajamovich GH, et al. DCE-MRI of the liver: Effect of linear and nonlinear conversions on hepatic perfusion quantification and reproducibility: DCE-MRI of the Liver. Journal of Magnetic Resonance Imaging. 2014;40(1):90–98.
32. Yamamoto A, Zhang JL, Rusinek H, et al. Quantitative evaluation of acute renal transplant dysfunction with low-dose three-dimensional MR renography. Radiology. 2011;260(3):781–789.
33. Chandarana H, Block TK, Ream J, et al. Estimating Liver Perfusion From Free-Breathing Continuously Acquired Dynamic Gadolinium-Ethoxybenzyl-Diethylenetriamine Pentaacetic Acid-Enhanced Acquisition With Compressed Sensing Reconstruction. Invest Radiol. 2014;
34. Orczyk C, Rusinek H, Rosenkrantz AB, et al. Preliminary experience with a novel method of three-dimensional co-registration of prostate cancer digital histology and in vivo multiparametric MRI. Clinical Radiology. 2013;68(12):e652–e658.
35. Depeursinge A, Foncubierta-Rodriguez A, Van De Ville D, Müller H. Three-dimensional solid texture analysis in biomedical imaging: Review and opportunities. Medical Image Analysis. 2014;18(1):176–196.
36. de la Taille A, Katz AE, Bagiella E, et al. Microvessel density as a predictor of PSA recurrence after radical prostatectomy. A comparison of CD34 and CD31. Am J Clin Pathol. 2000;113(4):555–562.
37. Vignati A, Mazzetti S, Giannini V, et al. Texture features on T2-weighted magnetic resonance imaging: new potential biomarkers for prostate cancer aggressiveness. Phys Med Biol. 2015;60(7):2685–2701.
38. Ginsburg SB, Algohary A, Pahwa S, et al. Radiomic features for prostate cancer detection on MRI differ between the transition and peripheral zones: Preliminary findings from a multi-institutional study. J Magn Reson Imaging. 2016;n/a – n/a.
39. Rosenkrantz AB, Mendrinos S, Babb JS, Taneja SS. Prostate Cancer Foci Detected on Multiparametric Magnetic Resonance Imaging are Histologically Distinct From Those Not Detected. The Journal of Urology. 2012;187(6):2032–2038.
40. Tan CH, Wei W, Johnson V, Kundra V. Diffusion-Weighted MRI in the Detection of Prostate Cancer: Meta-Analysis. American Journal of Roentgenology. 2012;199(4):822–829.
41. Siddiqui MM, Rais-Bahrami S, Turkbey B, et al. Comparison of MR/Ultrasound Fusion–Guided Biopsy With Ultrasound-Guided Biopsy for the Diagnosis of Prostate Cancer. JAMA. 2015;313(4):390.
42. Panebianco V, Barchetti F, Sciarra A, et al. Multiparametric magnetic resonance imaging vs. standard care in men being evaluated for prostate cancer: a randomized study. Urol Oncol. 2015;33(1):17.e1–e7.
43. Ahmed HU, Hu Y, Carter T, et al. Characterizing Clinically Significant Prostate Cancer Using Template Prostate Mapping Biopsy. The Journal of Urology. 2011;186(2):458–464.
44. Rosenkrantz AB, Ginocchio LA, Cornfeld D, et al. Interobserver Reproducibility of the PI-RADS Version 2 Lexicon: A Multicenter Study of Six Experienced Prostate Radiologists. Radiology. 2016;280(3):793–804.
45. Oto A, Yang C, Kayhan A, et al. Diffusion-weighted and dynamic contrast-enhanced MRI of prostate cancer: correlation of quantitative MR parameters with Gleason score and tumor angiogenesis. AJR Am J Roentgenol. 2011;197(6):1382–1390.
46. Verma S, Rajesh A, Morales H, et al. Assessment of Aggressiveness of Prostate Cancer: Correlation of Apparent Diffusion Coefficient With Histologic Grade After Radical Prostatectomy. American Journal of Roentgenology. 2011;196(2):374–381.
47. Choy B, Pearce SM, Anderson BB, et al. Prognostic Significance of Percentage and Architectural Types of Contemporary Gleason Pattern 4 Prostate Cancer in Radical

Prostatectomy: The American Journal of Surgical Pathology. 2016;40(10):1400–1406.
48. Epstein JI, Egevad L, Amin MB, et al. The 2014 International Society of Urological Pathology (ISUP) Consensus Conference on Gleason Grading of Prostatic Carcinoma: Definition of Grading Patterns and Proposal for a New Grading System. Am J Surg Pathol. 2016;40(2):244–252.
49. Villers A, Rubin MA. Re: Prognostic Significance of Percentage and Architectural Types of Contemporary Gleason Pattern 4 Prostate Cancer in Radical Prostatectomy. European Urology. 2017;71(2):301.
50. Moore CM, Giganti F, Albertsen P, et al. Reporting Magnetic Resonance Imaging in Men on Active Surveillance for Prostate Cancer: The PRECISE Recommendations-A Report of a European School of Oncology Task Force. Eur Urol. 2017;71(4):648–655.
51. O'Connor JPB, Aboagye EO, Adams JE, et al. Imaging biomarker roadmap for cancer studies. Nature Reviews Clinical Oncology. 2016;14(3):169–186.
52. Park B, Mikheev A, Zaim Wadghiri Y, et al. Optimal target VOI size for accurate 4D coregistration of DCE-MRI. 2016. p. 97881P – 97881P – 8http://dx.doi.org/10.1117/12.2214675. Accessed April 19, 2016.
53. Schneider CA, Rasband WS, Eliceiri KW. NIH Image to ImageJ: 25 years of image analysis. Nat Meth. 2012;9(7):671–675.

APPENDIX

Appendix 1 Computing quantitative maps using pharmacokinetic (PK) Toft model:

We used an in house developed software (Firevoxel, New York University, https://wp.nyu.edu/firevoxel), already used in other organs to compute pharmacokinetic models from 4D imaging (25,26), to generate the maps derived from the Toft model.

The two parameters were the Transfert Constant (Ktrans in ml/min) and Fraction of extracellular extravascular space (Ve, no unit).
The input function, Arterial Input Function (AIF), was patient specific.

1. Arterial Input Function (AIF):

The AIF was derived from a manually segmented region of interest (ROI) either from iliac or femoral artery over the 4D DCE data set.
The time point showing the time of peak of contrast media within this ROI was identified.
Then, threshold of 92.5% of the histogram was automatically applied to better reflect the maximum concentration of the contrast media at the level of the organ. AIF was then extracted from this adjusted ROI.

2. Approximation of contrast media concentration:

The conversion of signal intensity into approximated concentration of the contrast agent at a time point for a voxel was generated using the calculation

$$C(t) = -1 + {S(t)}/{S(0)}$$

Haematocrit was assumed equal to 0.4.

3. 4D Image registration and processing:

The prostate and immediate surroundings tissues were cropped in 4D to accelerate computation of the PK model as previously described(27).

Prior to computation of the pharmacokinetic model, motion artefacts across the different

time points were assessed. Motion artefacts across DCE acquisition can occur because of rectum motion, patient motion for example.

In case of visual large motion, the DCE sequence was registered in 4D to avoid artefacts in the resulting quantitative maps using the built-in algorithm of the software platform(28).

PK modelling is then computed using the specific AIF on the cropped 4D volume registered as the previous step, if needed.

The output are the Ktrans and Ve maps of the prostate and surroundings tissues.

Appendix 2 Assessment of consistency of histograms:

1. Methods:

The first level was a visual assessment of the histogram derived from the functional sequences and derivatives.
We undertook this level of investigation to check the interpatient consistency of the maps generated from the computation described previously.

To overcome the bias due to volume, all histograms were generated as normalised, meaning that the area under the curve is equal to 1 whatever is the VOI investigated.

Building the histogram was permitted using Image J (NIH, USA)(32) with a locally developed package.

For an imaging parameter, identical bin and range of values were carried out and applied for all the VOIs. A mask was applied for each VOIs.

2. Illustration of results:

This allows direct visual comparison of the enclosed information for each VOI. Results for the prostate VOI are displayed in the figure below for ADC, Ve and Ktrans.

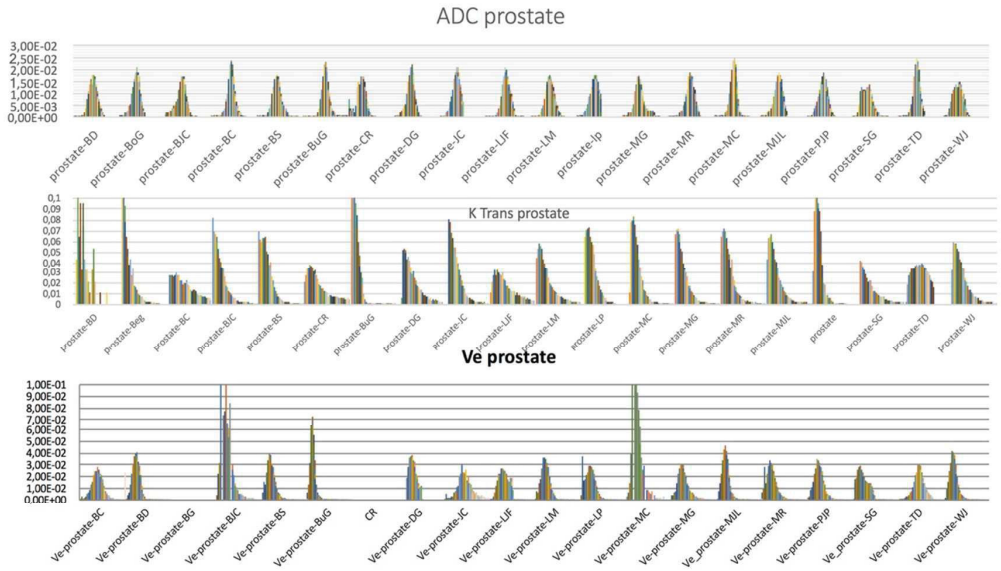

Appendix 3. Calibration of Entropy:

Entropy was computed as $\text{Entropy} = -\sum(\frac{h[i]}{N} \times \log\frac{h[i]}{N})$

where $h[i]$is the bin width of the histogram and N the number of voxels included in the analysis.

Entropy is a measurement of the quantity of information to be extracted for analysis. The information to be sampled has to be calibrated. As per the previous formula, the bin width directly influences the value of the Entropy. Therefore, we chose to calibrate the entropy to the critical information to be obtained.

We hypothesised that a heterogeneous lesion of 0.2cc comprising different Gleason patterns, considered as the lower threshold volume for significant disease, should be sampled by the calculation of the entropy.

As a result, the smaller volume sampled by a bin should be equal to the volume of 0.2cc lesion

Under the hypothesis that all the voxels from a 0.2cc volume would be captured by 1 bin width if homogeneous, this allows the computation of the total number of voxels to be plotted to sample the whole histogram accordingly.

$$tNb = 0.2 / VVx$$

where tNb is the total number of voxel of a bin and VVx is the volume of 1 voxel in cc.

And $$h[i] = [S] / tNb$$

Where [S] is the difference of the maximum and minimum value that can take the parameter to analyse.

As a results of the registration of all MRI maps and sequences in the same space, all parameters had the same voxel volume. In our study, tNb is equal to 310. Then the bin width depends of the range of value that can take the parameter to explore.

The following table summarizes bin width for the 4 different MRI features which were analysed using entropy.

MRI Feature	Signal Intensity range	Calculated bin width
ADC	1-2500	8.06
Ktrans	0.01-10	0.03
Ve	0.01-1.6	0.005
T2 WI	1-1000	3.22

Appendix 4. Computation of Kurtosis and Skewness:

The analysis also comprised computation of Kurtosis (K) and Skewness(Sk) for the different VOIS. Those were computed as followed

$$Sk = \frac{\sum (y_i\text{-ybar})^3}{(N\text{-}1) \times s^3}$$

and $$K = \frac{\sum (y_i\text{-ybar})^4}{(N\text{-}1)\times s^4} - 3$$

where ybar is the mean, *s* the standard deviation.

The Kurtosis describes the peakedness of distribution of the value of the parameter to explore such that the sharper peak indicates larger Kurtosis.

The Skewness interrogates the distribution of the asymmetry such larger positive and negative skew signifies longer tails to the right and the left of the mean.

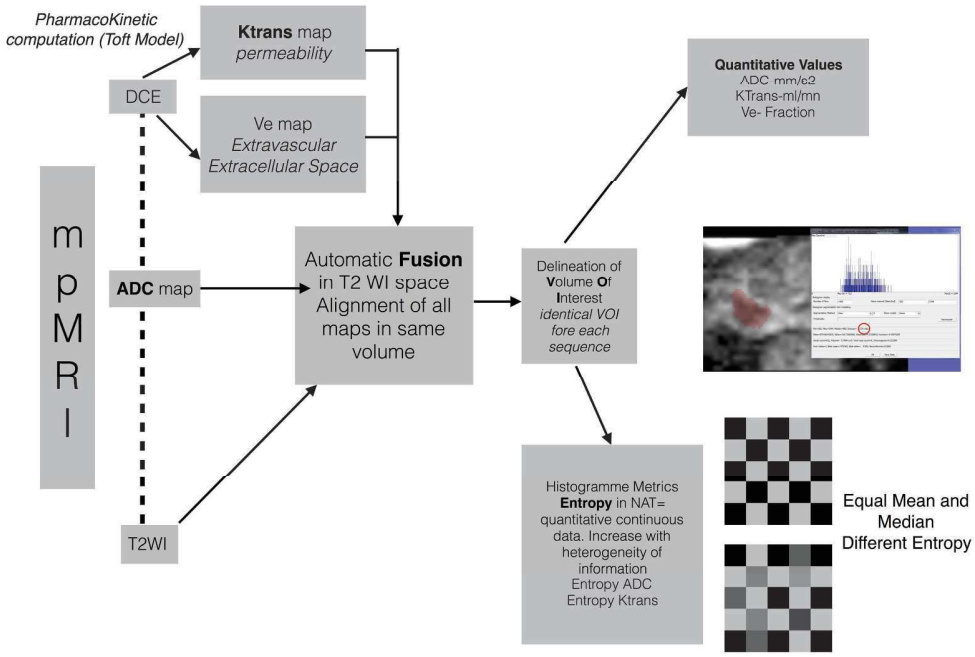

Figure 1. Image processing workflow

209x148mm (300 x 300 DPI)

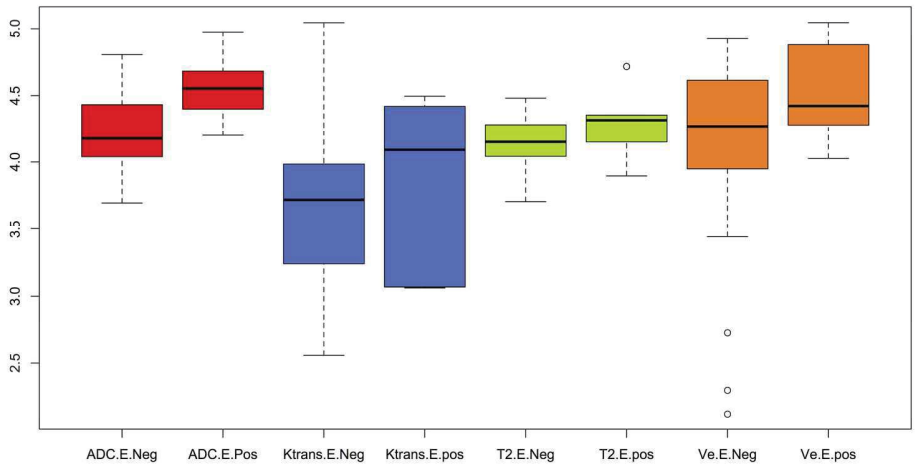

Figure 2: Comparison using boxplot of Entropy for the different MRI features between significant cancerous and non-cancerous targets

177x105mm (300 x 300 DPI)

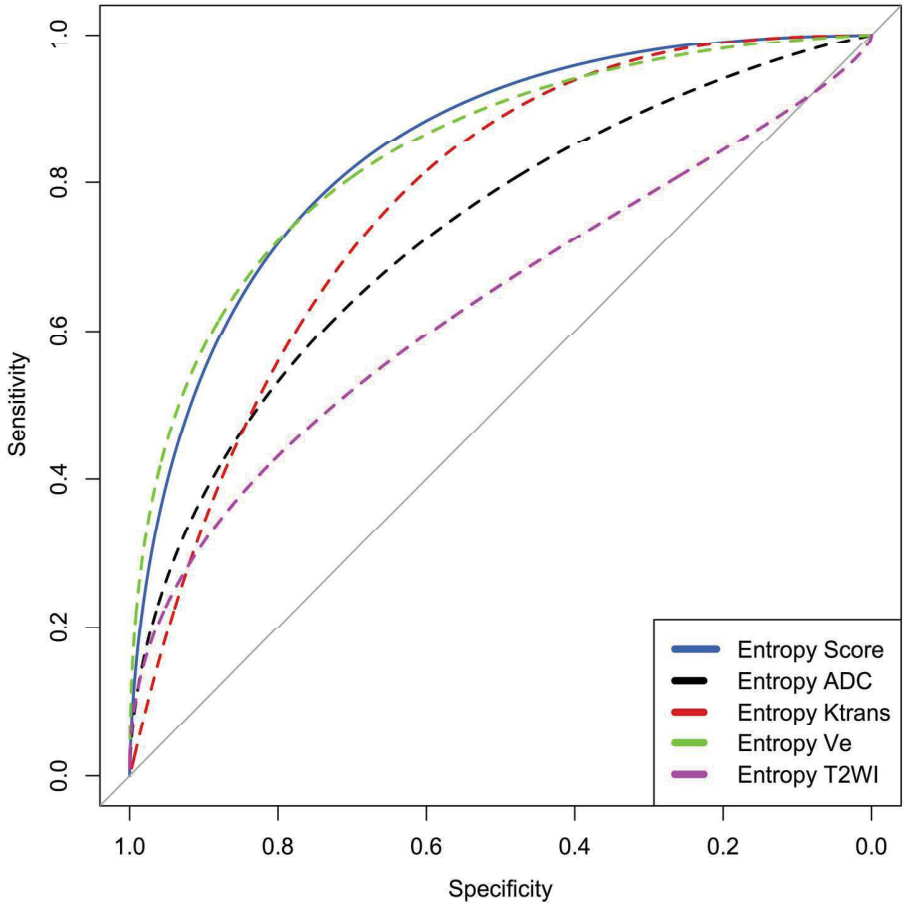

Figure 3 ROC curves for detection of significant cancer using entropy score and each of its component within normal tissue, MRI target and cancer 70 VOIS (A analysis)

177x177mm (300 x 300 DPI)

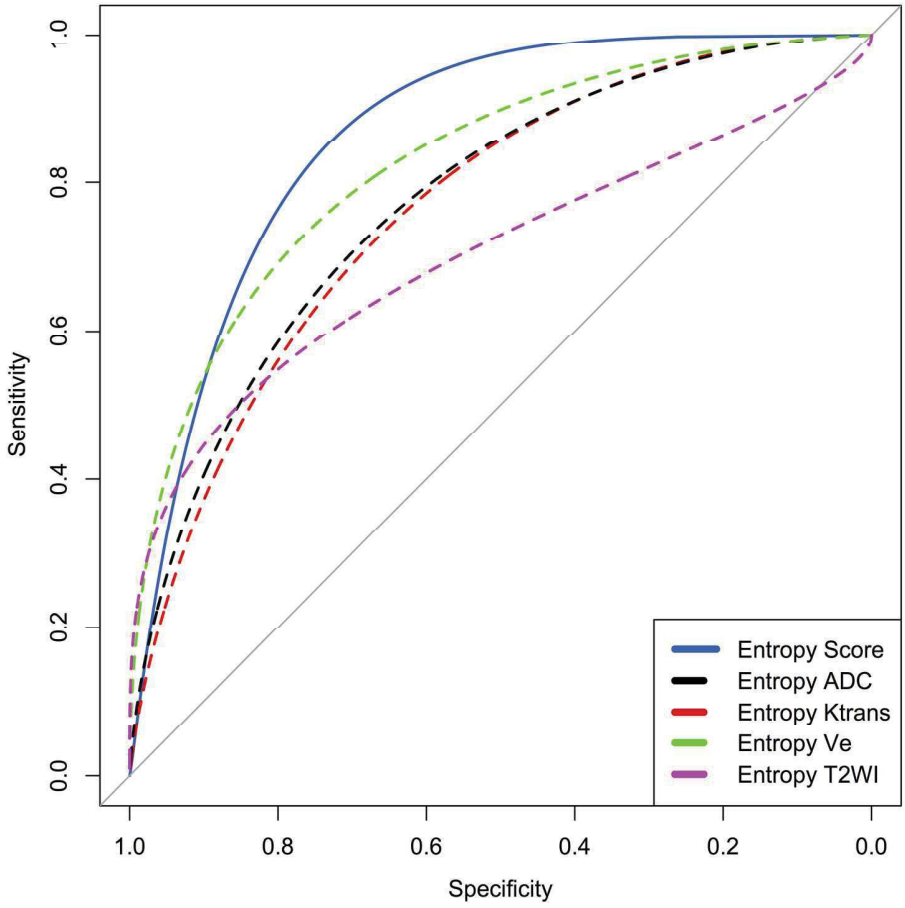

Figure 4 ROC curves for detection of significant cancer using entropy score and each of its component within the MRI target and cancer VOIS (B analysis

177x177mm (300 x 300 DPI)

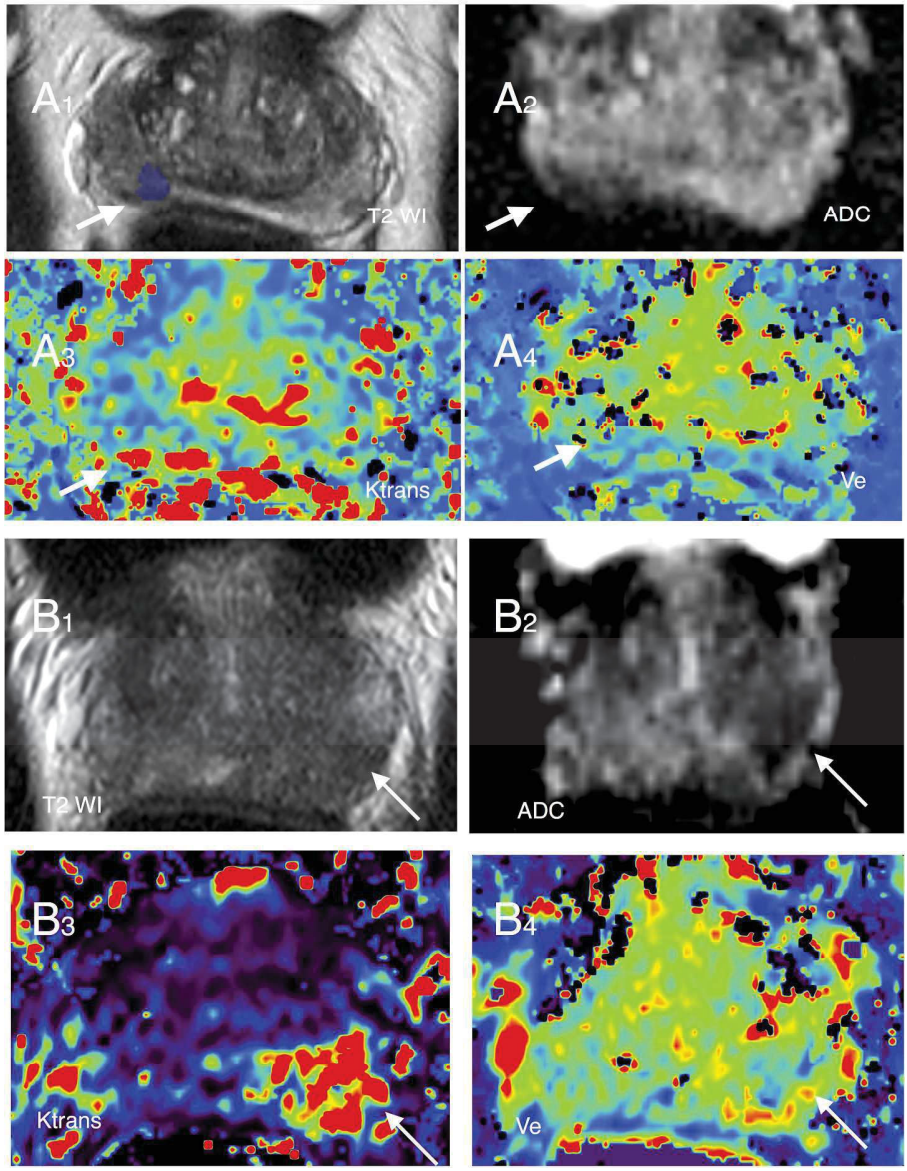

Figure 5 shows two examples of high and low entropy score of cancerous lesions of Gleason (3+3) (A) and (3+4) B with Entropy Score of 14.71 NAT and 18.75 NAT respectively‼ ┼ . A1, B1: T2 WI; A2, B2: ADC map; A3, B3: Ktrans map; A4, B4: Ve map. white arrows point the lesion.

219x284mm (300 x 300 DPI)

Section & Topic	No	Item	Reported on page #
TITLE OR ABSTRACT			
	1	Identification as a study of diagnostic accuracy using at least one measure of accuracy (such as sensitivity, specificity, predictive values, or AUC)	1
ABSTRACT			
	2	Structured summary of study design, methods, results, and conclusions (for specific guidance, see STARD for Abstracts)	1
INTRODUCTION			
	3	Scientific and clinical background, including the intended use and clinical role of the index test	2
	4	Study objectives and hypotheses	2
METHODS			
Study design	**5**	Whether data collection was planned before the index test and reference standard were performed (prospective study) or after (retrospective study)	3
Participants	**6**	Eligibility criteria	3
	7	On what basis potentially eligible participants were identified (such as symptoms, results from previous tests, inclusion in registry)	3
	8	Where and when potentially eligible participants were identified (setting, location and dates)	3
	9	Whether participants formed a consecutive, random or convenience series	3
Test methods	**10a**	Index test, in sufficient detail to allow replication	3
	10b	Reference standard, in sufficient detail to allow replication	3
	11	Rationale for choosing the reference standard (if alternatives exist)	3
	12a	Definition of and rationale for test positivity cut-offs or result categories of the index test, distinguishing pre-specified from exploratory	3, 6
	12b	Definition of and rationale for test positivity cut-offs or result categories of the reference standard, distinguishing pre-specified from exploratory	3, 6
	13a	Whether clinical information and reference standard results were available to the performers/readers of the index test	3
	13b	Whether clinical information and index test results were available to the assessors of the reference standard	3
Analysis	**14**	Methods for estimating or comparing measures of diagnostic accuracy	6
	15	How indeterminate index test or reference standard results were handled	6
	16	How missing data on the index test and reference standard were handled	6
	17	Any analyses of variability in diagnostic accuracy, distinguishing pre-specified from exploratory	7
	18	Intended sample size and how it was determined	3
RESULTS			
Participants	**19**	Flow of participants, using a diagram	Fig1
	20	Baseline demographic and clinical characteristics of participants	Table 1
	21a	Distribution of severity of disease in those with the target condition	Table 1
	21b	Distribution of alternative diagnoses in those without the target condition	Table 1
	22	Time interval and any clinical interventions between index test and reference standard	6
Test results	**23**	Cross tabulation of the index test results (or their distribution) by the results of the reference standard	8
	24	Estimates of diagnostic accuracy and their precision (such as 95% confidence intervals)	8,9 table 6
	25	Any adverse events from performing the index test or the reference standard	3
DISCUSSION			
	26	Study limitations, including sources of potential bias, statistical uncertainty, and generalisability	12
	27	Implications for practice, including the intended use and clinical role of the index test	12
OTHER INFORMATION			
	28	Registration number and name of registry	Cover letter
	29	Where the full study protocol can be accessed	Cover letter
	30	Sources of funding and other support; role of funders	none

STARD 2015

AIM

STARD stands for "Standards for Reporting Diagnostic accuracy studies". This list of items was developed to contribute to the completeness and transparency of reporting of diagnostic accuracy studies. Authors can use the list to write informative study reports. Editors and peer-reviewers can use it to evaluate whether the information has been included in manuscripts submitted for publication.

EXPLANATION

A **diagnostic accuracy study** evaluates the ability of one or more medical tests to correctly classify study participants as having a **target condition.** This can be a disease, a disease stage, response or benefit from therapy, or an event or condition in the future. A medical test can be an imaging procedure, a laboratory test, elements from history and physical examination, a combination of these, or any other method for collecting information about the current health status of a patient.

The test whose accuracy is evaluated is called **index test.** A study can evaluate the accuracy of one or more index tests. Evaluating the ability of a medical test to correctly classify patients is typically done by comparing the distribution of the index test results with those of the **reference standard**. The reference standard is the best available method for establishing the presence or absence of the target condition. An accuracy study can rely on one or more reference standards.

If test results are categorized as either positive or negative, the cross tabulation of the index test results against those of the reference standard can be used to estimate the **sensitivity** of the index test (the proportion of participants *with* the target condition who have a positive index test), and its **specificity** (the proportion *without* the target condition who have a negative index test). From this cross tabulation (sometimes referred to as the contingency or "2x2" table), several other accuracy statistics can be estimated, such as the positive and negative **predictive values** of the test. Confidence intervals around estimates of accuracy can then be calculated to quantify the statistical **precision** of the measurements.

If the index test results can take more than two values, categorization of test results as positive or negative requires a **test positivity cut-off**. When multiple such cut-offs can be defined, authors can report a receiver operating characteristic (ROC) curve which graphically represents the combination of sensitivity and specificity for each possible test positivity cut-off. The **area under the ROC curve** informs in a single numerical value about the overall diagnostic accuracy of the index test.

The **intended use** of a medical test can be diagnosis, screening, staging, monitoring, surveillance, prediction or prognosis. The **clinical role** of a test explains its position relative to existing tests in the clinical pathway. A replacement test, for example, replaces an existing test. A triage test is used before an existing test; an add-on test is used after an existing test.

Besides diagnostic accuracy, several other outcomes and statistics may be relevant in the evaluation of medical tests. Medical tests can also be used to classify patients for purposes other than diagnosis, such as staging or prognosis. The STARD list was not explicitly developed for these other outcomes, statistics, and study types, although most STARD items would still apply.

DEVELOPMENT

This STARD list was released in 2015. The 30 items were identified by an international expert group of methodologists, researchers, and editors. The guiding principle in the development of STARD was to select items that, when reported, would help readers to judge the potential for bias in the study, to appraise the applicability of the study findings and the validity of conclusions and recommendations. The list represents an update of the first version, which was published in 2003.

More information can be found on http://www.equator-network.org/reporting-guidelines/stard.

Partie 3 : Suivi longitudinal en 3D d'une thérapie focale du cancer de prostate basé sur le recalage-fusion d'image déformable

Les performances de la méthode de recalage non rigide ont été testée de manière longitudinale entre pré et post thérapie focale. L'objet du dernier chapitre a été d'étudier la méthode de recalage entre l'IRM de planning thérapeutique et celles de suivi afin de permettre d'établir une cible biopsique pour le suivi de la thérapie focale. La lésion traitée n'étant virtuellement plus détectable par l'imagerie. Les données de 10 patients traités par thérapie focale (photothérapie dynamique et ablation laser interstitielle) sont étudiées. Les examens pré traitement, post traitement et de suivi à 6 mois sont recalés de manière non rigide et rigide (comme contrôle) en utilisant l'algorithme d'Information Mutuelle au sein de la même plateforme logicielle. L'ensemble de prostate se déforme et perd significativement du volume après un traitement focal avec une perte volume moyenne de 14%, les déformations les plus accentuées étant au niveau de la zone d'ablation. Le recalage est évalué en termes de recouvrement avec l'indice de Dice et de distances avec la distance de Hausdorff. Le recalage déformable de la zone d'ablation atteint des performances de l'ordre de 1,99mm (0.72mm/ml, p=0.0019) significativement meilleure que le recalage rigide, pertinentes dans le suivi oncologique. La localisation virtuelle du tissu résiduel après une ablation focale pourrait permettre un suivi oncologique robuste et objectif notamment pour focaliser l'examen radiologique sur une zone précise, définir la zone à revisiter par biopsie en contrôle, d'établir les marges effectives de traitement ou encore distinguer récidive intra ou extra zone traitée.

Se référant à :

"3D registration of mpMRI for assessment of prostate cancer focal therapy."

Article en révision - Academic Radiology

Clément Orczyk, Andrew B Rosenkrantz, Arnauld Villers, Artem Mikheev, Myriam Bernaudin, Samir S Taneja, Samuel Valable, Henry Rusinek

Elsevier Editorial System(tm) for Academic Radiology

Manuscript Draft

Manuscript Number:

Title: 3D registration of mpMRI for assessment of prostate cancer focal therapy

Article Type: Original Investigation

Corresponding Author: Dr. Clement Orczyk, M.Sc.,MD.

Corresponding Author's Institution: University College London Hospitals

First Author: Clement Orczyk, M.Sc.,MD.

Order of Authors: Clement Orczyk, M.Sc.,MD.; Andrew B Rosenkrantz, MD; Artem Mikheev; Arnauld Villers, M.D., P.h.D; Myriam Bernaudin, P.h.D.; Samir S Taneja, M.D.; Samuel Valable, P.h.D.; Henry Rusinek, P.h.D.

Abstract: Purpose:
To assess a novel method of 3D co-registration of prostate MRI exams performed before and after prostate cancer focal therapy.

Material and method:
We developed a software platform for automatic 3D deformable co-registration of prostate MRI at different time points and applied this method to ten patients who underwent focal ablative therapy. MRI exams were performed preoperatively, as well as one week and six months post-treatment. Rigid registration served as reference for assessing co-registration accuracy and precision.

Results:
Segmentation of preoperative and postoperative prostate revealed a significant post-operative volume decrease of the gland that averaged 6.49 cc (p=0.017). Applying deformable transformation based upon Mutual Information (MI) from 120 pairs of MRI slices, we refined by 2.9 mm (max 6.25mm) the alignment of the ablation zone (AZ), segmented from contrast-enhanced images on the one-week post-operative exam, to the 6-month post-operative T2-weighted images. This represented a 500% improvement over the rigid approach (p=0.001), corrected by volume. The dissimilarity by Dice index of the mapped AZ using deformable transformation vs. rigid control was significantly (p=0.04) higher at the ablation site compared to the whole gland.

Conclusion:
Our findings illustrate our method's ability to correct for deformation at the ablation site. The preliminary analysis suggests that deformable transformation computed from MI of pre-operative and follow-up MRI is accurate in co-registration of MRI exams performed before and after focal therapy. The ability to localize the previously ablated tissue in 3D space may improve targeting for image-guided follow-up biopsy within focal therapy protocols.

Title

3D registration of mpMRI for assessment of prostate cancer focal therapy

Short Title

Assessment of prostate cancer focal therapy

Authors:
Clément Orczyk MSc MD [1,2,4], Andrew B Rosenkrantz MD[3], Artem Mikheev[3], Arnauld Villers, MD PhD[5], Myriam Bernaudin, PhD [4], Samir S Taneja, MD [2,3] Samuel Valable, PhD [4], Henry Rusinek PhD[3]

[1.] The prostate unit, Department of Urology, University College London Hospitals, London, United Kingdom
[2.] Division of Urologic Oncology, Department of Urology, New York University Langone Medical Center, New York, NY
[3.] Department of Radiology, New York University Langone Medical Center, New York, NY
[4.] Normandie Univ, UNICAEN, CEA, CNRS, CHU Caen, ISTCT/CERVOxy group, 14000 Caen, France.
[5.] Department of Urology, Université Lille Nord de France, 59000 Lille, France

Corresponding Author:
Clément Orczyk, M.Sc M.D.

Corresponding Author's Institution:

The prostate unit, Department of Urology, University College London Hospitals, London, United Kingdom

Dr Clement Orczyk, clementorczyk@yahoo.fr ; c.orczyk@ucl.ac.uk

Current address:
Research Department of Urology, Division of Surgery and Interventional Sciences, University College London
132 Hampstead Road, Room 4.23, 4th Floor,
London NW1 2PS
Phone : +44 7 958 550 727

Funding: Supported by the Joseph and Diane Steinberg Charitable Trust and Grant 1UL1RR029893 from the National Center for Research Resources, National Institutes of Health

Title

3D registration of mpMRI for assessment of prostate cancer focal therapy

Short Title

Assessment of prostate cancer focal therapy

Introduction:

Contemporary methods of multi-parametric MRI (mpMRI) of the prostate have greatly improved the ability of radiologists and urologists to detect prostate cancer [1]. mpMRI allows physicians to diagnose clinically significant cancer in its early stage, to plan prostatectomy and radiation therapy, and to detect local recurrence.

Combined with the trend of earlier detection, noninvasive prostate cancer therapies are gaining interest. Focal therapies (FT) aim to combine oncologic benefit with preserved continence and erectile function. The use of this tissue preservation approach is evolving and FT is being applied to more aggressive disease than when initially proposed [23]. Clinical FT trials depend on mpMRI for tumor localization, treatment planning, and post-treatment follow-up [4 5 6 7].

There is no consensus regarding optimal assessment of oncologic success of FT [3,5,8]. Current criteria of successful FT involve negative histology at the treatment site. Different methods have been proposed to detect cancer recurrence after FT. While invasive transrectal prostate biopsy or transperineal mapping biopsy are often performed, mpMRI-targeted biopsy has shown promising results [910]. Such assessment by MRI requires an ability to delineate on imaging the ablation zone (AZ) that is characterized histologically by homogeneous coagulation necrosis [1112]. In addition, it has been suggested [713], that mpMRI underestimates the total tumor

volume, requiring to include some surrounding margin within the AZ for a complete focal ablation. After treatment, dynamic contrast-enhanced (DCE) MRI delineates AZ as a devascularized, non-enhancing area [4]. Within several weeks after treatment, the AZ shrinks, often leading to a changed configuration of the gland [14 8].

These novel therapeutic developments require a reliable and accurate software system for assessment of the changes in the prostate gland, including tissue necrosis, due to ablation. To be effective, such a system must depict how the viable tissue is reorganized around the AZ. Thereby requiring a comparison of pre-treatment and post treatment images of the prostate. Development of image registration methods for this application is challenging. First, one must register longitudinal MRI, including different sequences, across different time points. Second, inherent in focal therapy, the tissue changes are inhomogeneous. Third, the variations in shape between the preoperative and postoperative exams are highly dependent on treatment delivery, location of the tumor, energy choice, as well as surrounding tissues. These factors makes it difficult to use a normative atlas to facilitate registration.

Fei et al. [15] described a mutual Information based rigid-transform method to align a preoperative prostate T2 weighted (T2W) imaging sequence to an intra operative sequence. Wu et al. [16] combined mutual Information measure with low-order polynomial transformation to register spectroscopy with the prostate deformed by inflated intra-rectal balloon. Using a finite elements method (FEM), Marami et al [17] validated a registration approach between MRI acquired with an endorectal coil and the intraoperative MRI. Toth et al. [18] also used FEM to model the changes in prostate shape after laser ablation.

It has been have previously demonstrated that the deformation of the gland after surgery is well captured by the affine transformation *T* that incorporates nonisotropic 3D sheer and stretch factors [19]. This technique was also found to accurately define a 3D target for focal therapy based on MRI findings [7]. We have now implemented an image-based framework for accurate estimation of the affine transform from the pre-FT to the post-FT MRI. This study evaluates the method using longitudinal mpMRI acquired before and after modern interstitial laser[20] and photodynamic FT[21]. This study aims to assess this novel method of 3D co-registration of prostate MRI exams performed before and after prostate cancer focal therapy, in order to facilitate focal therapy follow up.

Material and Methods

Patients

Ten male patients, aged 65 +/- 6.4 years, diagnosed with localized prostate cancer at biopsy (median PSA 5.1ng/ml, median Gleason Score 6) underwent FT. Five patients were treated by interstitial laser procedure within the MRI bore [4] and five by photodynamic therapy, included in an earlier publication[21]. Local institutional review board approved this study.

Image acquisition

All patients underwent a pre-operative mpMRI, and two follow-up post-operative mpMRI (one week and 6 months after treatment, fig.1) using 3T Magnetom Trio system equipped with a pelvic phase array (Siemens Healthcare, Erlangen, Germany). Each exam used identical MpMRI protocol that included a T2W sequence, a diffusion-weighted sequence, and a DCE-MRI exam specified in detail below.

The anatomical T2W images through the pelvis were acquired using turbo spin-echo sequence with parameters: TR = 4950 ms, TE = 122 ms, axial orientation, 256 x 256 acquisition matrix, no interslice gap, 180 x 180 mm field of view, 3 mm slice thickness, 3 signal averages.

Diffusion weighted sequence was based on axial fat-suppressed single shot echoplanar imaging with TR=4100 ms, TE=86 ms, diffusion gradient b-values of 50 and 1000 s/mm^2; slice thickness 3 mm; 100 x 100 matrix; 200 x 200 mm field of view,10 signal averages. ADC maps were reconstructed inline.

DCE-MRI exam consisted of continuous acquisition of T1-weighted 3 mm thick contiguous images (240 x 240 mm field of view; matrix 128 x 128) every 15 sec after IV administration of 0.1 mmol/kg of gadopentetate dimeglumine (Magnevist; Bayer HealthCare Pharmaceuticals, Montville, NJ). The contrast agent was administered as an intravenous bolus via power injector (Spectris; Medrad, Warrendale, Pa), followed by a 20-mL saline flush, both administered at a 3 mL/sec injection rate.

Image analysis

Our image processing workflow (figure 2) includes estimating 3D rigid body coregistration of mpMRI modalities within each exam; and image coregistration across-exams using non-rigid (affine) transform.

Coregistration framework

The user interaction consists of a rough outline of the prostate gland that can be done in few seconds. There are several novel features of the system: 1) the

parameters of the affine transform T are estimated only from prostate tissue, thus ignoring confounding signal from adjacent regions like the muscle, rectum or the bladder; 2) the iterative voxel-similarity algorithm is supplemented by the multi-dimensional gridding of initial parameters. The goal is to make the estimate of T insensitive of the initial value and to avoid being trapped in a suboptimal local optimum; and 3) the software is designed to take advantage of multi-threaded, multi-core platforms to improve performance and cost-efficiency.

Image coregistration consists of two tasks: determining the transformation T that relates points in the source image V_1 with the corresponding points in the target image V_2 and applying the transformation T to the source image, resulting in the coregistered volume $V_2' = T(V_1)$. Signal interpolation is another necessary step. Our coregistration process is controlled using the dialog box shown in figure 3. The optimization is done in two stages:

1) “Autofocus” stage: exhaustive search over multiple initial approximations drawn from a discrete grid of parameters that define T (6 parameters for rigid body, 12 parameters for affine transform). The most promising candidates (those having largest similarity measure) are passed to the second, fine-tune stage. The number of selected candidates is controlled by the "power" factor P. Large values of P mayimprove the accuracy of coregistration at the cost of longer processing time.

2) “Fine-tune” stage: iterative search for a local maximum of the similarity measure (initialized at P settings from autofocus stage). The available measures include signal intensity differences[22], signal correlation [23], uniformity of ratio image[24,25], and mutual information (MI) and normalized MI [26–29]. Mutual information was used in this study.

Our framework allows the user to restrict the similarity measure to a predefined 3D region called "target". In this study the target region was the prostate and immediately (5 mm margin) surrounding tissue [30]. The idea is to focus the similarity on the organ of interest, while ignoring possible misalignment of background structures as well as confounding image (curves of bladder neck or anterior wall of rectum).

Estimating transformations within-exam and across exams

The parameters for coregistering different MRI sequences within each exam were: target ROI=yes, subsample=3, autofocus grid = 10mm, rotation = 10°, transform = rigid, measure = mutual information, interpolation = sinc. Coregistration of MRI sequences across exams used the similar parameters except transform = affine, scale deformation=2 and shear=5. Here a rigid method was explored as a control for affine, to assess the significance of deformation (stretching and sheering) induced by therapy and to describe local changes that take place following FT.

For each patient and each exam, the resulting transformations were saved for later recall, to be applied to landmarks or subregion masks (ROI) placed within the source volume. This allowed visualization of AZ from the 1 week post-FT MRI superimposed over the prostate 6-month post-FT.

The coregistration software was written in C++ using Microsoft Foundation Class and Intel Threading Building Blocks libraries. The program exploits parallel processing.

Error analysis and segmentation of prostate gland and ablation zone

To analyze registration error, two operators with experience in prostate anatomy manually segmented in consensus the different 3D masks (or ROIs): preoperative prostate, 6 months post operative prostate, and AZ. ROIs excluded the seminal vesicles. The first two ROIs were traced on T2W images. Segmentation of the AZ, which was visualized in all 10 cases, was derived from the latest DCE time-point from the 1-week post-FT MRI (Fig. 4B). The geometrical transformations *T* estimated in the process of coregistration were applied to these 3D ROIs.

The ROIs served to assess the accuracy of rigid and deformable transformation models (Fig. 5). It should be noted here that a future clinical/surgical use of the system does not require fine manual segmentation of the whole prostate.

We have measured the mismatch between transformed pre-op region and the region manually segmented at follow-up, the latter considered as the ground truth. Three types of error measures were evaluated:

1) volume changes -- while important, this measure is the least informative, as unlike the other two measures it doesn't capture subtle shape changes.

2) the Hausdorff distance (HD), defined here as the maximum distance (in millimeters) between the structure boundaries [7]. The HD was obtained for each slice composing an ROI. For each multislice ROI, the average of the maximum HD for each slice was calculated resulting in an average maximum HD. The purpose is to have 3D information for each ROI.

3) Dice index [19] was defined as the volume ratio Di=$2 \times (A \cap B)/(A \cup B)$. The Dice index measures the normalized similarity between two different 3D masks ROIs based on their overlap.

The co-registration process aims to transfer the location of the ablated zone AZ to its residual location within the late control MRI. We further analyzed how the rigid *Tr*(V1) and deformable *Ta*(V1) transforms computed from mutual information measure for the entire gland (M=mask of whole gland) is able to align the AZ on V2 (late post-FT), as illustrated in figure 2. This entails direct comparison of the derived target for post-FT follow-up between the compensated $AZ_{2'}$=*Ta*(*Tdce*(AZ)) and non-compensated deformations $AZ_{2''}$=*Tr*(*Tdce*(AZ)). We compared Di $AZ_{2'}$/ $AZ_{2''}$ to Di M_2'=*Ta*(M)/ M_2''=*Tr*(M) (figure 6, C). This compares the performances of the two algorithms at the location of the AZ to those for whole gland mapping. Analogously, we compared the HD for the same ROIs, resulting of $AZ_{2'}$- $AZ_{2''}$ and M_2'- M_2'' (figure 5, C), normalized by volume.

These measures were compared using the paired *t*-test or Wilcoxon signed rank test (for data that didn't satisfy Shapiro-Wilk test of normality). A p value less than 0.05 was used to establish significance. All tests were done using R statistical software, (version 3.0.2, Sep 2013, R foundation for Statistical Computing, Vienna, Austria).

Results

Volumetric analysis

There was a significant ~14% reduction in prostate volume (table 1, figure 6) between an average of 46.5 ml pre-FT to 40.0 ml post-FT (p=0.017, paired T-test, mean 6.50, 95% confidence interval (CI) [1.46 - 11.54]). The volume of the AZ obtained by direct segmentation was significantly correlated (R=0.738, p= 0.015) with the difference in prostate volume between the pre-FT and post-FT examinations. However, the volume of AZ was on the average 13.8 ml, approximately double the difference D in pre-FT and post-FT volumes (table 1) and statistically different from D (paired t-test, T=-2.38, p=0.04; mean diff 7.33, 95% CI [0.38 - 14.27]).

The blue bars in figure 6 illustrates the significant difference in volume between the rigid and deformable transforms of the whole prostate over the late post operative prostate at 6 months MRI, i.e.. *M_2' vs M_2''*.

Analysis of image coregistration

The 10 cases represented MRI volumes composed in total of 120 pair of slices for pre operative and late follow up T2 WI. In all cases, the mutual information algorithm converged successfully and we were able to assess both deformable and rigid transformation for coregistration of the pre-FT and post-FT images. The software architecture successfully exploited multi-core processor parallelism and shown by high loading on a 12-core CPU system (figure 7). A representative example is shown in figure 4.

Table 2 compares of volume between the rigid M_2'', which serves as a control, and deformable M_2' transforms of the whole gland. The transforms of the pre-FT prostate to the post-FT prostate yielded a significantly lower volume (p=0.041; mean difference 2.3, 95% IC[0.1132 ; 4.4868])) using deformable transformation

compared to the rigid approach (table 2). The difference of less than 1% of prostate volume after rigid transformation might be imputable to the interpolation errors, as rigid transformation conserve volume through.

Table 3 lists the average values of Dice index and HD for the alignment of the whole gland described in Figure 6, AB. While the alignment is better (smaller HD, larger overlap) for affine transform, the difference didn't reach significance (p=0.10 and 0.20). These comparisons suggest a trend for higher accuracy using the deformable transformation.

Analysis of AZ

When whole gland was taken in account, the deformable transformation *Ta* provided better description of AZ than rigid transformation *Tr* (see table 4), reaching 1.99 mm HD (or 0.72mm/ml, p=0.0019) and Di= 0.87 (p=0.046) versus HD=3.83 mm (or 0.15mm mm/ml), and Di=0.93.

Figure 8 illustrates the changes between pre and post treatment MRI at the ablated location, with a 3D reconstruction of the prostate.

Discussion

The role of image registration in prostate cancer pathway

Image coregistration plays an increasingly important role in prostate cancer. It permits us to characterize MR signal and image texture of cancer tissue through

histological validation [19,31,32]. There is a great interest in developing ultrasound biopsy fused to MRI [33–36]. Image registration will also play an important role in both planning and follow-up of FT. This entails accurate mapping of lesion mask derived from pre-treatment mpMRI to the space of treatment and post treatment images [7].

The ability of contrast enhanced imaging, either ultrasound or MRI to visualize necrotic tissue permits initial assessment of FT [37]. Several studies [3,5,8] converge by defining oncologic success of FT as negative biopsy at the treated area. (PSA is not helpful for monitoring FT outcome [38]). Histologic post FT assessment depends on either random transrectal or transperineal approach [3814]. Transrectal option is prone to substantial sampling error and a high rate of false negative results. Transperineal mapping option requires repeat general anesthesia [39]. mpMRI offers the promise to guide post-FT biopsy and overcome these limitations [40384142]. However there are obvious concerns related to tissue displacement [40].

A critical step is to accurately locate AZ at follow-up biopsy to (a) evaluate the energy deposition within AZ, and/or (b) sample the surrounding tissue (tumor margin). The objective is to detect and manage treatment failure or cancer recurrence and possibly offer re-treatment. This task requires detecting low-volume cancer [38] and it requires exquisite precision. Ven et al. [43] estimated that, given a 0.3 ml target, a precision of 1.9 mm is necessary to correctly grade 95% of aggressive tumor component in peripheral zone. The report of the START consortium concludes that defining the target for biopsy and being able to reliably sample such area remain fundamental problems [3]. The challenge is intensified if a lesion is poorly demarcated on the post-FT images or it there are significant spatial deformations between pre- and post-FT

images. To address this need, our study estimated the margin of error in AZ using affine transform and a novel coregistration framework. We chose rigid registration as a control.

Challenge for image registration

The current standard in radiologic in oncology are RECIST criteria, that unfortunately are subjective and don't involve image registration. There is very limited literature on longitudinal registration describing the deformation of the gland after local treatment [1441]. A recent report [18] aims to quantify changes of the gland after focal laser ablation using the finite elements method (FEM) align pre- and post-operative T2W images. The study notes the importance of knowing biomechanical properties of the tissue, including surrounding bladder and rectum.

Post-treatment volume loss

We have observed a mean decrease in gland volume of 6.50 cc or 12.9%. This is significantly lower than the volume of the AZ, although the two measures were significantly correlated. Toth et al. [18] reported a similar decrease in gland volume at the same follow-up time delay in response to laser ablation. Volume shrinkage is likely due to the process of *cicatrization* with fibrosis [44]. If confirmed, accounting for volume change will be an important requirement of any longitudinal analysis software. Clearly, volume-preserving rigid body coregistration is not capable to reflect volume loss, whereas the affine transform appears to correctly represent the volume loss due to FT.

Coregistration accuracy

Our image coregistration technique helps to assess FT and demonstrates that local treatment influences the deformation of the entire gland. We have observed the similarity of boundary changes at the gland (global) and the AZ (local) level. Both Dice Index and HD show the effect of deformable algorithm at AZ. The change in mean HD of 2.9 mm (maximum ~6 mm) between rigid and a deformable mapped AZ indicates the advantage of the deformable model to define an area of interest. This observation is important because it implies that currently available systems that ignore shrinkage may leave unsampled residual tissue and fail to detect residual/recurrent disease.

We have also demonstrated that changes in AZ are well modeled by the affine transform. Normalized HD resulting from affine compensation was 0.75 mm/cc for the AZ, which is almost five times better than 0.15 mm/cc for the whole gland. The lower Dice index at the AZ location (0.88) in this experiment compared to the whole gland (0.93) indicates the higher dissimilarity of the rigid and deformable transforms at this very zone of interest. These data indicate that the residual tissue at the former AZ location is more accurately mapped in the post-FT MRI using the deformable approach than without such compensation. no break This important finding shows the ability to successfully model tissue changes at the location of cancer that can be visualized on baseline mpMRI. Intensity changes at the location of the ablation were also reported by Toth et al. [18].

We have evaluated the registration technique using volumetric and linear metrics (Dice index and HD) rather than using more conventional landmark approach. Clearly identifiable landmarks are hard to detect on post-operative images.

We attribute good performance of longitudinal coregistration (all the attempted registrations were successful) to the use of discrete parameter gridding, introduced to avoid being trapped in local maxima. Moreover, our method computes the similarity measures from prostate alone. The reduced field of view decreases the computational effort and is not influenced by tissue motion outside the prostate. The implementation of multi-core parallelism enables one to complete this complex task on standard desktop computer in a few minutes.

Clinical implications

This work suggests that longitudinal image transformation may guide the location of targeted biopsy after FT. The shrinkage of AZ can be modeled prior to follow-up biopsy and incorporated in a US-guided sampling system [45]. A recent study evocated the benefit of a TRUS-MRI fusion platform that corrects for deformation on ultrasound due to the probe insertion, as compared to "cognitive registration" [10]. Such implementation could also be used for in MR bore biopsy procedure[46]. Using longitudinal coregistration, one could consistently re-visit the same gland location [47], without limitations of implantable/imageable pellets proposed recently by Ghai et Tranchtenberg [48]. Recently, Natarajan et al. [49] rose the question of assessment of treatment margin in their report of a phase 1 trial about focal therapy using in bore laser ablation with a transrectal approach. Our method may assist to discriminate

infield/ outfield recurrence after focal therapy. Figure 9 summarizes the potential clinical implementation of our findings in focal therapy pathway and follow up.

Toth and associates [18] provide preliminary validation of a competing framework based on FEM and requiring modeling the elastic effects of the bladder and the rectum. A direct comparison between FEM and purely image-based framework would be of interest. While further work is needed to validate software for accurate and safe focal therapy procedures, our preliminary experience suggests the clinical utility of affine algorithms for mapping mpMRI findings between pre- and post-FT scans. Our workflow could be also extended to transformation models that involve higher degree of freedom. The longitudinal coregistration technique could also be applied to other image-guided procedures like liver ablation[50] or focal kidney-sparing cancer therapy [51].

In summary, we have proposed a novel coregistration framework that has potential to provide image-guided target for post-FT biopsy. The affine algorithm can compensate and correct the deformation of an ablated zone and reach the needed accuracy of several millimeters. The technique offers the possibility to re-visit cancer location which was targeted and to plan follow up biopsy, facilitating accurate and safe follow up of focal therapy of prostate cancer.

Figures legends:

Figure 1: Timeline of treatment and imaging exams.

Figure 2: Image analysis workflow.

Figure 3: The dialogue box defines the registration process

Figure 4: Illustrative case of affine registration between pre-treatment (A) and post-treatment (photodynamic therapy) T2W volumes (C). Panel (B) shows delayed DCE image of the treated area, with ablated gland shown as non enhancing region. The bottom panel displays a postoperative T2W image overlayed with the corresponding preoperative image.

Figure 5: Schematic illustration of various measures assesses in current study. A: analysis of errors in whole gland definition for rigid transform model M_2 vs M_2''; B: analysis of errors for affine transform model M_2 vs M_2'; C: analysis of errors in defining AZ ($AZ_{2'}$-$AZ_{2''}$) vs (M_2'- M_2'').

Figure 6: Comparison between median pre-operative and 6 months post-operative volumes of the prostate (orange bars). Comparison between median volume generated with rigid and deformable transforms (blue bars) shows that deformable trans-formation compensates better for volume loss due to focal therapy.

Figure 7: Demonstration of high CPU core usage on a 12-core computer achieved during registration.

Figure 8: Post-surgical changes for a representative case involving dynamic phototherapy on left lobe. A,B: 3D rendering before and post treatment. Changes in shape and volume loss are observed in the left part of the gland. The pre-treatment view shows in red the lesion 10 mm in axial diameter, Gleason 6 (3+3). The post-treatment view displays in yellow the location of the ablated zone. This yellow area needs to be sampled to rule out cancer at follow-up biopsy. The green line segment is the needle path for transperineal targeted biopsy. C: preoperative T2W image. D: preoperative ADC map. E: preoperative DCE image through the cancer focus (white arrow). F: late postoperative T2W image. G, post operative ADC map H: DCE image at the same level. Changes in shape and MRI signal are discernible at the site of ablation on the left side of the gland.

Figure 9: graphical summary of implementation of 3D registration of mpMRI into focal therapy of prostate cancer pathway.

References

1. Dickinson L, Ahmed HU, Allen C, et al. Magnetic resonance imaging for the detection, localisation, and characterisation of prostate cancer: recommendations from a European consensus meeting. *Eur*. *Urol*. 2011;59(4):477–494.

2. Orczyk C a, Emberton M a, Ahmed HU a. What tumours should we treat with focal therapy based on risk category, grade, size and location?. *Current Opinion in Urology*. 2015;25(3):212–219.

3. Donaldson IA, Alonzi R, Barratt D, et al. Focal Therapy: Patients, Interventions, and Outcomes—A Report from a Consensus Meeting. *European Urology*. 2015;67(4):771–777.

4. Oto A, Sethi I, Karczmar G, et al. MR Imaging–guided Focal Laser Ablation for Prostate Cancer: Phase I Trial. *Radiology*. 2013;267(3):932–940.

5. van den Bos W, Muller BG, Ahmed H, et al. Focal Therapy in Prostate Cancer: International Multidisciplinary Consensus on Trial Design. *European Urology*. 2014;65(6):1078–1083.

6. Le Nobin J, Orczyk C, Deng F-M, et al. Prostate tumour volumes: evaluation of the agreement between magnetic resonance imaging and histology using novel co-registration software: Prostate tumour volume: co-registration between MRI and pathology. *BJU International*. 2014;114(6b):E105–E112.

7. Le Nobin J, Rosenkrantz AB, Villers A, et al. Image Guided Focal Therapy for Magnetic Resonance Imaging Visible Prostate Cancer: Defining a 3-Dimensional Treatment Margin

Based on Magnetic Resonance Imaging Histology Co-Registration Analysis. *The Journal of Urology*. 2015;194(2):364–370.

8. Muller BG, van den Bos W, Brausi M, et al. Follow-up modalities in focal therapy for prostate cancer: results from a Delphi consensus project. *World Journal of Urology*. 2015. Available at: http://link.springer.com/10.1007/s00345-014-1475-2. Accessed February 9, 2015.

9. Rosenkrantz AB, Taneja SS. Targeted Prostate Biopsy: Opportunities and Challenges in the Era of Multiparametric Prostate Magnetic Resonance Imaging. *The Journal of Urology*. 2012;188(4):1072–1073.

10. Wysock JS, Rosenkrantz AB, Huang WC, et al. A prospective, blinded comparison of magnetic resonance (MR) imaging-ultrasound fusion and visual estimation in the performance of MR-targeted prostate biopsy: the PROFUS trial. *Eur*. *Urol*. 2014;66(2):343–351.

11. Lindner U, Lawrentschuk N, Weersink RA, et al. Focal Laser Ablation for Prostate Cancer Followed by Radical Prostatectomy: Validation of Focal Therapy and Imaging Accuracy. *European Urology*. 2010;57(6):1111–1114.

12. Huang Z, Haider MA, Kraft S, et al. Magnetic resonance imaging correlated with the histopathological effect of Pd-bacteriopheophorbide (Tookad) photodynamic therapy on the normal canine prostate gland. *Lasers Surg Med*. 2006;38(7):672–681.

13. Bratan F, Melodelima C, Souchon R, et al. How Accurate Is Multiparametric MR Imaging in Evaluation of Prostate Cancer Volume? *Radiology*. 2014:140524.

14. Rouvière O, Gelet A, Crouzet S, et al. Prostate focused ultrasound focal therapy—imaging for the future. *Nature Reviews Clinical Oncology*. 2012;9(12):721–727.

15. Fei B, Wheaton A, Lee Z, et al. Automatic MR volume registration and its evaluation for the pelvis and prostate. *Phys Med Biol*. 2002;47(5):823–838.

16. Wu X, Dibiase SJ, Gullapalli R, et al. Deformable image registration for the use of magnetic resonance spectroscopy in prostate treatment planning. *International Journal of Radiation Oncology*Biology*Physics*. 2004;58(5):1577–1583.

17. Marami B, Sirouspour S, Ghoul S, et al. Elastic registration of prostate MR images based on estimation of deformation states. *Medical Image Analysis*. 2015;21(1):87–103.

18. Toth R, Sperling D, Madabhushi A. Quantifying Post- Laser Ablation Prostate Therapy Changes on MRI via a Domain-Specific Biomechanical Model: Preliminary Findings. *PLOS ONE*. 2016;11(4):e0150016.

19. Orczyk C, Rusinek H, Rosenkrantz AB, et al. Preliminary experience with a novel method of three-dimensional co-registration of prostate cancer digital histology and in vivo multiparametric MRI. *Clinical Radiology*. 2013;68(12):e652–e658.

20. Oto A, Sethi I, Karczmar G, et al. MR Imaging-guided Focal Laser Ablation for Prostate Cancer: Phase I Trial. *Radiology*. 2013.

21. Taneja SS, Bennett J, Coleman J, et al. Final Results of a Phase I/II Multicenter Trial of WST11 (TOOKAD® Soluble) Vascular-Targeted Photodynamic Therapy (VTP) for

Hemiablation of the Prostate in Men with Unilateral Low Risk Prostate Cancer Conducted in the United States. *J. Urol*. 2016.

22. Hajnal JV, Saeed N, Oatridge A, et al. Detection of subtle brain changes using subvoxel registration and subtraction of serial MR images. *J Comput Assist Tomogr*. 1995;19(5):677–691.

23. Lemieux L, Wieshmann UC, Moran NF, et al. The detection and significance of subtle changes in mixed-signal brain lesions by serial MRI scan matching and spatial normalization. *Med Image Anal*. 1998;2(3):227–242.

24. Woods RP, Grafton ST, Holmes CJ, et al. Automated image registration: I. General methods and intrasubject, intramodality validation. *J Comput Assist Tomogr*. 1998;22(1):139–152.

25. Woods RP, Grafton ST, Watson JD, et al. Automated image registration: II. Intersubject validation of linear and nonlinear models. *J Comput Assist Tomogr*. 1998;22(1):153–165.

26. Collignon A, Maes F, Delaere D, et al. Automated multi-modality image registration based on information theory. *In: Bizais*. 1995.

27. Maes F, Collignon A, Vandermeulen D, et al. Multimodality image registration by maximization of mutual information. *IEEE Trans Med Imaging*. 1997;16(2):187–198.

28. Viola P, Wells WM. Alignment by maximization of mutual information. In: *, Fifth International Conference on Computer Vision, 1995. Proceedings.*; 1995:16–23.

29. Wells WM 3rd, Viola P, Atsumi H, et al. Multi-modal volume registration by maximization of mutual information. *Med Image Anal*. 1996;1(1):35–51.

30. Park B, Mikheev A, Zaim Wadghiri Y, et al. Optimal target VOI size for accurate 4D coregistration of DCE-MRI. In: Vol 9788.; 2016:97881P–97881P–8. Available at: http://dx.doi.org/10.1117/12.2214675. Accessed April 19, 2016.

31. Gibson E, Crukley C, Gaed M, et al. Registration of prostate histology images to ex vivo MR images via strand-shaped fiducials. *J Magn Reson Imaging*. 2012;36(6):1402–1412.

32. Patel P, Chappelow J, Tomaszewski J, et al. Spatially weighted mutual information (SWMI) for registration of digitally reconstructed ex vivo whole mount histology and in vivo prostate MRI. In: IEEE; 2011:6269–6272. Available at: http://ieeexplore.ieee.org.ezproxy.med.nyu.edu/xpls/abs_all.jsp?arnumber=6091547&tag=1. Accessed March 2, 2012.

33. Hawkes DJ, Barratt D, Blackall JM, et al. Tissue deformation and shape models in image-guided interventions: a discussion paper. *Medical Image Analysis*. 2005;9(2):163–175.

34. Hu Y, Carter T, Ahmed H, et al. Modelling Prostate Motion for Data Fusion during Image-guided Interventions. *IEEE Trans Med Imaging*. 2011. Available at: http://www.ncbi.nlm.nih.gov/pubmed/21632296. Accessed July 12, 2011.

35. Hu Y, Morgan D, Ahmed HU, et al. A statistical motion model based on biomechanical simulations for data fusion during image-guided prostate interventions. *Med Image Comput Comput Assist Interv*. 2008;11(Pt 1):737–744.

36. Mitra J, Kato Z, Martí R, et al. A spline-based non-linear diffeomorphism for multimodal prostate registration. *Medical Image Analysis*. 2012;16(6):1259–1279.

37. Rouvière O, Glas L, Girouin N, et al. Prostate cancer ablation with transrectal high-intensity focused ultrasound: assessment of tissue destruction with contrast-enhanced US. *Radiology*. 2011;259(2):583–591.

38. Barret E, Harvey-Bryan K-A, Sanchez-Salas R, et al. How to diagnose and treat focal therapy failure and recurrence?: *Current Opinion in Urology*. 2014;24(3):241–246.

39. Muller BG, Fütterer JJ, Gupta RT, et al. The role of magnetic resonance imaging (MRI) in focal therapy for prostate cancer: recommendations from a consensus panel: Role of MRI in focal therapy for prostate cancer. *BJU International*. 2014;113(2):218–227.

40. De Visschere PJ, De Meerleer GO, Fütterer JJ, et al. Role of MRI in follow-up after focal therapy for prostate carcinoma. *AJR Am J Roentgenol*. 2010;194(6):1427–1433.

41. Del Vescovo R, Pisanti F, Russo V, et al. Dynamic contrast-enhanced MR evaluation of prostate cancer before and after endorectal high-intensity focused ultrasound. *Radiol Med*. 2013;118(5):851–862.

42. Muller BG, van den Bos W, Pinto PA, et al. Imaging modalities in focal therapy: patient selection, treatment guidance, and follow-up. *Current Opinion in Urology*. 2014;24(3):218–224.

43. Ven WJM, Hulsbergen–van de Kaa CA, Hambrock T, et al. Simulated required accuracy of image registration tools for targeting high-grade cancer components with prostate biopsies. *European Radiology*. 2012;23(5):1401–1407.

44. Shah TT, Kasivisvanathan V, Jameson C, et al. Histological outcomes after focal high-intensity focused ultrasound and cryotherapy. *World J Urol*. 2015:1–10.

45. Mozer P, Baumann M, Chevreau G, et al. Mapping of transrectal ultrasonographic prostate biopsies: quality control and learning curve assessment by image processing. *J Ultrasound Med*. 2009;28(4):455–460.

46. Engelhard K, Kühn R, Osten A, et al. Impact of magnetic resonance imaging-guided prostate biopsy in the supine position on the detection of significant prostate cancer in an inhomogeneous patient cohort. *Scand J Urol*. 2016;50(2):110–115.

47. Ukimura O, Gross ME, de Castro Abreu AL, et al. A novel technique using three-dimensionally documented biopsy mapping allows precise re-visiting of prostate cancer foci with serial surveillance of cell cycle progression gene panel: Re-Visiting Biopsy From Known Prostate Cancer. *The Prostate*. 2015;75(8):863–871.

48. Ghai S, Trachtenberg J. Prostate cancer: A consensus on trial design for focal therapy. *Nat Rev Urol*. 2014;11(4):190–192.

49. Natarajan S, Raman S, Priester AM, et al. Focal Laser Ablation of Prostate Cancer: Phase I Clinical Trial. *The Journal of Urology*. 2016;196(1):68–75.

50. Lencioni R, de Baere T, Martin RC, et al. Image-Guided Ablation of Malignant Liver Tumors: Recommendations for Clinical Validation of Novel Thermal and Non-Thermal Technologies - A Western Perspective. *Liver Cancer*. 2015;4(4):208–214.

51. Singla N, Gahan J. New technologies in tumor ablation. *Curr Opin Urol*. 2016;26(3):248–253.

Table 1: Distribution of prostate volumes estimated from T2W images acquired before and after ablation (late control) and distribution of volume of ablated zone (AZ).

	Prostate volume from T2W images			Ablated Volume (cc) from DCE MRI
	Initial volume (cc)	Post-ablation volume (cc)	Difference D (cc)	
median	51.64	46.73	6.70	7.88
mean	46.49	39.99	6.50	13.82
SD	23.67	20.25	7.05	13.67
min	8.42	6.80	-3.60	1.07
max	87.16	65.52	21.64	37.35

Table 2. Comparison of volumes between original T2 WI and their transform using rigid and deformable methods.

	Transformed Volumes	
	Rigid Preop Transform volume (cc)	Deformable Preop Transform volume (cc)
median	50.71	48.22
mean	45.41	43.23
SD	22.81	21.17
min	7.99	7.17
max	81.02	73.67

Table 3: Alignment between whole gland obtained by mapping from pre-operative to post-operative T2W image and whole gland traced directly on post-operative image: comparison between rigid and affine coregistrations.

	Rigid registration *Tr*	Affine registration *Ta*
	Hausdorff distance (mm)	
median	7.73	7.29
mean	8.14	6.91
max	9.46	9.98
min	5.31	4.64
SD	1.45	1.60
p value	p=0.20	
	Dice index	
mean	0.82	0.84
median	0.85	0.85
max	0.91	0.92
min	0.68	0.72
SD	0.08	0.06
p value	p=0.10	

Table 4. Compensation of the local deformation by affine algorithm: comparison between mapping accuracy of the location of the ablated zone and the whole gland, referring to measures shown in figure 6 C.

	Ta(AZ) vs *Tr* (AZ)	*Ta*(M) vs *Tr* (M)
	Hausdorff distance (mm)	
median	1.99	3.83
mean	2.99	3.84
max	6.25	7.05
min	1.10	1.10
SD	2.10	2.21
	Normalized Hausdorff distance (mm/ml)	
mean	0.72	0.15
median	0.22	0.09
max	1.09	0.55
min	0.05	0.03
sd	0.57	0.17
p value	**p=0.0019**	
	Dice index	
mean	0.87	0.93
median	0.87	0.92
max	0.96	0.98
min	0.59	0.88
SD	0.11	0.04
p value	**p=0.046**	

Figure1
Click here to download high resolution image

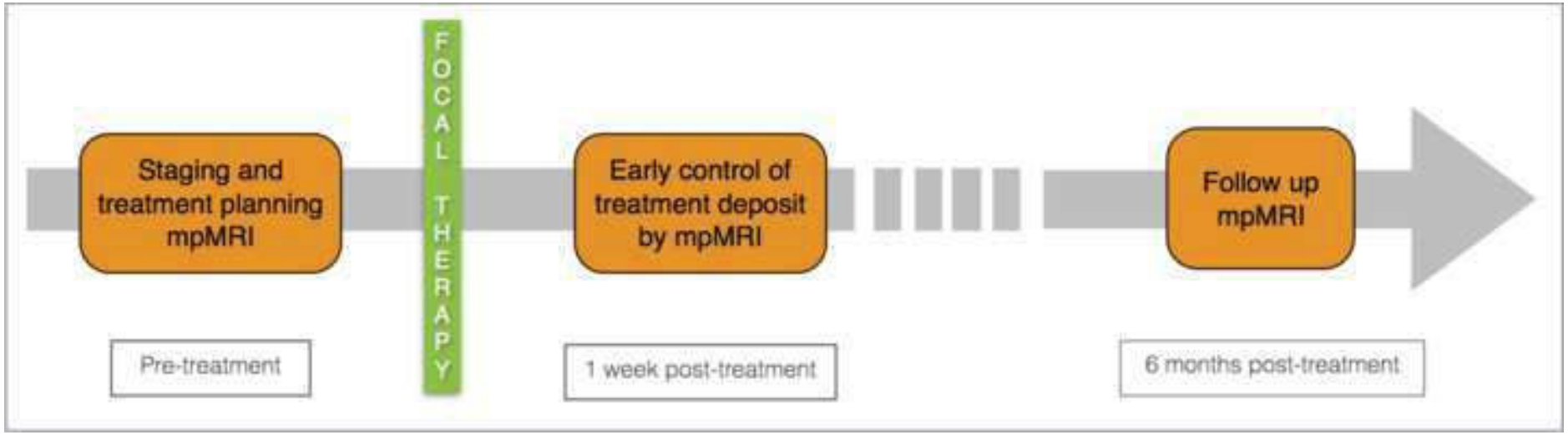

Figure2
Click here to download high resolution image

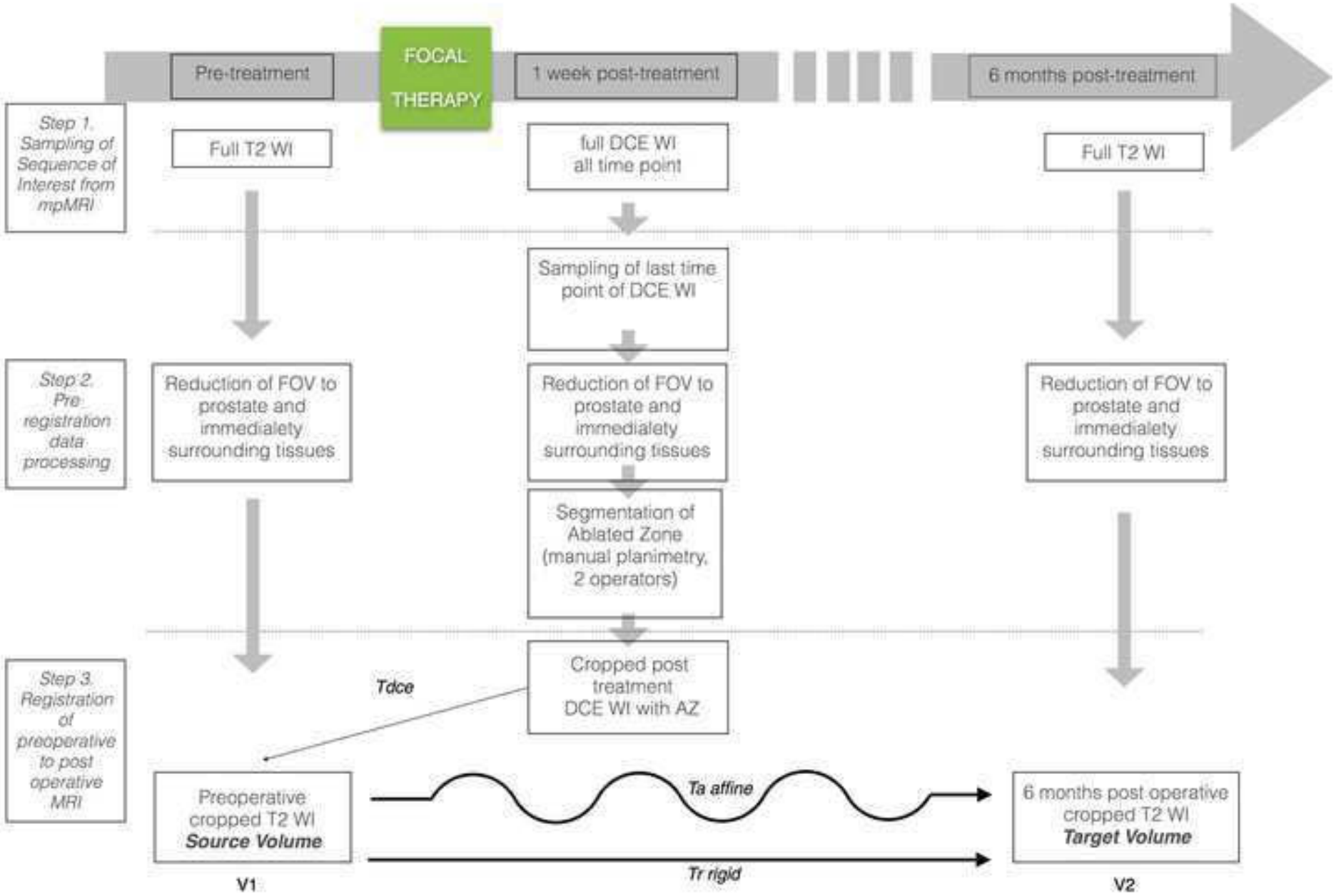

Figure3
Click here to download high resolution image

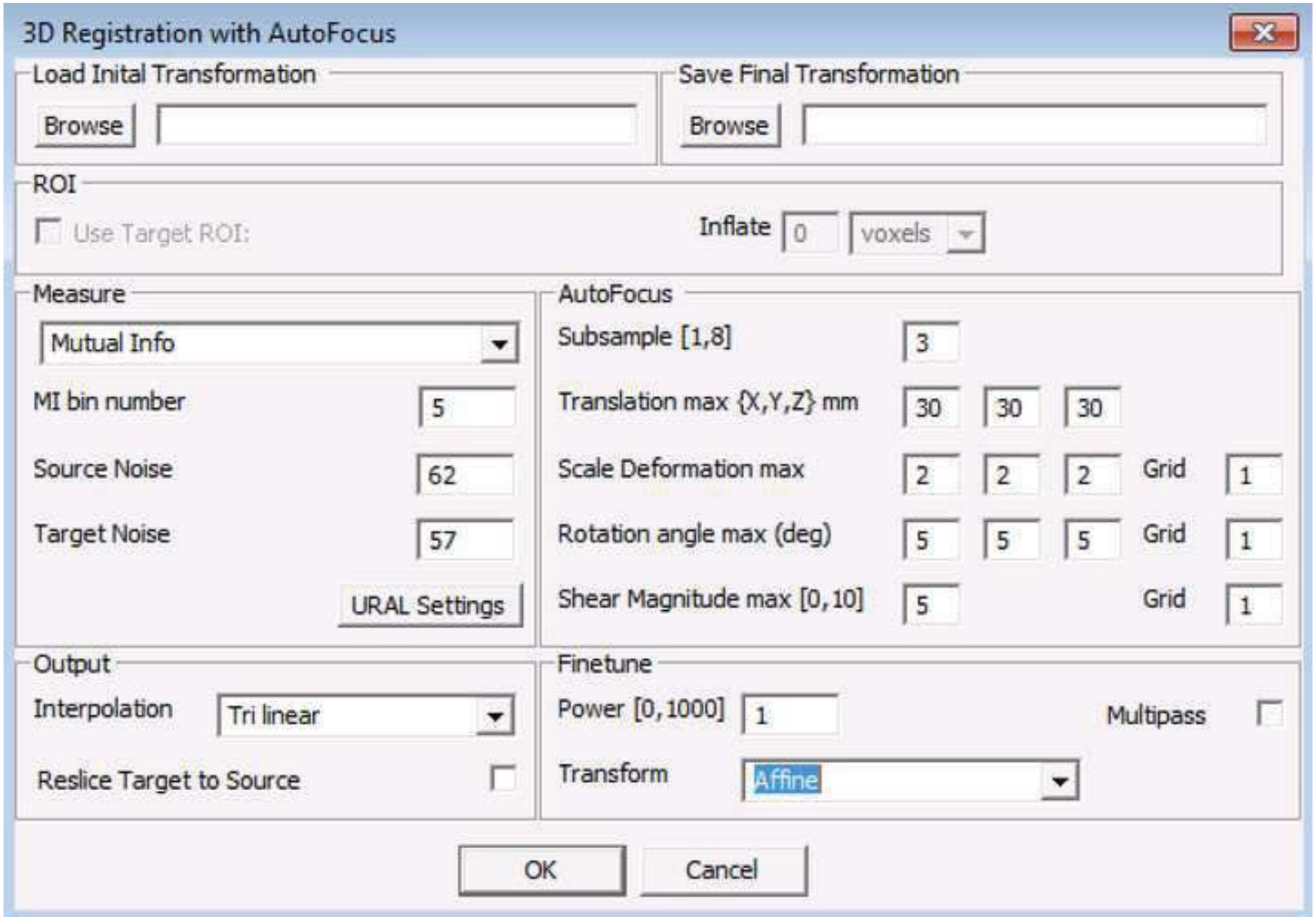

Figure4

Click here to download high resolution image

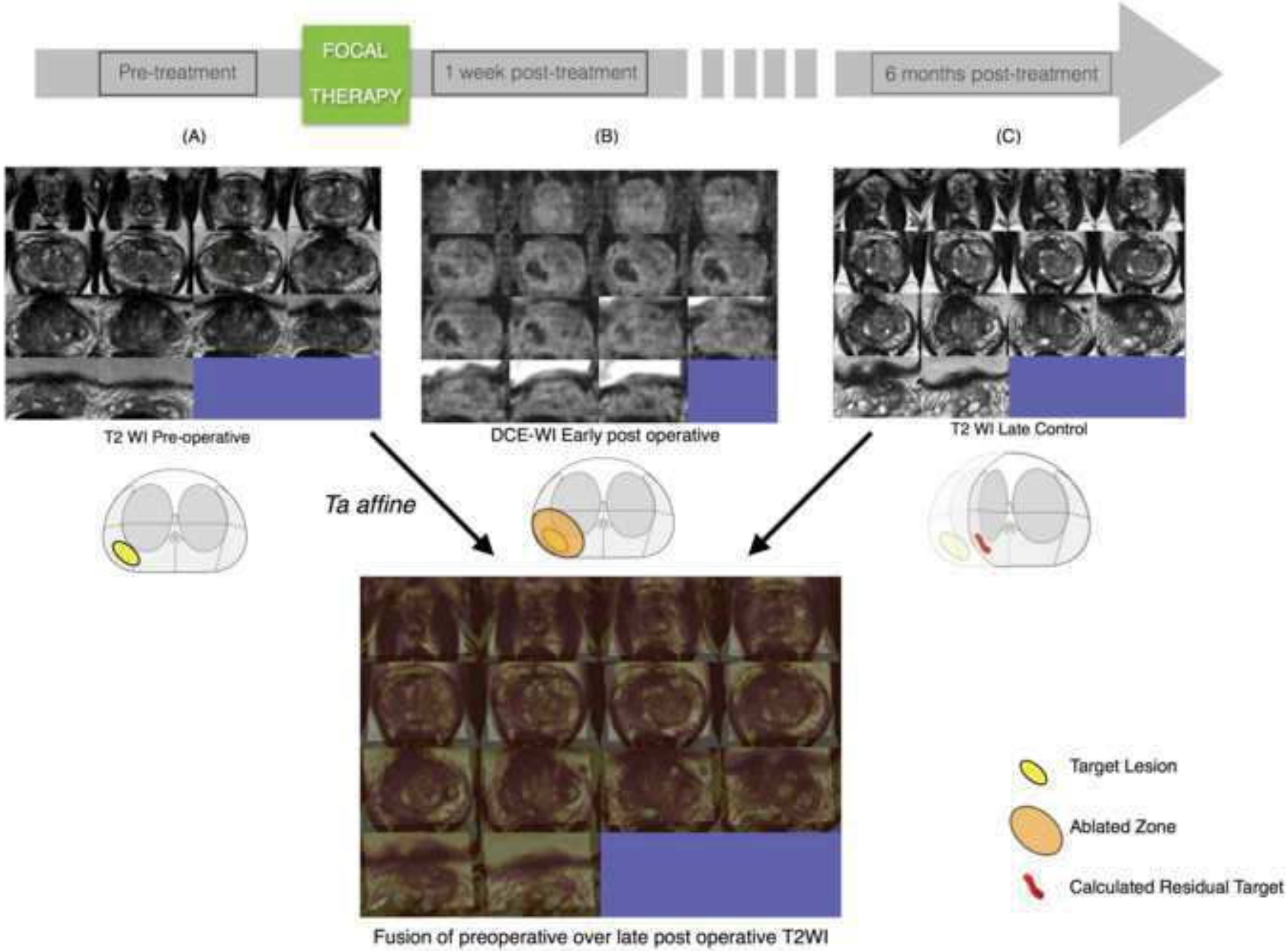

Figure5

Click here to download high resolution image

Figure6
Click here to download high resolution image

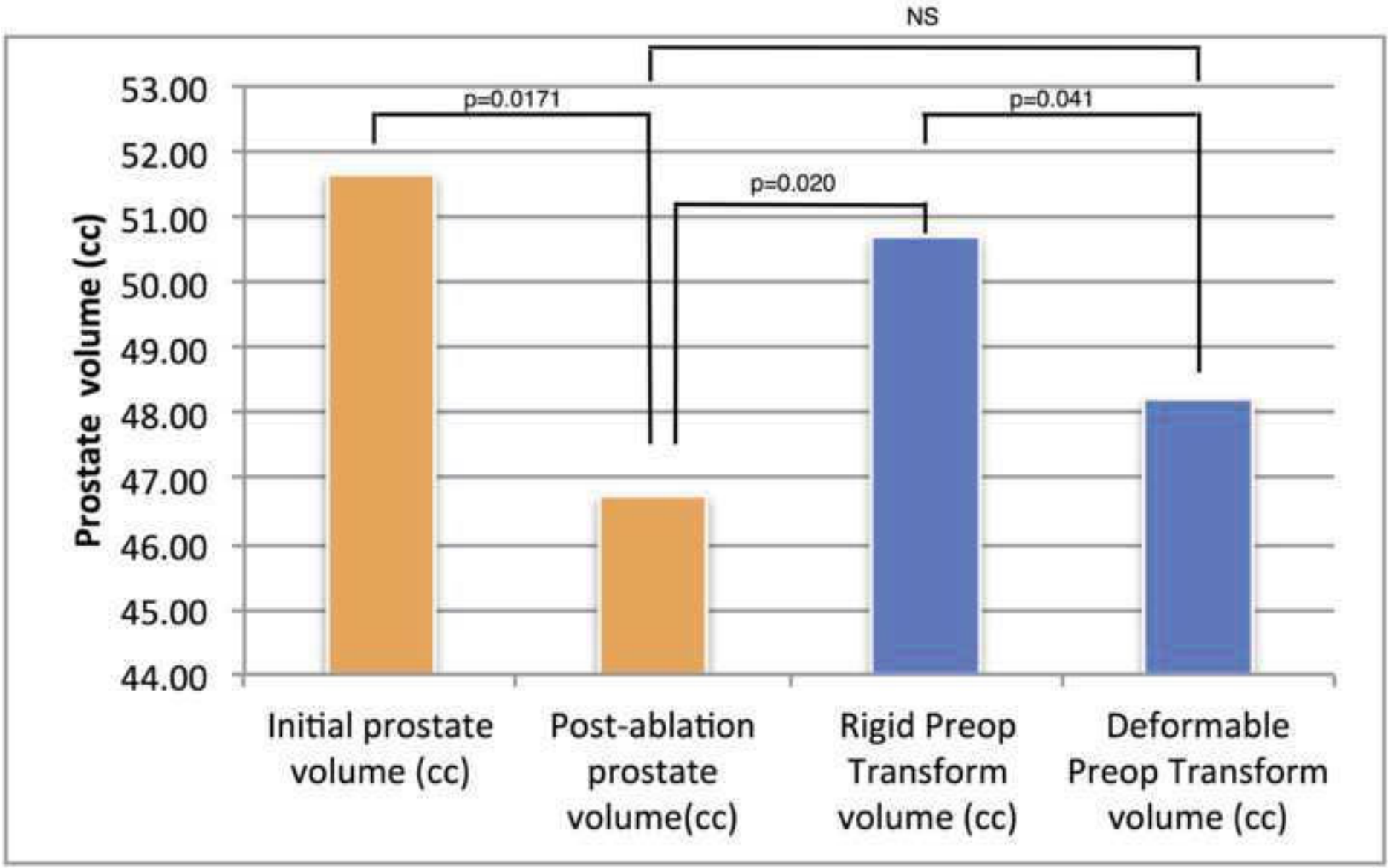

Figure7
Click here to download high resolution image

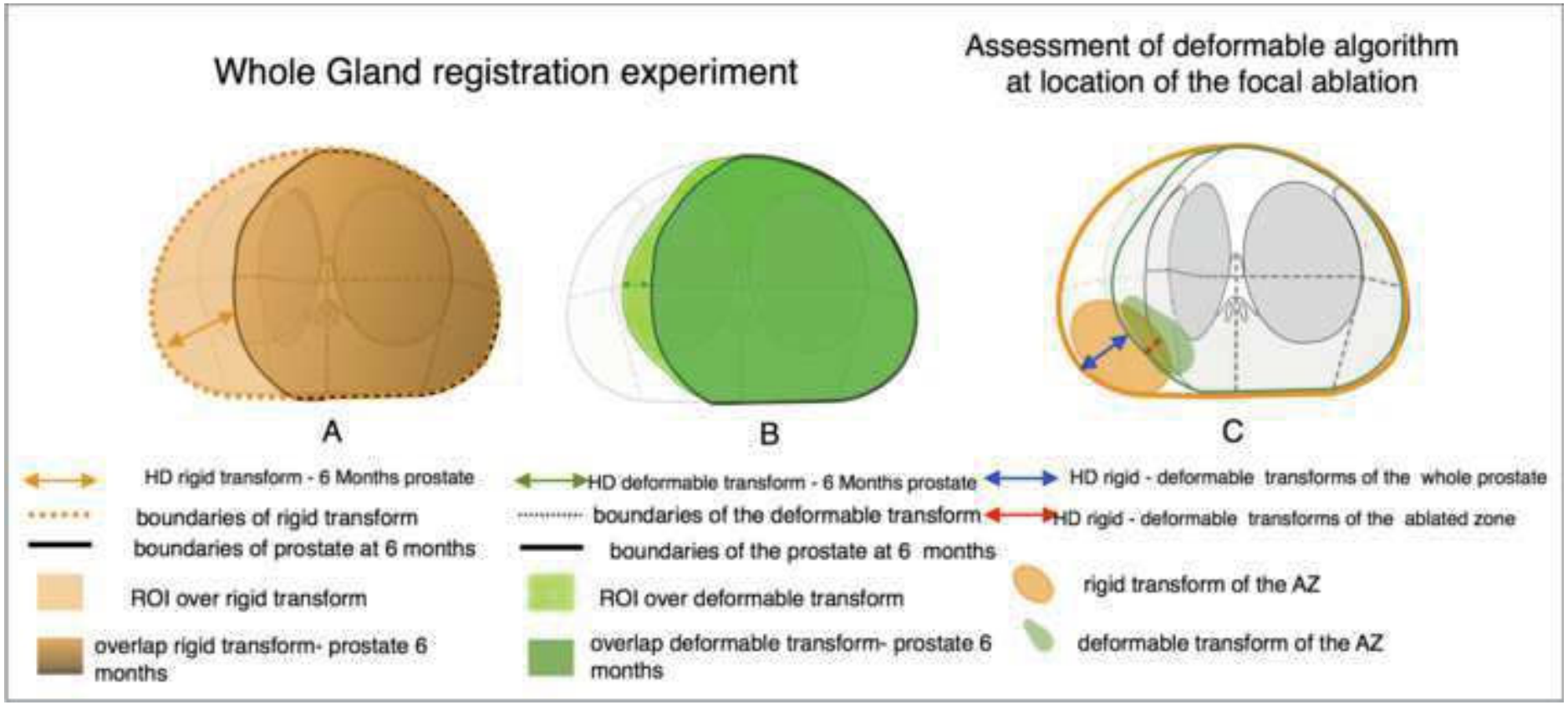

Figure8

Click here to download high resolution image

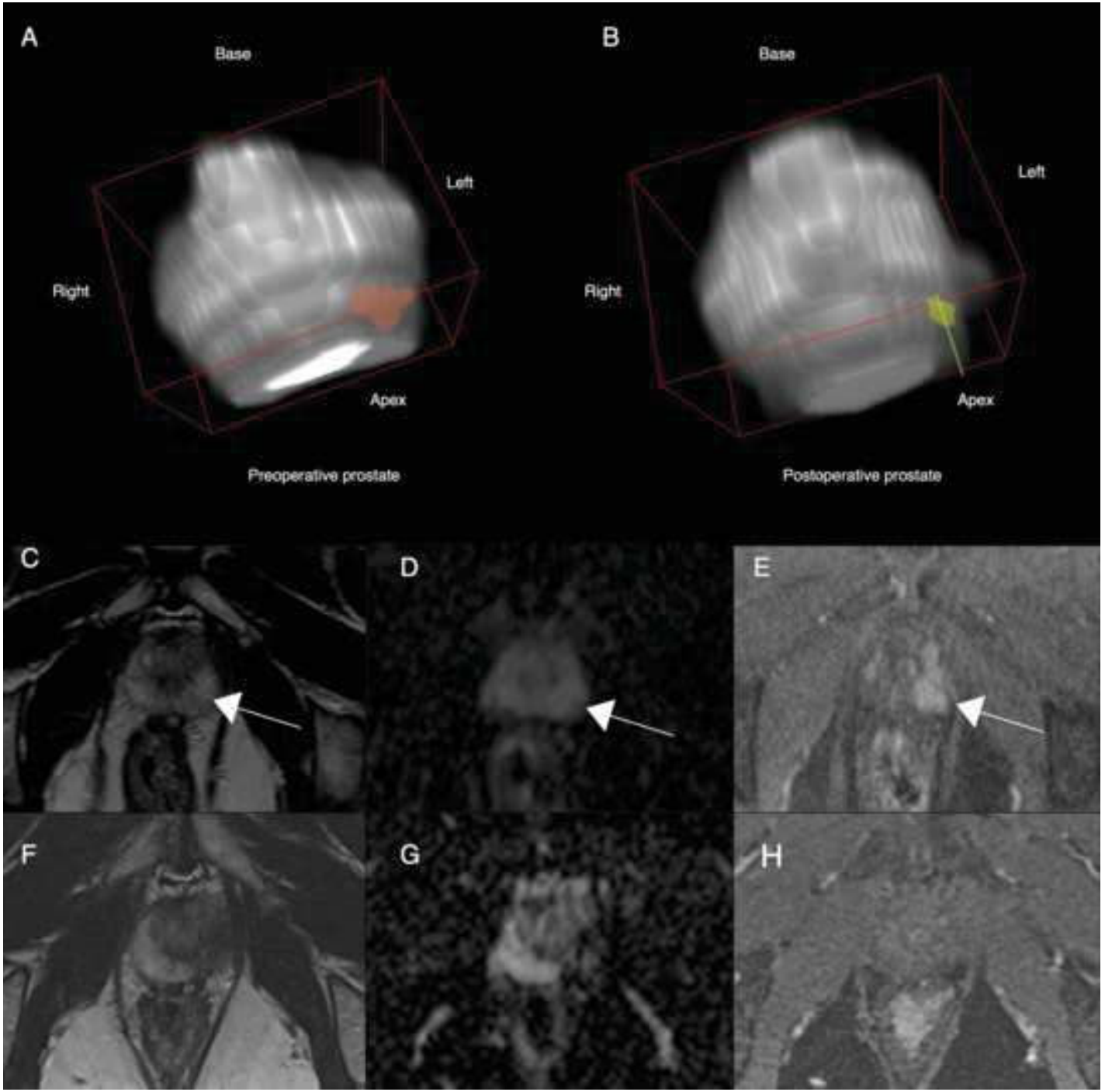

Figure9
Click here to download high resolution image

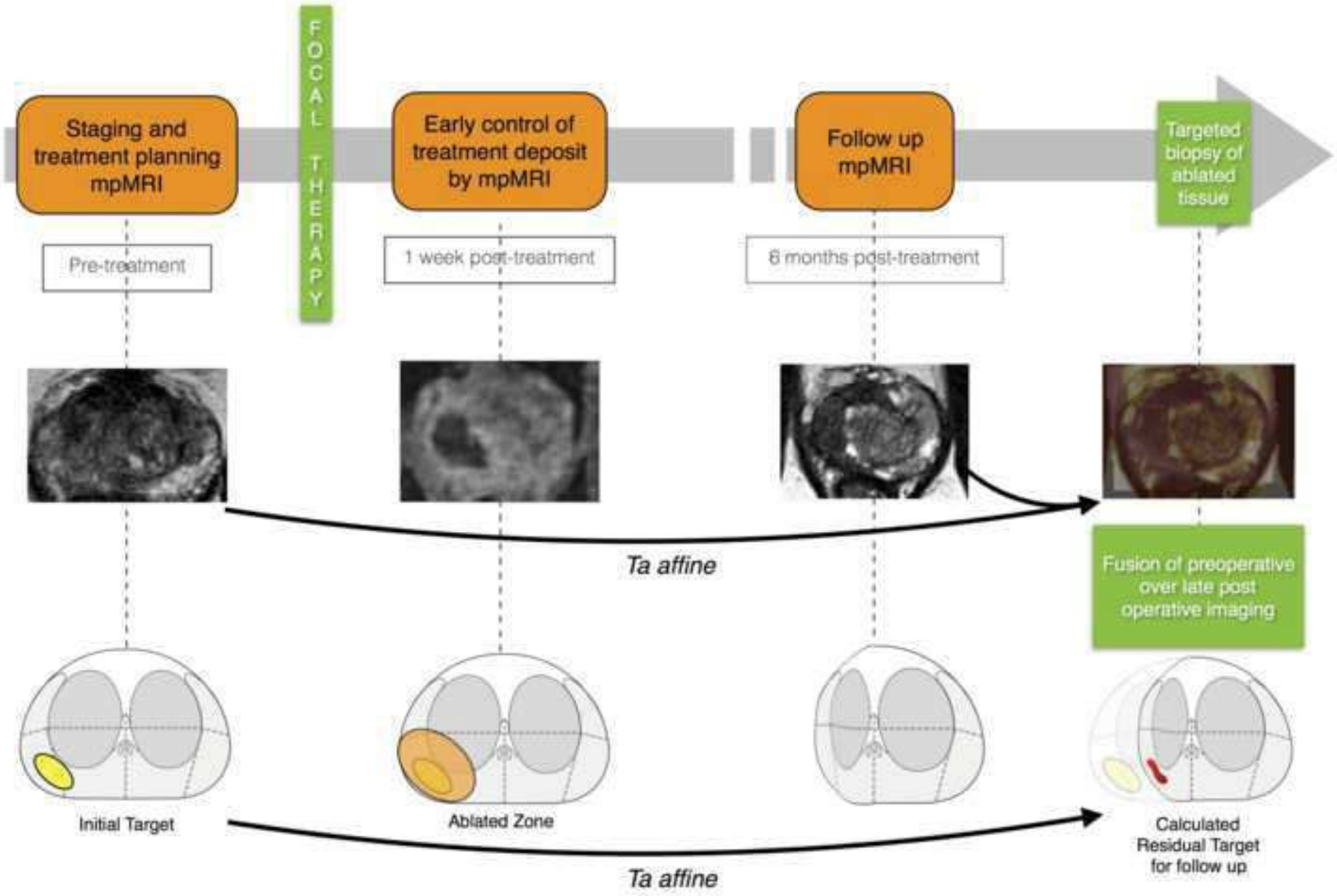

Synthèse et Perspectives

Synthèse :

Ce travail basé sur l'implémentation d'un test radiologique dans un environnement chirurgical, urologique, s'est axé sur l'utilisation de méthodes, des outils de recalage fusion et traitement d'image pour permettre une approche contrôlée et quantifiée des résultats radiologiques en termes de détection, de stratification et suivi oncologique du cancer de la prostate.

En partant du modèle histologique post chirurgie, il a été montré que la prostate est un organe plastique et hétérogène. Les modélisations proposées ont montré leur pertinence dans des études rétrospectives, principalement après chirurgie ou la biopsie. Cette pertinence nécessité confirmation pour une utilisation en clinique de routine ou lors d'essais clinique prospectifs.

Une étape de validation in vivo apparaît donc nécessaire de manière prospective lors d'essai clinique.

Les perspectives de cette thèse s'articulent autour des thèmes abordés de diagnostic et stratification, de traitement focal et de son planning chirurgical mais aussi sur l'histoire naturelle de la maladie elle-même.

Perspectives diagnostiques :

L'équipe de UCL est d'ores et déjà passée à une approche de biopsie ciblée exclusive par voie transpérinéale. Cette approche, l'utilisation de l'IRMmp de manière systématique ainsi que l'expérience acquise lors de cette thèse en analyse d'image suscitent plusieurs questions sur la définition de la cible biopsique (et potentiellement thérapeutique) et la dimension pronostique de celle-ci.

Définition de la cible biopsique :

Il est apparu lors des travaux sur l'imagerie qu'une lésion présente une hétérogénité intrasèque que l'imagerie est à même de détecter et de localiser dans l'espace.

Signification des « hot spots » fonctionnels de l'imagerie :

Les différentes cartographies quantitatives issues de l'IRMmp présentent une hétérogénité avec des « sous-lésions » au sein d'une lésion présentant une valeur quantitative potentiellement plus extrêmes traduisant virtuellement une agressivité plus importantes. Par exemple, l'ADC est connu comme négativement corrélé au Score de Gleason. Quelle serait la valeur de biopsie directement dirigée non pas sur la lésion mais sur ces zones démontrant ces valeurs, limitant de biais d'échantillonage d'une lésion ?

Une analyse rétrospective des données de l'essai clinique PROMIS est en cours. Dans cet essai tous les patients, naïfs de biopsie, ont été soumis à une IRMmp avant une biopsie en saturation par voie transperineale tous les 5 mm (test index) et une biopsie classique par voie transrectale. Une carte histologique basée sur la reconstruction 3D des biopsies transpérinéales est recalée à l'IRMmp selon une plateforme logicielle.

Les outils de recalage d'image développés dans cette thèse sont utilisés pour tenter de trouver un intérêt à ces « hot spots » en termes de détection et de stratégie biopsique.

En cas de positivé de la relation entre ces hot spots et l'histologie pour la stratification du cancer, un essai clinique prospectif de validation sera envisagé.

Approche morphométrique des lésions IRMmp :

La même population de l'étude PROMIS est actuellement en cours d'étude pour la planification biopsique : que doit-on viser avec la biopsie ciblée, quel densité échantilonage doit être réalisée ?

Un foyer cancéreux prostatique est hétérogène. Au sein d'une lésion coexistent plusieurs patterns de grade de Gleason différents. Doit-on viser le centre d'une lésion pour obtenir le grade le plus agressif ?

Une première analyse qui sera présenté au congrès de l'AUA à Boston en mai 2017 suggère que le centroïde de la lésion IRM ne contient pas la carotte biopsique présentant le score de Gleason le plus élévé et la longueur maximale de cancer.

Des analyses morphométriques complémentaires sont en cours et pourrait déboucher sur un essai clinique prospectif.

Perspectives de stratification et pronostiques :

Imagerie comme biomarqueur du cancer de la prostate ?

Le score visuel de suspicion d'une lésion IRM, qu'il soit sur l'échelle PIRADS 2 ou Likert, présente une probabilité de présence de cancer significatif. Les scores 3 restent problématiques présentant entre 20 et 40% de cancer significatifs (en fonction des définitions) et représentent la majorité des lésions IRM(86). Aussi, certaines lésions de score 4 ou 5 reviennent négatives pour cancer après biopsie dirigées, posant la question clinique du faux positif de l'IRMmp ou du faux négatif des biopsies.

L'analyse de texture décrite dans ce travail avec le Score d'Entropie pourrait présenter un intérêt pour la sélection des lésions à biopsier et conforter la décision du clinicien dans le choix du suivi de faux positifs de l'IRMmp.

L'intégration de ces données à un système de « Computer Assisted Diagnosis » pourrait permettre un aide au diagnostic. L'utilité clinique serait à vérifier lors dans une population diagnostique, confronté à l'expertise de radiologique.

L'analyse de texture, simple dans ce travail puisque de 1er ordre, soulève aussi la question du phénomène sous-jacent. S'agit-il de la traduction à l'imagerie d'une structure histologique, d'un processus fonctionnel, biomoléculaire ou alors de nouvelle propriété participant au pronostic du patient ?

Un récent consensus européen (66) faisant écho au FDA–NIH Biomarker Working Group propose une feuille de route détaillée pour l'émergence et la validation de l'imagerie en tant que biomarqueur. La corrélation à l'histologie et biologie moléculaire ainsi que le traitement d'image tiennent une place de premier ordre dans ces futures investigations, regroupées sous le terme de « radiogenomics ».

Des travaux de validation externe des travaux de cette thèse sur une population plus large doivent être réalisés pour d'abord passer l'étape de validation comme un potentiel sujet de recherche clinique.
Ceci devrait s'intégrer dans un programme de recherche plus large sur l'utilisation des outils d'imagerie en tant que biomarqueur.

Histoire naturelle du cancer de prostate et imagerie, vers de nouvelles définitions ? :

Les classifications pronostiques (D'Amico(87)) et nomogrammes (tables de Partin(88)ou nomogram du MSKCC (89)), couramment utilisés comme outils de prediction clinique ne tiennent pas compte des nouvelles données de l'IRM.

De récent travaux (90) intègrent l'IRM dans la prédiction de récidive après traitement local à moyen terme en montrant un avantage sur les modèles originaux. Ceci indique le potentiel prédictif de l'IRMmp.

Les définitions originales de maladie significatives selon Epstein et Stamey (6,91) devraient être revisitées à la lumière des caractéristiques IRM des lésions ou leur absence. Ceci nécessite de larges cohortes avec un suivi significativement long pour refléter l'histoire naturelle du cancer de la prostate.

Des travaux rétrospectifs ont été initiés à UCL sur une série d'environ 5000

patients ayant eu une IRM avec séquence(s) fonctionnelle(s) sur la période 2007-2015.

Les futurs travaux de recherche translationnelle et clinique s'attacheront donc à combiner les approches diagnostique et pronostique pour affiner le risque d'un patient de présenter une maladie potentiellement significative et s'ouvrant sur approche individualisée du traitement.

Perspectives thérapeutiques :

Détermination de la cible thérapeutique pour la thérapie focale :

Indépendamment de nature l'énergie utilisée pour réaliser la thérapie focale, cette nouvelle stratégie de traitement et son succès, tant fonctionnel qu'oncologique, dépend de la précision du planning thérapeutique et de la cible.

Les travaux de cette thèse et subséquents (92) ont montré une différence entre le volume à l'imagerie en séquence pondérée T2 et la cartographie ADC. Une première approche des marges autour d'une lésion a été proposée en utilisant les specimen de prostatectomies comme référence.

Cependant, ces travaux souffrent du biais du test index, le specimen de prostatectomie totale. En effet, il existe un bais de sélection des patients recevant ce traitement radical avec une maladie potentiellement plus agressive, spécifiquement dans les centres proposant thérapie focale et surveillance active. L'agressivité du cancer a montré être corrélée avec une différence de volume IRM-histologie (92,93) dont la direction reste controversée. De plus, il s'agit d'un test ex vivo avec une réponse a posteriori.

C'est pourquoi, la même population de l'étude PROMIS décrite ci-dessus est aussi étudiée sous l'angle de la marge de tissu cancéreux autour d'une lésion IRM. Outre la robustesse de la sélection de la population, le test de référence est in vivo et potentiellemnt reflète ce qui peut être atteint par biopsie. Les résultats initiaux de

corrélation à l'imagerie anatomique pondéree T2 seront présentés au congrès de l'AUA à Boston en mai 2017. L'étude en cours des séquences fonctionnelles correspond au second volet de l'analyse et s'appuie directement sur les travaux de cette thèse.

L'implication en termes de succès oncologique des marges autour d'une zone à traiter (temps avant récidive, survie sans re-traitement ou autre thérapie) sera à évaluer. La forme de l'évaluation reste à déterminer, s'offrant la possibilité de registres prospectifs ou d'un essai clinique.

Surveillance active, vers l'imagerie comme biomarqueur ?

La récente parution des recommandations sur l'utilisation de l'IRMmp en surveillance active (The PRECISE recommandations(94)) renforce l'utilisation de l'imagerie dans le suivi du cancer de la prostate.

Les techniques de recalage longitudinal développées dans ces thèses combinées avec des mesures quantitatives et de radiomique (comme l'entropie) pourrait permettre une standardisation quantitative du suivi de ces patients placés sous surveillance et définir la progression radiologique ou au contraire la stabilité par ce test non invasif d'imagerie.

L'application dans la cohorte de surveillance active de UCLH est envisagée.

Perspectives de terrains de recherche et professionnelles :

Les projets de recherche ci-dessus sont envisagés au sein de University College London, Department of Surgery and Interventional Sciences, et de University College London Hospitals, The prostate Unit, Department of Urology. Ces institutions universitaire et hospitalière ont démontré leur excellence dans leur partenariat sur la thématique du cancer de prostate.

Les possibilités de collaboration s'offrent dans des domaines de recherche et de soins variés de biologie moléculaire (Centre for Molecular Intervention (COMET)-

Dr Whitaker), de l'imagerie (Center for Medical Imaging-Dr Punwani) ou encore de l'ingénierie-traitement d'image (CMIC-Center for Medical Image Computing- Dr Barrat).

L'ouverture prochaine en 2017 à UCL d'un nouvelle entité « Center for Surgical and Interventional Sciences » sous la direction commune des Pr Ourselin et Pr Emberton ambitionne de regrouper problématique d'ingénierie et clinique. En particulier, le centre développera les sciences de l'ingénierie dans l'imagerie intraopératoire et dans la perception, la fusion et extraction de données, l'interface humain-technologie, la modélisation tissulaire, l'instrumentation et la navigation chirurgicale.

Il pourrait être proposé de rejoindre l'équipe de seniors par un poste partagé clinique /recherche –enseignement entre les deux institutions à part égale.

Les collaborations internationales développées et maintenues durant cette thèse seront approfondies.

Bibliographie :

1. Ferlay J, Soerjomataram I, Dikshit R, Eser S, Mathers C, Rebelo M, et al. Cancer incidence and mortality worldwide: sources, methods and major patterns in GLOBOCAN 2012. Int J Cancer. 1 mars 2015;136(5):E359‑86.

2. Binder-Foucard F, Bossard N, Delafosse P, Belot A, Woronoff A-S, Remontet L. Cancer incidence and mortality in France over the 1980–2012 period: Solid tumors. Revue d'Épidémiologie et de Santé Publique. avr 2014;62(2):95‑108.

3. McNeal JE. Normal histology of the prostate. Am J Surg Pathol. août 1988;12(8):619‑33.

4. Johansson JE, Andren O, Andersson SO, Dickman PW, Holmberg L, Magnuson A, et al. Natural history of early, localized prostate cancer. JAMA. 2004;291:2713‑9.

5. Epstein JI, Walsh PC, Carmichael M, Brendler CB. Pathologic and Clinical Findings to Predict Tumor Extent of Nonpalpable (Stage T1 c) Prostate Cancer. JAMA: The Journal of the American Medical Association. Février 1994;271(5):368‑74.

6. Stamey TA, Freiha FS, McNeal JE, Redwine EA, Whittemore AS, Schmid HP. Localized prostate cancer. Relationship of tumor volume to clinical significance for treatment of prostate cancer. Cancer. 1 févr 1993;71(3 Suppl):933‑8.

7. Franks LM. Latent carcinoma of the prostate. J Pathol. 1 oct 1954;68(2):603‑16.

8. Gleason DF. Classification of prostatic carcinomas. Cancer Chemother Rep. mars 1966;50(3):125‑8.

9. Epstein JI, Egevad L, Amin MB, Delahunt B, Srigley JR, Humphrey PA, et al. The 2014 International Society of Urological Pathology (ISUP) Consensus Conference on Gleason Grading of Prostatic Carcinoma: Definition of Grading Patterns and Proposal for a New Grading System. Am J Surg Pathol. févr 2016;40(2):244‑52.

10. Welch HG, Gorski DH, Albertsen PC. Trends in Metastatic Breast and Prostate Cancer — Lessons in Cancer Dynamics. New England Journal of Medicine. 29 oct 2015;373(18):1685‑7.

11. Hodge KK, McNeal JE, Stamey TA. Ultrasound guided transrectal core biopsies of the palpably abnormal prostate. J Urol. juill 1989;142(1):66‑70.

12. Walsh PC. Radical retropubic prostatectomy with reduced morbidity: an anatomic approach. NCI Monogr. 1988;(7):133‑7.

13. Salomon L, Bastide C, Beuzeboc P, Cormier L, Fromont G, Hennequin C, et al. Recommandations en onco-urologie 2013 du CCAFU : Cancer de la prostate. Progrès en Urologie. nov 2013;23, Supplement 2:S69‑101.

14. Schroder FH, Hugosson J, Roobol MJ, Tammela TL, Ciatto S, Nelen V, et al. Screening and prostate-cancer mortality in a randomized European study. N Engl J Med. 2009;360:1320‑8.

15. Andriole GL, Crawford ED, Grubb III RL, Buys SS, Chia D, Church TR, et al. Mortality results from a randomized prostate-cancer screening trial. New England Journal of Medicine.

2009;360(13):1310‑9.

16. More on Reevaluating PSA Testing Rates in the PLCO Trial. New England Journal of Medicine. 13 oct 2016;375(15):1500‑1.

17. Schröder FH, Hugosson J, Roobol MJ, Tammela TLJ, Zappa M, Nelen V, et al. Screening and prostate cancer mortality: results of the European Randomised Study of Screening for Prostate Cancer (ERSPC) at 13 years of follow-up. Lancet. 6 déc 2014;384(9959):2027‑35.

18. Heijnsdijk EAM, Wever EM, Auvinen A, Hugosson J, Ciatto S, Nelen V, et al. Quality-of-Life Effects of Prostate-Specific Antigen Screening. New England Journal of Medicine. 16 août 2012;367(7):595‑605.

19. Wilt TJ, Brawer MK, Jones KM, Barry MJ, Aronson WJ, Fox S, et al. Radical Prostatectomy versus Observation for Localized Prostate Cancer. New England Journal of Medicine. 2012;367(3):203‑13.

20. Hamdy FC, Donovan JL, Lane JA, Mason M, Metcalfe C, Holding P, et al. 10-Year Outcomes after Monitoring, Surgery, or Radiotherapy for Localized Prostate Cancer. New England Journal of Medicine. 13 oct 2016;375(15):1415‑24.

21. Bibbins-Domingo K, Grossman DC, Curry SJ. The US Preventive Services Task Force 2017 Draft Recommendation Statement on Screening for Prostate Cancer: An Invitation to Review and Comment. JAMA [Internet]. 11 avr 2017 [cité 30 avr 2017]; Disponible sur: http://jama.jamanetwork.com/article.aspx?doi=10.1001/jama.2017.4413

22. Noldus J, Graefen M, Haese A, Henke RP, Hammerer P, Huland H. Stage migration in clinically localized prostate cancer. European urology. 2000;38(1):74‑8.

23. Hu JC, Gu X, Lipsitz SR, Barry MJ, D'Amico AV, Weinberg AC, et al. Comparative effectiveness of minimally invasive vs open radical prostatectomy. JAMA. 14 oct 2009;302(14):1557‑64.

24. Sanda MG, Dunn RL, Michalski J, Sandler HM, Northouse L, Hembroff L, et al. Quality of life and satisfaction with outcome among prostate-cancer survivors. N Engl J Med. 20 mars 2008;358(12):1250‑61.

25. Cooperberg MR, Lubeck DP, Meng MV, Mehta SS, Carroll PR. The changing face of low-risk prostate cancer: trends in clinical presentation and primary management. J Clin Oncol. 2004;22:2141‑9.

26. Klotz L, Zhang L, Lam A, Nam R, Mamedov A, Loblaw A. Clinical results of long-term follow-up of a large, active surveillance cohort with localized prostate cancer. J Clin Oncol. 28:126‑31.

27. Carter HB, Kettermann A, Warlick C, Metter EJ, Landis P, Walsh PC, et al. Expectant management of prostate cancer with curative intent: an update of the Johns Hopkins experience. J Urol. 2007;178:2359‑64; discussion 2364‑5.

28. Duffield AS, Lee TK, Miyamoto H, Carter HB, Epstein JI. Radical prostatectomy findings in patients in whom active surveillance of prostate cancer fails. J Urol. 2009;182:2274‑8.

29. Kanthabalan A, Emberton M, Ahmed HU. Biopsy strategies for selecting patients for focal therapy for prostate cancer: Current Opinion in Urology. mai 2014;24(3):209‑17.

30. de la Rosette J, Ahmed H, Barentsz J, Johansen TB, Brausi M, Emberton M, et al. Focal therapy in prostate cancer-report from a consensus panel. J Endourol. mai 2010;24(5):775‑80.

31. Boccon-Gibod LM, de Longchamps NB, Toublanc M, Boccon-Gibod LA, Ravery V. Prostate saturation biopsy in the reevaluation of microfocal prostate cancer. J Urol. 2006;176:961‑3; discussion 963‑4.

32. Abraham NE, Mendhiratta N, Taneja SS. Patterns of repeat prostate biopsy in contemporary clinical practice. J Urol. avr 2015;193(4):1178‑84.

33. Ouzzane A, Puech P, Lemaitre L, Leroy X, Nevoux P, Betrouni N, et al. Combined Multiparametric MRI and Targeted Biopsies Improve Anterior Prostate Cancer Detection, Staging, and Grading. Urology. déc 2011;78(6):1356‑62.

34. Schiffmann J, Connan J, Salomon G, Boehm K, Beyer B, Schlomm T, et al. Tumor volume in insignificant prostate cancer: Increasing threshold gains increasing risk. Prostate. 4 oct 2014;

35. Orczyk C a, Emberton M a, Ahmed HU a. What tumours should we treat with focal therapy based on risk category, grade, size and location?. Current Opinion in Urology. mai 2015;25(3):212‑9.

36. Valerio M, Cerantola Y, Eggener SE, Lepor H, Polascik TJ, Villers A, et al. New and Established Technology in Focal Ablation of the Prostate: A Systematic Review. European Urology. janv 2017;71(1):17‑34.

37. Valerio M, Ahmed HU, Emberton M, Lawrentschuk N, Lazzeri M, Montironi R, et al. The Role of Focal Therapy in the Management of Localised Prostate Cancer: A Systematic Review. European Urology. oct 2014;66(4):732‑51.

38. Haffner J, Potiron E, Bouyé S, Puech P, Leroy X, Lemaitre L, et al. Peripheral zone prostate cancers: Location and intraprostatic patterns of spread at histopathology. Prostate. févr 2009;69(3):276‑82.

39. Bouye S, Potiron E, Puech P, Leroy X, Lemaitre L, Villers A. Transition zone and anterior stromal prostate cancers: zone of origin and intraprostatic patterns of spread at histopathology. Prostate. 2009;69:105‑13.

40. Nevoux P, Ouzzane A, Ahmed HU, Emberton M, Montironi R, Presti JC, et al. Quantitative tissue analyses of prostate cancer foci in an unselected cystoprostatectomy series. BJU Int. août 2012;110(4):517‑23.

41. Mouraviev V, Villers A, Bostwick DG, Wheeler TM, Montironi R, Polascik TJ. Understanding the pathological features of focality, grade and tumour volume of early-stage prostate cancer as a foundation for parenchyma-sparing prostate cancer therapies: active surveillance and focal targeted therapy. BJU Int. oct 2011;108(7):1074‑85.

42. Haffner J, Potiron E, Bouye S, Puech P, Leroy X, Lemaitre L, et al. Peripheral zone prostate cancers: location and intraprostatic patterns of spread at histopathology. Prostate. 2009;69:276‑82.

43. Villers A, McNeal JE, Freiha FS, Stamey TA. Multiple cancers in the prostate. Morphologic features of clinically recognized versus incidental tumors. Cancer. 1992;70:2313‑8.

44. Liu W, Laitinen S, Khan S, Vihinen M, Kowalski J, Yu G, et al. Copy number analysis indicates monoclonal origin of lethal metastatic prostate cancer. Nat Med. mai 2009;15(5):559‑65.

45. Villers A, Puech P, Mouton D, Leroy X, Ballereau C, Lemaitre L. Dynamic Contrast Enhanced, Pelvic Phased Array Magnetic Resonance Imaging of Localized Prostate Cancer for Predicting Tumor Volume: Correlation With Radical Prostatectomy Findings. The Journal of Urology. Décembre 2006;176(6):2432‑7.

46. Haffner J, Lemaitre L, Puech P, Haber G-P, Leroy X, Jones JS, et al. Role of magnetic resonance imaging before initial biopsy: comparison of magnetic resonance imaging-targeted and systematic biopsy for significant prostate cancer detection. BJU Int [Internet]. 22 mars 2011 [cité 24 mars 2011]; Disponible sur: http://www.ncbi.nlm.nih.gov/pubmed/21426475

47. Fütterer JJ, Briganti A, De Visschere P, Emberton M, Giannarini G, Kirkham A, et al. Can Clinically Significant Prostate Cancer Be Detected with Multiparametric Magnetic Resonance Imaging? A Systematic Review of the Literature. European Urology. déc 2015;68(6):1045‑53.

48. Lemaitre L, Puech P, Poncelet E, Bouye S, Leroy X, Biserte J, et al. Dynamic contrast-enhanced MRI of anterior prostate cancer: morphometric assessment and correlation with radical prostatectomy findings. Eur Radiol. 2009;19:470‑80.

49. Panebianco V, Barchetti F, Sciarra A, Ciardi A, Indino EL, Papalia R, et al. Multiparametric magnetic resonance imaging vs. standard care in men being evaluated for prostate cancer: a randomized study. Urol Oncol. janv 2015;33(1):17.e1‑7.

50. Dickinson L, Ahmed HU, Allen C, Barentsz JO, Carey B, Futterer JJ, et al. Magnetic resonance imaging for the detection, localisation, and characterisation of prostate cancer: recommendations from a European consensus meeting. Eur Urol. avr 2011;59(4):477‑94.

51. Wysock JS, Rosenkrantz AB, Huang WC, Stifelman MD, Lepor H, Deng F-M, et al. A Prospective, Blinded Comparison of Magnetic Resonance (MR) Imaging–Ultrasound Fusion and Visual Estimation in the Performance of MR-targeted Prostate Biopsy: The PROFUS Trial. European Urology [Internet]. [cité 29 nov 2013]; Disponible sur: http://www.sciencedirect.com/science/article/pii/S030228381301186X

52. Rosenkrantz AB, Kim S, Lim RP, Hindman N, Deng F-M, Babb JS, et al. Prostate Cancer Localization Using Multiparametric MR Imaging: Comparison of Prostate Imaging Reporting and Data System (PI-RADS) and Likert Scales. Radiology. 20 juin 2013;

53. Weinreb JC, Barentsz JO, Choyke PL, Cornud F, Haider MA, Macura KJ, et al. PI-RADS Prostate Imaging – Reporting and Data System: 2015, Version 2. European Urology. janv 2016;69(1):16‑40.

54. Hambrock T, Somford DM, Huisman HJ, van Oort IM, Witjes JA, Hulsbergen-van de Kaa CA, et al. Relationship between Apparent Diffusion Coefficients at 3.0-T MR Imaging and Gleason Grade in Peripheral Zone Prostate Cancer. Radiology [Internet]. 14 déc 2011 [cité 28 mars 2012]; Disponible sur: http://www.ncbi.nlm.nih.gov/pubmed/21406633

55. Hambrock T, Somford DM, Huisman HJ, van Oort IM, Witjes JA, Hulsbergen-van de Kaa

CA, et al. Relationship between apparent diffusion coefficients at 3.0-T MR imaging and Gleason grade in peripheral zone prostate cancer. Radiology. mai 2011;259(2):453‑61.

56. Verma S, Rajesh A, Morales H, Lemen L, Bills G, Delworth M, et al. Assessment of Aggressiveness of Prostate Cancer: Correlation of Apparent Diffusion Coefficient With Histologic Grade After Radical Prostatectomy. American Journal of Roentgenology. 21 janv 2011;196(2):374‑81.

57. Turkbey B, Shah VP, Pang Y, Bernardo M, Xu S, Kruecker J, et al. Is apparent diffusion coefficient associated with clinical risk scores for prostate cancers that are visible on 3-T MR images? Radiology. févr 2011;258(2):488‑95.

58. Rosenkrantz AB, Mendrinos S, Babb JS, Taneja SS. Prostate Cancer Foci Detected on Multiparametric Magnetic Resonance Imaging are Histologically Distinct From Those Not Detected. The Journal of Urology [Internet]. avr 2012 [cité 18 avr 2012]; Disponible sur: http://linkinghub.elsevier.com/retrieve/pii/S0022534712002054

59. Villers A, Puech P, Mouton D, Leroy X, Ballereau C, Lemaitre L. Dynamic Contrast Enhanced, Pelvic Phased Array Magnetic Resonance Imaging of Localized Prostate Cancer for Predicting Tumor Volume: Correlation With Radical Prostatectomy Findings. The Journal of Urology. Décembre 2006;176(6):2432‑7.

60. Verma S, Turkbey B, Muradyan N, Rajesh A, Cornud F, Haider MA, et al. Overview of Dynamic Contrast-Enhanced MRI in Prostate Cancer Diagnosis and Management. American Journal of Roentgenology. juin 2012;198(6):1277‑88.

61. Rosenkrantz AB, Taneja SS. Radiologist, be aware: ten pitfalls that confound the interpretation of multiparametric prostate MRI. AJR Am J Roentgenol. janv 2014;202(1):109‑20.

62. Tofts PS, Brix G, Buckley DL, Evelhoch JL, Henderson E, Knopp MV, et al. Estimating kinetic parameters from dynamic contrast-enhanced T(1)-weighted MRI of a diffusable tracer: standardized quantities and symbols. J Magn Reson Imaging. sept 1999;10(3):223‑32.

63. Langer DL, van der Kwast TH, Evans AJ, Plotkin A, Trachtenberg J, Wilson BC, et al. Prostate tissue composition and MR measurements: investigating the relationships between ADC, T2, K(trans), v(e), and corresponding histologic features. Radiology. mai 2010;255(2):485‑94.

64. Franiel T, Lüdemann L, Rudolph B, Rehbein H, Staack A, Taupitz M, et al. Evaluation of normal prostate tissue, chronic prostatitis, and prostate cancer by quantitative perfusion analysis using a dynamic contrast-enhanced inversion-prepared dual-contrast gradient echo sequence. Invest Radiol. juill 2008;43(7):481‑7.

65. Gillies RJ, Kinahan PE, Hricak H. Radiomics: Images Are More than Pictures, They Are Data. Radiology. 18 nov 2015;278(2):563‑77.

66. O'Connor JPB, Aboagye EO, Adams JE, Aerts HJWL, Barrington SF, Beer AJ, et al. Imaging biomarker roadmap for cancer studies. Nature Reviews Clinical Oncology. 11 oct 2016;14(3):169‑86.

67. Franiel T, Ludemann L, Rudolph B, Lutterbeck E, Hamm B, Beyersdorff D. Differentiation of prostate cancer from normal prostate tissue: role of hotspots in pharmacokinetic MRI and histologic evaluation. AJR Am J Roentgenol. 194:675‑81.

68. Rosenkrantz AB, Triolo MJ, Melamed J, Rusinek H, Taneja SS, Deng F-M. Whole-lesion apparent diffusion coefficient metrics as a marker of percentage Gleason 4 component within Gleason 7 prostate cancer at radical prostatectomy. J Magn Reson Imaging. 25 févr 2014;

69. Ahmed HU, Bosaily AE-S, Brown LC, Gabe R, Kaplan R, Parmar MK, et al. Diagnostic accuracy of multi-parametric MRI and TRUS biopsy in prostate cancer (PROMIS): a paired validating confirmatory study. The Lancet [Internet]. 19 janv 2017 [cité 20 janv 2017];0(0). Disponible sur: /journals/lancet/article/PIIS0140-6736(16)32401-1/abstract

70. Ahmed HU, Hu Y, Carter T, Arumainayagam N, Lecornet E, Freeman A, et al. Characterizing Clinically Significant Prostate Cancer Using Template Prostate Mapping Biopsy. The Journal of Urology. août 2011;186(2):458‑64.

71. Mozer P, Baumann M, Chevreau G, Moreau-Gaudry A, Bart S, Renard-Penna R, et al. Mapping of transrectal ultrasonographic prostate biopsies: quality control and learning curve assessment by image processing. J Ultrasound Med. avr 2009;28(4):455‑60.

72. Mazaheri Y, Bokacheva L, Kroon D-J, Akin O, Hricak H, Chamudot D, et al. Semi-automatic deformable registration of prostate MR images to pathological slices. J Magn Reson Imaging. nov 2010;32(5):1149‑57.

73. Hawkes DJ. Algorithms for radiological image registration and their clinical application. J Anat. oct 1998;193 (Pt 3):347‑61.

74. Soulié M, Portier G, Salomon L. Principes oncologiques du contrôle local de la tumeur primitive. Progrès en Urologie. nov 2015;25(15):918‑32.

75. Tewari A, Sooriakumaran P, Bloch DA, Seshadri-Kreaden U, Hebert AE, Wiklund P. Positive surgical margin and perioperative complication rates of primary surgical treatments for prostate cancer: a systematic review and meta-analysis comparing retropubic, laparoscopic, and robotic prostatectomy. Eur Urol. juill 2012;62(1):1‑15.

76. Ukimura O, Gill IS. Key to Successful Focal Therapy: Location, Location, Location. European Urology. avr 2012;

77. Schmid HP, McNeal JE. An abbreviated standard procedure for accurate tumor volume estimation in prostate cancer. Am J Surg Pathol. févr 1992;16(2):184‑91.

78. Orczyk C, Mikheev A, Rosenkrantz A, Melamed J, Taneja SS, Rusinek H. Imaging of prostate cancer: a platform for 3D co-registration of in-vivo MRI ex-vivo MRI and pathology. In 2012 [cité 2 sept 2012]. p. 83162M ‑ 83162M ‑ 13. Disponible sur: http://proceedings.spiedigitallibrary.org/proceeding.aspx?articleid=1285718

79. Epstein JI. Prognostic significance of tumor volume in radical prostatectomy and needle biopsy specimens. J Urol. sept 2011;186(3):790‑7.

80. Ahmed HU, Freeman A, Kirkham A, Sahu M, Scott R, Allen C, et al. Focal therapy for localized prostate cancer: a phase I/II trial. J Urol. avr 2011;185(4):1246‑54.

81. Shannon C. A Mathematical Theory of Communication. oct 1948;27:379‑423.

82. Maes F, Collignon A, Vandermeulen D, Marchal G, Suetens P. Multimodality image registration by maximization of mutual information. IEEE Trans Med Imaging. avr

1997;16(2):187‑98.

83. McNeal JE, Villers AA, Redwine EA, Freiha FS, Stamey TA. Histologic differentiation, cancer volume, and pelvic lymph node metastasis in adenocarcinoma of the prostate. Cancer. 1990;66:1225‑33.

84. Villers AA, McNeal JE, Freiha FS, Stamey TA. Development of prostatic carcinoma. Morphometric and pathologic features of early stages. Acta Oncol. 1991;30:145‑51.

85. Sala E, Mema E, Himoto Y, Veeraraghavan H, Brenton JD, Snyder A, et al. Unravelling tumour heterogeneity using next-generation imaging: radiomics, radiogenomics, and habitat imaging. Clinical Radiology. janv 2017;72(1):3‑10.

86. Rosenkrantz AB, Meng X, Ream JM, Babb JS, Deng F-M, Rusinek H, et al. Likert score 3 prostate lesions: Association between whole-lesion ADC metrics and pathologic findings at MRI/ultrasound fusion targeted biopsy: Whole-Lesion ADC Metrics in Likert 3 Prostate Lesions. Journal of Magnetic Resonance Imaging. févr 2016;43(2):325‑32.

87. D'Amico AV, Whittington R, Malkowicz SB, Schultz D, Blank K, Broderick GA, et al. Biochemical outcome after radical prostatectomy, external beam radiation therapy, or interstitial radiation therapy for clinically localized prostate cancer. Jama. 1998;280:969‑74.

88. Partin AW, Kattan MW, Subong EN, Walsh PC, Wojno KJ, Oesterling JE, et al. Combination of prostate-specific antigen, clinical stage, and Gleason score to predict pathological stage of localized prostate cancer. A multi-institutional update. JAMA. 1997;277:1445‑51.

89. Stephenson AJ, Scardino PT, Eastham JA, Bianco FJ, Dotan ZA, DiBlasio CJ, et al. Postoperative Nomogram Predicting the 10-Year Probability of Prostate Cancer Recurrence After Radical Prostatectomy. J Clin Oncol. 1 oct 2005;23(28):7005‑12.

90. Zhang Y-D, Wu C-J, Bao M-L, Li H, Wang X-N, Liu X-S, et al. MR-based prognostic nomogram for prostate cancer after radical prostatectomy. J Magn Reson Imaging. févr 2017;45(2):586‑96.

91. Epstein JI. Evaluation of radical prostatectomy capsular margins of resection. The significance of margins designated as negative, closely approaching, and positive. Am J Surg Pathol. juill 1990;14(7):626‑32.

92. Le Nobin J, Rosenkrantz AB, Villers A, Orczyk C, Deng F-M, Melamed J, et al. Image Guided Focal Therapy for Magnetic Resonance Imaging Visible Prostate Cancer: Defining a 3-Dimensional Treatment Margin Based on Magnetic Resonance Imaging Histology Co-Registration Analysis. The Journal of Urology. août 2015;194(2):364‑70.

93. Bratan F, Melodelima C, Souchon R, Hoang Dinh A, Mège-Lechevallier F, Crouzet S, et al. How accurate is multiparametric MR imaging in evaluation of prostate cancer volume? Radiology. avr 2015;275(1):144‑54.

94. Moore CM, Giganti F, Albertsen P, Allen C, Bangma C, Briganti A, et al. Reporting Magnetic Resonance Imaging in Men on Active Surveillance for Prostate Cancer: The PRECISE Recommendations-A Report of a European School of Oncology Task Force. Eur Urol. 24 juin 2016;

Annexe

CHUCaen

Protocole XXX*

Recherche observationnelle

TITRE : Etude préliminaire des paramètres quantitatifs de la perfusion en IRM prostatique en situation de pré-diagnostique pour la détection et stratification du cancer de la prostate

.....

.....

.....

INVESTIGATEUR(S) –COORDINATEUR(S)

Dr Clément Orczyk .....
Service D'urologie .....
CHU de CAEN
Tél : 02.31.06.58.07/06 22 48 26 44 .....
Fax : 02.31.06.49.47 .....
Mail :clementorczyk@yahoo.fr / orczyk-c@chu-caen.fr

INVESTIGATEURS – ASSOCIES

Dr Samuel Valable .....
UMR 6301-ISTCT, Equipe CERVOXy .....
GIP Cyceron
Tél : 02.31.47.01.08 .....
Fax : 02.31.47.02.22 .....
Mail :valable@cyceron.fr .....

☐ Version initiale V0	Date de la version V0 : .. / .. / ….
☐ Version amendée V	Date de la version V .... : .. / .. / ….
Si version amendée, objet de la modification substantielle :	
☐ Validation par le CPP Nord Ouest III	Date de validation : .. / .. / ….

***Acronyme**

HISTORIQUE DES MISES A JOUR DU PROTOCOLE

VERSION	DATE	RAISON DE LA MISE A JOUR
	.. / .. / ….	Soumis pour informations au CPP

SOMMAIRE – TABLE DES MATIERES

1. INFORMATIONS GENERALES

1.1 Investigateurs participants

- CHU de CAEN, Service d'Urologie
- UMR 6301 Imagerie et Stratégie Thérapeutique des pathologies Cérébrales et Tumorales- Equipe CERVOxy- GIP Cyceron-CNRS-CEA-Université de Caen

1.2 Pôle de recherche et d'épidémiologie clinique

Cellule de promotion de la recherche clinique, CHU Caen

M. F. CHAILLOT
Chargé des affaires réglementaires
CHU Côte de Nacre
14033 CAEN Cedex
☏ : 02 31 06 57 74
Courriel : chaillot-f@chu-caen.fr

1.3 Abréviations

IRM mp : Imagerie par Résonance Magnétique Multiparamétrique
PSA : Prostatic Specific Antigen

2. SYNOPSIS

Titre de l'étude	Etude préliminaire de l'apport des paramètres quantitatifs de l'imagerie de perfusion en IRM pour la détection et la stratification du cancer de la prostate en situation de pré diagnostique .....
Protocole	QDCEPROST
Investigateur coordinateur	Dr Clément Orczyk, 7 rue de la chaussée 14920 MATHIEU
Population concernée	Patients en situation de diagnostique du cancer de prostate par biopsie écho guidée de la prostate, chez qui a été indiqué une IRM prostatique
Objectifs de l'étude	Objectif <u>principal</u> : -Efficacité : Etablir a posteriori les valeurs quantitatives (Ktrans, Ve, Vp) de perfusion en IRM et leur hétérogénéité pour les zones cancéreuses ou non en intra et interpatient. Les résultats histologiques des biopsies sont le test de référence. .... Objectif(s) <u>secondaire</u>(s) : -Mesure de l'apport d'information par la perfusion en IRM par rapport à l'imagerie en diffusion et anatomique (T2) --Déterminer les caractéristiques d'une fonction d'entrée artérielle compatible avec la modélisation de paramètres quantitatifs ..... -comparaison de deux plateformes logicielles de modélisation de la perfusion - Amélioration de qualité du recalage de l'échographie lors des biopsies à l'IRM et évaluation in silico d'une nouvelle méthode de recalage d'image multimodale ....
Critères d'inclusion	-Patient (majeur) présentant une suspicion de cancer de la prostate ..... -Patients pour lequel des biopsies échoguidées de la prostate ont été réalisée -Suspicion adressée par l'urologue devant élévation du PSA et/ou un toucher rectal modifié et un traitement est envisagée ..... -Ayant une IRM prostatique au CHU de Caen .....
Critères de non-inclusion	-Patient présentant une IRM prostatique ne répondant pas aux séquences IRM exigées -Patient précédemment traité pour cancer de la prostate ..... -Patient traité pour une hypertrophie prostatique par Inhibiteur de la 5 αréductase.....
Critères d'évaluation / jugement	Principal : -Mesure du KTrans, Ve, Vp (Moyenne, Deviation standard, Médiane, Max) en

	zone cancéreuse et non cancéreuse (adénome, zone périphérique). Mesure de paramètres d'histogramme (Kurtosis, Skewness,) des valeurs quantitatives en fonction de l'agressivité (score de Gleason biopsique) du cancer ou de la bénignité..... Secondaire(s) : -- Mesure de paramètres d'histogramme reflétant l'heterogénéité (Kurtosis, Skewness, entropie) sur les différentes séquences d'IRM pour une région d'intérêt Mesure : de l'index de Dice et de la distance de Hausdorff après recalage de l'échographie sur l'IRM.
Définition des groupes si applicable	Un seul groupe-cohorte observationnelle
Nombre de patients	25 patients (1 groupe, chaque patient est son témoin): Différence de Ktrans de 0.05 min-1 Risque alpha de 5%, Puissance de 90 %, test bilatéral, non apparié
Nombre de centres	1centre : CHU de Caen
Agenda prévisionnel	Début des inclusions : 01/09/212..... Fin des inclusions : 11/11/2014 Fin d'étude : 31/10/2015
Procédure d'inclusion	Rétrospective

3. RESUME

Depuis la large adoption du dosage sérique du PSA (prostatic specific antigen) et des biopsies prostatiques sous guidage échographique (pour repérage de la glande) à la fin des années 1980(1), le cancer de la prostate est maintenant diagnostiqué à un stade plus précoce et localisé. Cependant, cette stratégie de diagnostique a engendré un surdiagnostique et surtraitement de lésion dite indolente(2) d'une part et la non détection de lésion agressive d'autre part. Ceci est en partie du tant à la faible spécificité du PSA qu'au mode d'échantillonnage systématisé de la glande(3). L'IRM multiparamétrique de prostate avec séquences de diffusion et perfusion a en partie permis d'optimiser la stratégie biopsique en établissant une cible au sein de la prostate(4). Cependant, l'estimation actuelle de la malignité d'une lésion à l'IRM est basée sur un système de score visuel(5). Bien qu'ayant fait l'objet de consensus(6), celui reste dépendant de l'expertise de l'opérateur et limite la dissémination de la technique. De plus, certains phénomènes tissulaires (adénome, prostatite chronique, artefact biopsique) imitent la prise de contraste liée (7)(8) à la néoangiogenèse cancéreuse réduisant la spécificité de la méthode.

Nous proposons donc une étude in silico des paramètres objectifs et quantitatifs de la perfusion en IRM évaluant de manière préliminaire l'efficacité intrinsèque de ces paramètres, mais aussi leur hétérogénéité, dans la détection et la stratification du cancer de prostate.

Cette étude doit inclure de manière rétrospective 25 patients présentant une suspicion clinique de cancer de prostate, à qui une série de biopsie de prostate a été réalisée et ayant eu une IRM de prostate indiquée par le praticien.

Le but de ce travail est d'évaluer les paramètres de perfusion selon le modèle Toft modifié (9)tel que le KTrans, le Ve, le Vp avec comme référence histologiques les biopsies réalisées. La méthodologie s'appuiera sur l'expertise en imagerie de l'équipe CERVOxy et une collaboration avec le New York University Medical Center. Une nouvelle technique de recalage multimodalité entre l'échographie et l'IRM sera testée et évaluée sur le jeu de données ainsi constitué.....

mots clés : cancer de la prostate ; IRM ; perfusion ; échographie ; imagerie multimodale ; image processing .....

4. JUSTIFICATION SCIENTIFIQUE ET DESCRIPTION GENERALE DE LA RECHERCHE

Le cancer de la prostate est le premier cancer chez l'homme de plus de 50 ans dans les pays industrialisés. En France, le nombre de nouveaux cas diagnostiqués en 2008 était de 67640 (10). Malgré leur efficacité carcinologique, les thérapeutiques radicales validées pour le traitement curatif du cancer de la prostate (chirurgie, radiothérapie, curiethérapie..) s'accompagnent d'une morbidité uro-génitale et rectale altérant la qualité de vie des patients. Depuis 1989 et l'avènement des biopsies écho guidées de la prostate(1), les techniques de détection du cancer de la prostate ont peu évolué. L'échographie a depuis cette époque montré son incapacité à détecter le cancer de la prostate en tant que modalité d'imagerie isolée (11)et sert principalement de guidage des biopsies ainsi qu'à l'exploration de pathologies annexes.

L'utilisation large du PSA en routine a permis de diagnostiquer le cancer de la prostate à un stade plus précoce (12,13)et localisé permettant un traitement radical de la maladie et une diminution de la mortalité(14). Cependant, l'utilisation combinée du PSA et des biopsies de prostate échoguidées ont mené à une tendance au sur diagnostic et au surtraitement, comme l'a montré une étude multicentrique européenne (2). En effet, le PSA présente une spécificité faible (de l'ordre de 20%(15) selon les études) et le cancer de la prostate peut présenter des formes indolentes de petits volumes et de bas grade. Ces formes indolentes pourraient ne pas évoluer ni localement ni à distance et ne pas altérer l'espérance de vie(16–18). Ces formes, si elles sont traitées par une thérapie radicale qui concerne l'ensemble de la glande (par chirurgie ou radiothérapie) font l'objet d'un surtraitement et les patients présentent de potentiels effets secondaires, notamment en terme de dysérection et de continence, avec un bénéfice oncologique limité. Pour réduire le surtraitement lié au surdiagnostic, la surveillance active a été proposée comme option pour les cas de cancer de prostate dits à faible risque de progression. De l'autre côté du spectre, des limitations du schéma conventionnel de détection se situent les lésions qui sont sous évaluées au niveau de leur extension ou de leur grade. L'évaluation préopératoire du cancer de la prostate reste un challenge et un quart à un tiers des patients en surveillance active nécessite un traitement dans les 2 à 5 années qui suivent le diagnostic en raison d'une sous estimation initiale de la maladie ou d'une progression rapide(19,20). De plus, 73% des patients éligibles à une surveillance active avaient un cancer significatif sur la pièce opératoire de prostatectomie totale dans une série récente(21). Le retentissement psychosocial négatif de la surveillance active est également un élément à prendre en compte (21). Typiquement les lésions de la partie antérieure de la glande sont mal échantillonnées par les biopsies systématisées(22). L'accès au volume lésionnel, qui détermine en partie la significativité clinique d'une lésion(23), ne se faisait qu'à travers le prisme dépoli des longueurs de cancer sur les biopsies de prostate réalisées à l'aveugle.

L'ensemble de ces éléments a contribué à l'émergence du concept de thérapie focale. La méthodologie consiste à sélectionner des patients par des stratégies de biopsies et/ou d'imagerie par IRM, à appliquer un traitement focal limitée à la partie tumorale de la glande par ultrasons focalisés de haute intensité (HIFU), photothérapie dynamique (PDT), thermothérapie Laser interstitielle (LITT), chirurgie partielle ou cryoablation tout en préservant les structures nerveuses et sphinctériennes

nécessaires au maintien de la continence et des érections. Ces techniques sont en cours d'évaluation. Les études morphométriques des pièces de prostatectomies totales ont permis de préciser l'histoire naturelle du cancer de la prostate, d'améliorer les stratégies de biopsies et de valider les résultats de l'imagerie moderne qui sont nécessaires pour la planification du traitement focal (24,25). Cependant, la multifocalité fréquente des cancers de la prostate qui représente environ 70% des cas(25,26) constitue une réserve au développement de cette modalité thérapeutique. Néanmoins, et malgré cette multifocalité, seules les lésions significatives (volume > 0,5 cc ou > 0,2 cc avec présence de grade de Gleason 4/5(17)) semblent à risque de progression métastatique dans les 5 à 10 ans et sont donc une indication de traitement qui peut être focal (16). Cette hypothèse a été confortée récemment par une étude autopsique de patients décédés d'un cancer de prostate et qui suggère une origine monoclonale des cellules tumorales responsables des métastases(27). La possibilité de détecter et de quantifier les foyers tumoraux en préopératoire constitue donc un pré-requis indispensable au développement des modalités de thérapie focale. Cela est désormais possible grâce aux progrès de l'imagerie moderne par IRM multiparamétrique couplée aux biopsies dirigées. En effet, l'IRM couplée aux biopsies dirigées possède une sensibilité et une spécificité de 86% et 94% respectivement pour le diagnostic des tumeurs significatives de plus de 0,5cc de volume après corrélation avec les pièces opératoires de prostatectomies totales [12]. De plus, l'IRM a également été validée pour la détection et la localisation des cancers antérieurs de la prostate inaccessibles aux biopsies systématisée réalisées par voie postérieure trans-rectale (28).

Ceci a abouti à la réalisation d'un consensus sur les modalités de réalisation de l'IRM dite multiparamétrique (IRMmp) de prostate et son interprétation(6).Plusieurs études ont montré l'apport potentiel de l'IRMmp en situation prébiopsique (4,29), c'est-à-dire prédiagnostique, en permettant d'augmenter le taux de détection de lésion dite signifiante, et évitant le surdiagnostique de lésion indolente. Ceci a notamment abouti à l'adoption dans les recommandations française sur le diagnostic du cancer de la prostate à incorporer l'IRM dans la stratégie diagnostique en cas de première série négative et persistance de la suspicion clinique(30).

Toutefois, l'utilisation de l'IRMmp requiert une expertise à l'interprétation. Celle-ci tient en partie au fait que le résultat de l'IRMmp est rendu par le radiologue sous la forme d'un score visuel d'estimation (5)(Score de Likert ou score PiRADS) qui, bien que standardisé ,n'apporte pas la robustesse nécessaire à large dissémination de la technique.

Ainsi, les paramètres quantitatifs de l'imagerie fonctionnelle pourraient apporter une reproductibilité inter et intra centre des résultats fournis par l'IRMmp. Une restriction du coefficient de diffusion apparent (ou ADC) calculé avec l'IRM de diffusion a déjà montré une corrélation avec la détection des foyers cancéreux mais aussi avec l'agressivité de la maladie(31–34). Néanmoins, toutes les lésions ne sont pas détectées par cette cartographie ADC(35), reflétant ainsi l'hétérogénéité de la maladie. L'imagerie de la néoangiogenèse tumorale est en partie réalisée avec la séquence de perfusion (DCE-MRI) après injection d'un agent de contraste(36). L'estimation visuelle par la prise rapide de

contraste et da décroissance du signal permet déjà de détecter certaines lésions(37). Malgré cela, il existe des faux positifs en se basant sur cette estimation visuelle. Ainsi, l'anatomie zonale de la prostate montre différent type de tissu au sein de la glande(38) et la zone de transition, notamment lorsqu'elle est adénomateuse peut présenter une prise de contraste très rapide(7). C'est pourquoi ,notre approche vise à établir le profil quantitatif des lésion prostatiques en utilisant des modèles pharmacocinétiques connus dans d'autre organes (modèle de Toft, Toft modifié(9)). Langer et Al.(39) ont ainsi montré une différence significative de Ktrans (constante de transfert de l'agent de contraste du compartiment vasculaire vers le parenchyme) entre les cancers de la zone périphérique et le tissu normal de cette même zone. Franiel et al.(40) ont étudié une modalité de perfusion en IRM montrant des différences modestes entre tissu cancéreux et tissu pathologique mais non cancéreux (prostatite). L'obtention de paramètres objectifs doit permettre la distinction entre les lésions cancéreuses et les lésions bénignes affichant des caractères similaires d'un point de vue visuel ou semi-quantitatifs(37). De manière additionnelle, nos prévoyons d'explorer l'hétérogénéité de ces paramètres en fonction des lésions. Franiel et al. (41) ont initié une recherche sur l'échantillonnage d'une lésion pour en extraire les voxels montrant la prise de contraste, en le comparant à l'intégralité de la lésion. Nous formulons l'hypothèse qu'une lésion cancéreuse présentera des paramètres correspondant à la perfusion plus hétérogène que du tissu bénin. Ceci a été montré en imagerie de diffusion par Rosenkrantz et al.(42) notamment en se focalisant sur l'entropie de l'ADC. Ce paramètre n'a pas fait l'objet d'une évaluation en ce qui concerne la perfusion.

Notre approche est originale dans le sens où nous étudierons des patients ne présentant ou non du cancer, permettant une analyse des faux positifs de l'imagerie.

Pour terminer, le transfert des informations de l'IRM vers une modalité plus facilement accessible en clinique et à grande échelle, l'échographie, est un enjeu important(43). Ainsi, nous avons développé avec NYU une plateforme purement logicielle de recalage-fusion d'image entre l'IRM et l'échographie prostatique transrectale. Plusieurs type de systèmes existent actuellement, et nécessitent un rééquipement complet par de l'échographie 3D (44) ou une machine dédiée semi-robotisée(45). L'originalité du concept est le recalage de l'échographie standard en 2D vers l'IRM en 3D en se basant sur une analyse de la texture des images. Ce concept doit être évalué sur des données rétrospectives avant d'envisager une application clinique.

5. OBJECTIFS DE LA RECHERCHE

L'objectif principal de cette étude est de permettre une approche préliminaire des paramètres quantitatifs en perfusion par IRM en prédiagnostique et d'étudier leur hétérogénéité au sein d'une région d'intérêt. Il s'agira d'établir les valeurs correspondantes à différents types de tissu au sein de l'anatomie zonale de la prostate, pathologique ou non. Ceci sera mené en intra et inter patient et avec deux types d'approche de

la modélisation pharmacocinétique de la perfusion (plateforme CERVOxy et NYU-droit cédé pour l'étude).
Un objectif secondaire est d'étudier de manière objective et quantifiée la valeur ajoutée par l'information fournie par la séquence de perfusion par rapport aux séquences anatomique T2 et de diffusion (carte de coefficient de diffusion apparent) sur différentes régions d'intérêt.
De même, la précision d'un nouveau type de recalage multi modalité IRM-échographie sera étudiée sur les données recueillies.

6. CRITERES D'EVALUATION

Après traitement des données brutes IRM, seront calculés pour les différentes zones de tissu tumoral ou non et en fonction de l'anatomie zonale, en se référant aux résultats des biopsies, les valeurs :

- Coefficient d'échange (Ktrans en min-1),
- la fraction de volume extracellulaire extraplasmatique Ve (%),
- la fraction de volume plasmatique (%)

L'analyse sera réalisée par région d'intérêt et la prostate entière.
Les données de Ktrans, Ve et Vp seront ensuite traitées pour en mesurer l'hétérogénéité par des paramètres de dispersion : kurtosis, skewness et entropies exprimés de manière absolue.

Ensuite, ces mêmes paramètres de dispersion seront calculés pour les séquences T2 et la carte ADC.

L'évaluation du recalage entre l'échographie et l'IRM sera appréciée par le calcul entre l'image source et cible de trois paramètres :

- d'un indice de recouvrement (index de Dice)
- la mesure de l'erreur résiduelle en millimètre pour des points de repères d'intérêt
- Le calcul de la distance de Hausdorff en millimètre, correspondant à la distance entre les contours de la prostate après recalage.

7. CONCEPTION DE LA RECHERCHE

Il s'agit d'une étude mono centrique observationnelle comprenant un seul groupe de patient. Chaque patient sera son propre témoin. La prostate est divisée en différentes régions d'intérêt, présentant ou non une anomalie à l'imagerie ou à l'histologie.

8. SELECTION ET EXCLUSION DES PERSONNES DE LA RECHERCHE

8.1 Critère d'inclusion des personnes qui se prêtent à la recherche

Pour être éligibles, les sujets doivent vérifier l'ensemble des critères d'inclusion définis :

- Patient masculin, majeur
- Présenter une suspicion de cancer de la prostate pour lequel un traitement est envisagé ou une réévaluation de celui en cas de surveillance active.
- Avoir eu une série de biopsie de prostate échoguidées
- Avoir eu une IRM prostatique au CHU de Caen avec séquence de perfusion et diffusion, indiquée par le praticien référent.
- L'IRM doit répondre à un critère de qualité permettant l'exploitation des données (Rapport Signal sur bruit suffisant).

8.2 Critères de non-inclusion

Les sujets vérifiant un seul des critères de non-inclusion ne peuvent être éligibles pour participer à la recherche. Ces critères sont :

- Traitement antérieur du cancer de prostate par radiothérapie ou HIFU.
- Traitement en cours, ou arrêté depuis moins de 3 mois, par un inhibiteur de la 5-α-réductase
- Présenter une IRM prostatique dont les caractéristiques de réalisation des séquences de perfusion sont inexploitables pour les calculs ultérieurs.

9. DEROULEMENT PRATIQUE DE L'ETUDE

Une consultation spécialisée en urologie établit la suspicion de cancer de prostate et programme les biopsies, conformément au soin courant. Le patient est informé des modalités de réalisation des biopsies et reçoit une information éclairée sur le geste, la réalisation de l'échographie par voie transrectale, les bénéfices attendus en terme de diagnostique et les potentielles complications. Les consignes de préparation du geste sont données au patient par le praticien qui indique le geste, de même que les prescriptions inhérentes. Lors de la réalisation du geste de biopsie, une échographie prostatique est systématiquement réalisée en tant que partie intégrante du geste. Les clichés sont sauvegardés dans l'appareil d'échographie de manière systématique.

Une IRM de prostate a été prescrite par le praticien en fonction du contexte clinique. Si celle-ci n'a pas été indiquée avant la réalisation des biopsies, elle pourra avoir été réalisée ultérieurement s'il existe une indication, notamment en cas de bilan d'extension ou de biopsie négative.

Une information orale a été systématiquement prodiguée par le même praticien (CO) sur la potentielle inclusion dans une étude et l'utilisation de l'imagerie et des résultats des biopsies.

Bilan d'inclusion

La liste des patients incluables est dressée à partir des actes réalisés de biopsies de prostate par un patricien du service (CO).

Sont ensuite vérifiés les critères d'inclusion suivant :

Critères d'inclusion	oui	non
Vérification des critères d'éligibilité clinique-suspicion de cancer		
Résultats des biopsies de prostate (soins courant) disponibles		
Présence d'une IRM mp réalisée au CHU		

10. DESCRIPTION DES DONNEES A RECUEILLIR

Seront recueillies :

Lors de la visite de programmation des biopsies :

Concernant les données cliniques du patient

- Les données démographiques : âge et date de naissance
- La valeur du dosage du PSA précédent les biopsies
- L'antécédent de biopsie prostatique, leur date et résultats
- Les données du toucher rectal
- L'antécédent de traitement instrumental prostatique
- L'antécédent d'infection urinaire

Concernant les données d'imagerie :

- Les clichés échographiques réalisés pour le soin, exportés de manière anonymisée au format DICOM
- L'examen d'IRM et ses différentes séquences, exportés de manière anonymisée au format DICOM.
- Rapport du radiologue, anonymisé, concernant l'IRM avec dose de produit de contraste injecté.

Concernant les données biopsiques :

- Le schéma de biopsie de routine, anonymisé, envoyé à l'anatomopathologie pour l'analyse des biopsies.

A la réception des résultats anatomopathologiques (selon le protocole de soins standard) :

- La présence de cancer ou non, en fonction de la localisation des biopsies
- La présence de pathologie bénigne (ASAP, Néoplasie intra épithéliale, prostatite aigue ou chronique)
- La longueur de chaque biopsie et du cancer si présent
- Le score histologique de Gleason
- Ces éléments sont reportés sur une fiche anonymisée schématique.

11. PARTICIPATION A L'ETUDE

Toutes les consultations auront eu lieu dans l'unité des consultations du service d'urologie du CHU de Caen.
La réalisation des biopsies aura eu lieu au CHU de Caen, soit au niveau des consultations soit au bloc opératoire du chu de Caen si une anesthésie générale était requise.
L'IRM de prostate doit être réalisée au CHU de Caen, service de radiologie comme critère d'inclusion.
Les dosages du PSA, préalable à l'inclusion, peuvent être réalisés dans un laboratoire extérieur au CHU.

12. METHODOLOGIE DE TRAITEMENTS DES DONNEES IRM ET RECALAGE

Nous disposons au sein de l'UMR 6301 de différentes plateformes de traitement logiciel des séquences d'IRM. Le premier est une plateforme développée en interne avec des macro pour Image J. Cette plateforme a déjà permis l'évaluation des paramètres quantitatifs de tumeurs d'autres organes(46).
La seconde plateforme est une développée par le New York University Medical Center, Firevoxel. Les droits d'utilisation de cette plateforme sont cédés pendant la durée de la thèse de sciences du Dr C. Orczyk.
Ce logiciel permet de réaliser du recalage en multimodalité et intramodalité, notamment en pathologie prostatique comme cela a été publié par l'investigateur principal (Orczyk et Al. Clinical Radiology 2013). Cette méthode de recalage a donc déjà été éprouvée et validée pour recaler des différentes séquences IRM entre elles (perfusion, diffusion, T2).
Firevoxel sera utilisé pour construire les différentes cartes quantitatives de perfusion selon le modèle de toft modifié. L'approche de calculs du modèle pharmacocinétique sous jacente a été validée par l'équipe de NYU sur différents organes comme le foie ou le rein (47,48).
Nous avons choisi une méthode individualisée pour établir la fonction d'entrée artérielle nécessaire au calcul des paramètres quantitatifs.
La mesure des paramètres d'hétérogénéité s'appuiera sur la méthodologie développée par l'équipe de NYU. Celle-ci a déjà testé ces paramètres sur les séquences de diffusion et la surtout la cartographie

ADC avec succès (42).

Enfin, il a été développé un nouveau concept pour réaliser de la fusion d'image IRM-échographie pour permettre à terme de guider précisément les biopsies sur une lésion précédemment détectée en IRM. Il s'agit d'un nouveau concept dans cette indication permettant de réaliser un recalage d'une image 2D en échographie vers l'IRM, imagerie tridimensionnelle. Le recalage s'appuie sur la texture de l'image et sur la détermination des contours. Cette méthodologie a été implémentée dans Firevoxel.

13. STATISTIQUES

La première étape consistera à une analyse descriptive des résultats.
Il est prévu de réaliser une analyse statistique en utilisant le logiciel R (Vienne, Autriche). La significativité des résultats est appréciée à $p<0,05$.
Pour chaque patient, un couple de donnée quantitative sera édité pour chaque paramètre étudié en fonction d'une variable binaire (cancer ou absence de cancer). Ces paires de variables continues quantitatives (Ktrans, Ve, Vp, Skewness, Entropie, Kurtosis) seront comparées en utilisant un test *t* de Student pour série appariées en cas de normalité de la distribution (vérifiée par un test de Shapiro Wilk). Dans le cas contraire un test des rangs signés de Wilcoxon sera utilisé.

Une analyse de variance sera utilisée pour étudier le comportement de chaque paramètre quantitatif continu d'imagerie en fonction de l'histologie (cancer agressif, cancer peu agressif, cancer de la zone périphérique, cancer de la zone de transition, prostatite, adénome, tissu normal).

Une régression logistique multinomiale sera ensuite effectuée pour modéliser l'association des différents paramètres quantitatifs d'imagerie avec les variables qualitatives avec une valeur clinique (cancer agressif, cancer peu agressif, cancer de la zone périphérique, cancer de la zone de transition).

Calcul du nombre de patients à inclure :
Le nombre de patients à inclure est calculé pour avoir une différence significative sur l'objectif principal. Il est décidé de privilégier une différence significative sur la mesure du Ktrans qui est la pierre angulaire du modèle de Toft modifié que nous utiliserons pour modéliser la perfusion en IRM.

Ainsi, d'après des données de la littérature (Langer et al. Radiology 2010(39)), la valeur du Ktrans en zone périphérique normale était de 0.25 min-1 et pour un cancer de la zone périphérique (70% des cancers de la prostate) de 0.30 min-1. L'écart type commun était 0.04. Ainsi, pour observer une différence significative entre les moyennes de ces deux valeurs au risque $\alpha=0.05$ et à la puissance $1-\beta=0.9$ et pour

un test bilatéral, le nombre de cas à étudier est de 14 dans chaque groupe, chaque patient étant son propre témoin (lésion et zone saine au sein de la même glande). Nous devons donc inclure 14 patients présentant un cancer. Or le taux de détection de cancer de la prostate au CHU de Caen dans la population cible de notre étude est de 58% (Thèse de Doctorat de Médecine, Dr Clément Orczyk). Il faut donc inclure 25 patients.

14. DROITS D'ACCES AUX DONNEES ET DOCUMENTS SOURCES

Conformément à la loi informatique et libertés et à la loi n° 2002-303 du 4 mars 2002, le patient pourra exercer à tout moment son droit d'accès et de rectification aux données recueillies. Le CHU de Caen tiendra informé les patients des résultats globaux de cette Recherche à la fin de l'étude.

15. CONSIDERATIONS ETHIQUES

Demande d'avis au CPP Nord Ouest

Ce projet de Recherche ne correspond pas à une « Recherche Biomédicale » au sens de l'article L. 1121-1 du code de la santé publique (loi n° 2004-806 du 9 août 2004 ainsi que de l'article R. 1121-1 du décret n° 2006-477 du 26/04/2006). Le protocole et le document d'information au patient seront soumis, pour information, au Comité de Protection des Personnes Nord Ouest III.

16. TRAITEMENT DES DONNEES ET CONSERVATION DES DOCUMENTS ET DES DONNEES RELATIVES A LA RECHERCHE

Demande d'autorisation CNIL pour le traitement de données automatisées :

Les recherches biomédicales relevant ou non de l'article L 1121-1 produisent de l'information à visée scientifique. Ces informations directement ou indirectement nominatives et codées entrent dans un cadre légal de fonctionnement des fichiers (Loi n° 78-17 du 6 janvier 1978 et loi n° 94-548 du 1er juillet 1994). La mise en œuvre d'un traitement automatisé de données ayant pour fin la recherche dans le domaine de la santé est soumis à l'avis d'un Comité Consultatif sur le Traitement d'Information en matière de Recherche dans le domaine de la Santé (CCTIRS) préalablement à l'autorisation de la Commission Informatique et des Libertés (CNIL). La mise en œuvre d'un traitement automatisé de données ayant pour fin la recherche dans le domaine de la santé sera soumise à l'avis d'un Comité Consultatif sur le Traitement d'Information en matière de Recherche dans le domaine de la Santé (CCTIRS).

L'étude observationnelle que nous proposons n'entraîne aucun surcoût médicaux ou paramédicaux. Elle s'intègre dans les pratiques de soins habituelles avec un suivi classique clinique et biologique.

17. REGLES DE PUBLICATIONS

Les règles de publication de l'article scientifique sont les suivantes ():

Toute personne désignée en tant qu'auteur doit en avoir la compétence : Chaque auteur doit avoir suffisamment participé au travail pour prendre la responsabilité publique de tout ou partie de son contenu. La crédibilité de la paternité de l'article est fondée sur des contributions essentielles :

- Conception et méthode et/ou analyse et interprétation des résultats
- Rédaction de l'article ou révisions critiques avec participation importante au contenu intellectuel
- Approbation finale de la version publiée

Ordre d'apparition des auteurs (investigateur(s) coordinateur(s), méthodologiste, investigateurs principaux des centres impliqués) : L'ordre tiendra compte de la participation des différents investigateurs à l'essai (nombre de patients inclus et évaluables) et de ceux qui viendraient apporter une contribution significative au cours de son déroulement.

Une mention indiquera de l'origine du financement.

En cas d'études annexes, les résultats de celles-ci ne pourront être publiés qu'avec l'accord des investigateurs principaux et du méthodologiste, et uniquement après publication de l'étude principale qui devra être citée.

L'investigateur coordinateur signera la version finale du rapport d'essai clinique pour cette étude, indiquant par là son accord avec les analyses, les résultats et les conclusions du rapport.

L'étude et ses résultats sont la propriété exclusive du Centre Hospitalo-Universitaire de Caen et les investigateurs sont tenus, selon les termes de la loi, au secret professionnel.

L'analyse des résultats fera l'objet de communications dans les congrès et de publications.

Le texte des publications et des communications sera discuté avec l'ensemble des investigateurs participants à l'essai.

18. BIBLIOGRAPHIE

Les références bibliographiques seront citées dans l'ordre d'apparition dans le texte et doivent respecter les règles d'écriture suivantes :

1. Hodge KK, McNeal JE, Stamey TA. Ultrasound guided transrectal core biopsies of the palpably abnormal prostate. J Urol. 1989 Jul;142(1):66–70.
2. Schroder FH, Hugosson J, Roobol MJ, Tammela TL, Ciatto S, Nelen V, et al. Screening and prostate-cancer mortality in a randomized European study. N Engl J Med. 2009;360:1320–8.
3. Rosenkrantz AB, Taneja SS. Targeted prostate biopsy: opportunities and challenges in the era of multiparametric prostate magnetic resonance imaging. J Urol. 2012 Oct;188(4):1072–3.
4. Haffner J, Lemaitre L, Puech P, Haber G-P, Leroy X, Jones JS, et al. Role of magnetic resonance imaging before initial biopsy: comparison of magnetic resonance imaging-targeted and systematic biopsy

for significant prostate cancer detection. BJU Int [Internet]. 2011 Mar 22 [cited 2011 Mar 24]; Available from: http://www.ncbi.nlm.nih.gov/pubmed/21426475
5. Rosenkrantz AB, Kim S, Lim RP, Hindman N, Deng F-M, Babb JS, et al. Prostate Cancer Localization Using Multiparametric MR Imaging: Comparison of Prostate Imaging Reporting and Data System (PI-RADS) and Likert Scales. Radiology. 2013 Jun 20;
6. Dickinson L, Ahmed HU, Allen C, Barentsz JO, Carey B, Futterer JJ, et al. Magnetic resonance imaging for the detection, localisation, and characterisation of prostate cancer: recommendations from a European consensus meeting. Eur Urol. 2011 Apr;59(4):477–94.
7. Rosenkrantz AB, Taneja SS. Radiologist, be aware: ten pitfalls that confound the interpretation of multiparametric prostate MRI. AJR Am J Roentgenol. 2014 Jan;202(1):109–20.
8. Van Niekerk CG, Witjes JA, Barentsz JO, van der Laak JAWM, Hulsbergen-van de Kaa CA. Microvascularity in transition zone prostate tumors resembles normal prostatic tissue. The Prostate. 2013;73(5):467–75.
9. Tofts PS, Brix G, Buckley DL, Evelhoch JL, Henderson E, Knopp MV, et al. Estimating kinetic parameters from dynamic contrast-enhanced T(1)-weighted MRI of a diffusable tracer: standardized quantities and symbols. J Magn Reson Imaging. 1999 Sep;10(3):223–32.
10. Crouzet S. KP. Etude des variations de l'incidence et de l'incidence par stade des cancers de prostate en France à partir de 5 centres. 2008.
11. Hodge KK, McNeal JE, Terris MK, Stamey TA. Random systematic versus directed ultrasound guided transrectal core biopsies of the prostate. J Urol. 1989 Jul;142(1):71–4; discussion 74–5.
12. Noldus J, Graefen M, Haese A, Henke RP, Hammerer P, Huland H. Stage migration in clinically localized prostate cancer. European urology. 2000;38(1):74–8.
13. Neppl-Huber C, Zappa M, Coebergh JW, Rapiti E, Rachtan J, Holleczek B, et al. Changes in incidence, survival and mortality of prostate cancer in Europe and the United States in the PSA era: additional diagnoses and avoided deaths. Ann Oncol. 2012 May;23(5):1325–34.
14. Schröder FH, Hugosson J, Roobol MJ, Tammela TLJ, Ciatto S, Nelen V, et al. Prostate-cancer mortality at 11 years of follow-up. N Engl J Med. 2012 Mar 15;366(11):981–90.
15. Stamey TA, Yang N, Hay AR, McNeal JE, Freiha FS, Redwine E. Prostate-specific antigen as a serum marker for adenocarcinoma of the prostate. N Engl J Med. 1987 Oct 8;317(15):909–16.
16. Stamey TA, Freiha FS, McNeal JE, Redwine EA, Whittemore AS, Schmid HP. Localized prostate cancer. Relationship of tumor volume to clinical significance for treatment of prostate cancer. Cancer. 1993 Feb 1;71(3 Suppl):933–8.
17. Epstein JI, Walsh PC, Carmichael M, Brendler CB. Pathologic and Clinical Findings to Predict Tumor Extent of Nonpalpable (Stage T1 c) Prostate Cancer. JAMA: The Journal of the American Medical Association. 1994 Février;271(5):368–74.
18. Epstein JI. Prognostic significance of tumor volume in radical prostatectomy and needle biopsy specimens. J Urol. 2011 Sep;186(3):790–7.
19. Klotz L, Zhang L, Lam A, Nam R, Mamedov A, Loblaw A. Clinical results of long-term follow-up of a large, active surveillance cohort with localized prostate cancer. J Clin Oncol. 28:126–31.
20. Carter HB, Kettermann A, Warlick C, Metter EJ, Landis P, Walsh PC, et al. Expectant management of prostate cancer with curative intent: an update of the Johns Hopkins experience. J Urol. 2007;178:2359–64; discussion 2364–5.
21. Duffield AS, Lee TK, Miyamoto H, Carter HB, Epstein JI. Radical prostatectomy findings in patients in whom active surveillance of prostate cancer fails. J Urol. 2009;182:2274–8.
22. Ouzzane A, Puech P, Lemaitre L, Leroy X, Nevoux P, Betrouni N, et al. Combined Multiparametric MRI and Targeted Biopsies Improve Anterior Prostate Cancer Detection, Staging, and Grading. Urology. 2011 Dec;78(6):1356–62.
23. Schiffmann J, Connan J, Salomon G, Boehm K, Beyer B, Schlomm T, et al. Tumor volume in insignificant prostate cancer: Increasing threshold gains increasing risk. Prostate. 2014 Oct 4;
24. Bouye S, Potiron E, Puech P, Leroy X, Lemaitre L, Villers A. Transition zone and anterior stromal prostate cancers: zone of origin and intraprostatic patterns of spread at histopathology. Prostate. 2009;69:105–13.
25. Haffner J, Potiron E, Bouye S, Puech P, Leroy X, Lemaitre L, et al. Peripheral zone prostate cancers: location and intraprostatic patterns of spread at histopathology. Prostate. 2009;69:276–82.
26. Villers A, McNeal JE, Freiha FS, Stamey TA. Multiple cancers in the prostate. Morphologic features of clinically recognized versus incidental tumors. Cancer. 1992;70:2313–8.

27. Liu W, Laitinen S, Khan S, Vihinen M, Kowalski J, Yu G, et al. Copy number analysis indicates monoclonal origin of lethal metastatic prostate cancer. Nat Med. 2009 May;15(5):559–65.
28. Lemaitre L, Puech P, Poncelet E, Bouye S, Leroy X, Biserte J, et al. Dynamic contrast-enhanced MRI of anterior prostate cancer: morphometric assessment and correlation with radical prostatectomy findings. Eur Radiol. 2009;19:470–80.
29. Wysock JS, Rosenkrantz AB, Huang WC, Stifelman MD, Lepor H, Deng F-M, et al. A Prospective, Blinded Comparison of Magnetic Resonance (MR) Imaging–Ultrasound Fusion and Visual Estimation in the Performance of MR-targeted Prostate Biopsy: The PROFUS Trial. European Urology [Internet]. [cited 2013 Nov 29]; Available from: http://www.sciencedirect.com/science/article/pii/S030228381301186X
30. Salomon L, Bastide C, Beuzeboc P, Cormier L, Fromont G, Hennequin C, et al. Recommandations en onco-urologie 2013 du CCAFU : Cancer de la prostate. Progrès en Urologie. 2013 Nov;23, Supplement 2:S69–101.
31. Hambrock T, Somford DM, Huisman HJ, van Oort IM, Witjes JA, Hulsbergen-van de Kaa CA, et al. Relationship between Apparent Diffusion Coefficients at 3.0-T MR Imaging and Gleason Grade in Peripheral Zone Prostate Cancer. Radiology [Internet]. 2011 Dec 14 [cited 2012 Mar 28]; Available from: http://www.ncbi.nlm.nih.gov/pubmed/21406633
32. Hambrock T, Somford DM, Huisman HJ, van Oort IM, Witjes JA, Hulsbergen-van de Kaa CA, et al. Relationship between apparent diffusion coefficients at 3.0-T MR imaging and Gleason grade in peripheral zone prostate cancer. Radiology. 2011 May;259(2):453–61.
33. Verma S, Rajesh A, Morales H, Lemen L, Bills G, Delworth M, et al. Assessment of Aggressiveness of Prostate Cancer: Correlation of Apparent Diffusion Coefficient With Histologic Grade After Radical Prostatectomy. American Journal of Roentgenology. 2011 Jan 21;196(2):374–81.
34. Turkbey B, Shah VP, Pang Y, Bernardo M, Xu S, Kruecker J, et al. Is apparent diffusion coefficient associated with clinical risk scores for prostate cancers that are visible on 3-T MR images? Radiology. 2011 Feb;258(2):488–95.
35. Rosenkrantz AB, Mendrinos S, Babb JS, Taneja SS. Prostate Cancer Foci Detected on Multiparametric Magnetic Resonance Imaging are Histologically Distinct From Those Not Detected. The Journal of Urology [Internet]. 2012 Apr [cited 2012 Apr 18]; Available from: http://linkinghub.elsevier.com/retrieve/pii/S0022534712002054
36. Villers A, Puech P, Mouton D, Leroy X, Ballereau C, Lemaitre L. Dynamic Contrast Enhanced, Pelvic Phased Array Magnetic Resonance Imaging of Localized Prostate Cancer for Predicting Tumor Volume: Correlation With Radical Prostatectomy Findings. The Journal of Urology. 2006 Décembre;176(6):2432–7.
37. Verma S, Turkbey B, Muradyan N, Rajesh A, Cornud F, Haider MA, et al. Overview of Dynamic Contrast-Enhanced MRI in Prostate Cancer Diagnosis and Management. American Journal of Roentgenology. 2012 Jun;198(6):1277–88.
38. McNeal JE. Normal histology of the prostate. Am J Surg Pathol. 1988 Aug;12(8):619–33.
39. Langer DL, van der Kwast TH, Evans AJ, Plotkin A, Trachtenberg J, Wilson BC, et al. Prostate tissue composition and MR measurements: investigating the relationships between ADC, T2, K(trans), v(e), and corresponding histologic features. Radiology. 2010 May;255(2):485–94.
40. Franiel T, Lüdemann L, Rudolph B, Rehbein H, Staack A, Taupitz M, et al. Evaluation of normal prostate tissue, chronic prostatitis, and prostate cancer by quantitative perfusion analysis using a dynamic contrast-enhanced inversion-prepared dual-contrast gradient echo sequence. Invest Radiol. 2008 Jul;43(7):481–7.
41. Franiel T, Ludemann L, Rudolph B, Lutterbeck E, Hamm B, Beyersdorff D. Differentiation of prostate cancer from normal prostate tissue: role of hotspots in pharmacokinetic MRI and histologic evaluation. AJR Am J Roentgenol. 194:675–81.
42. Rosenkrantz AB, Triolo MJ, Melamed J, Rusinek H, Taneja SS, Deng F-M. Whole-lesion apparent diffusion coefficient metrics as a marker of percentage Gleason 4 component within Gleason 7 prostate cancer at radical prostatectomy. J Magn Reson Imaging. 2014 Feb 25;
43. Ukimura O, Gill IS. Key to Successful Focal Therapy: Location, Location, Location. European Urology. 2012 Apr;
44. Baumann M, Mozer P, Daanen V, Troccaz J. Prostate biopsy assistance system with gland deformation estimation for enhanced precision. Med Image Comput Comput Assist Interv. 2009;12(Pt 1):67–74.
45. Xu S, Kruecker J, Turkbey B, Glossop N, Singh AK, Choyke P, et al. Real-time MRI-TRUS fusion

for guidance of targeted prostate biopsies. Comput Aided Surg. 2008 Sep;13(5):255–64.
46. Corroyer-Dulmont A, Pérès EA, Petit E, Guillamo J-S, Varoqueaux N, Roussel S, et al. Detection of glioblastoma response to temozolomide combined with bevacizumab based on µMRI and µPET imaging reveals [18F]-fluoro-L-thymidine as an early and robust predictive marker for treatment efficacy. Neuro-oncology. 2013 Jan;15(1):41–56.
47. Aronhime S, Calcagno C, Jajamovich GH, Dyvorne HA, Robson P, Dieterich D, et al. DCE-MRI of the liver: Effect of linear and nonlinear conversions on hepatic perfusion quantification and reproducibility: DCE-MRI of the Liver. Journal of Magnetic Resonance Imaging. 2014 Jul;40(1):90–8.
48. Yamamoto A, Zhang JL, Rusinek H, Chandarana H, Vivier P-H, Babb JS, et al. Quantitative evaluation of acute renal transplant dysfunction with low-dose three-dimensional MR renography. Radiology. 2011 Sep;260(3):781–9.

COMITE DE PROTECTION DES PERSONNES NORD OUEST III

CHU – niveau 03 – porte 03-508
14033 Caen cedex 9

Tel : 09.64.08.19.44.
Fax : 02.31.06.46.73.
E-mail : cppnordouest3@orange.fr

Caen, le 11 décembre 2014

Urologie
à l'attention de M. le Dr Clément ORCZYK
CHU – Niveau 07
14033 Caen cedex 9

Réf. CHU : A14-D66-VOL.23

Monsieur,

Le comité a été saisi d'une demande d'avis concernant le projet d'étude intitulé « Etude QDCEPROST : Etude préliminaire des paramètres quantitatifs de la perfusion en IRM prostatique en situation de pré-diagnostic pour la détection et stratification du cancer de la prostate » et conduit par M. le Dr Clément ORCZYK.

Extrait des délibérations du 06 décembre 2014 du Comité de Protection des Personnes Nord-Ouest III, dont la séance non publique s'est tenue au CHU de Caen à cette date à partir de 9 h 00, sur la convocation de ses membres par sa Présidente.

Siégeaient ensemble ce 06 décembre 2014, sous la présidence de Mme Charlotte GOURIO,

Membres du premier collège
au titre du 1° de l'article R.1123-4 du CSP
- M. Rémy MORELLO, médecin, personne qualifiée en raison de sa compétence en matière de biostatistique ou d'épidémiologie, membre titulaire,
- M. Jean-François HERON, médecin, membre titulaire,
- Mme Pascaline BERTHET, médecin, membre suppléant,
- M. Claude BAZIN, médecin, membre suppléant,

au titre du 2° de l'article R.1123-4 du CSP
- M. Bertrand VIENNOT, médecin généraliste, membre titulaire,

au titre du 3° de l'article R.1123-4 du CSP
- Mme Charlotte GOURIO, pharmacien hospitalier, membre titulaire,

Membres du second collège
au titre 2° de l'article R .1123-4 du CSP
- Mme Nadège ROCHE-LABARBE, maître de conférences en psychologie à l'UFR de psychologie de Caen, membre titulaire,

au titre 3° de l'article R .1123-4 du CSP
- Mme Sylvie BALP, conseillère technique à la direction générale adjointe de la solidarité du Conseil Général de Caen, membre titulaire,
- M. Simon FRANCOISE, représentant d'association agréée de malades ou d'usagers du système de santé, membre suppléant,

Délibération

Considérant les documents suivants :

- courrier de M. le Dr Clément ORCZYK du 03 novembre 2014,
- protocole, version 01 du 03 novembre 2014,

Le comité confirme le caractère non interventionnel de cette étude, tel que défini par l'article L.1121-1 de la loi n° 2004-806 du 9 août 2004 et l'article R.1121-2 du décret 2006-477 du 26 avril 2006 du CSP.

En revanche, il conviendrait d'adresser au comité pour avis le document d'information qu'il est prévu de remettre au patient.

Je vous prie d'agréer, Monsieur, mes salutations distinguées.

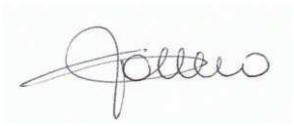

Mme Charlotte GOURIO,
Présidente

Résumé en français :

Dénommée multiparamétrique par adjonction de séquences fonctionnelle aux conventionnelles, L'IRM de prostate a montré ses performances pour la détection du cancer de prostate par un score radiologique visuel, subjectif. D'autres applications sont en cours d'investigations comme la stratification, le planning thérapeutique ou encore le suivi oncologique.

La première partie s'attache à décrire, élaborer et appliquer une méthodologie de recalage non rigide en 3D entre l'histologie du spécimen de prostatectomie totale et les différentes séquences de l'IRMmp. Après avoir capturé une déformation et un changement de volume de la prostate entre les états *in vivo et ex vivo* par IRM, la méthode de recalage multimodalité appliquée à une population de prostatectomie totale précédée d'une IRM démontre une sous-estimation du volume de cancer par l'IRM, sujette à une stratification. Les implications se trouvent dans la détection, la stratification et le planning thérapeutique.

La deuxième partie propose une analyse de texture des différentes séquences et cartographies quantitatives en diffusion et perfusion pour la détection et la stratification du cancer. Cette approche multiparamétrique de « Score d'Entropie » est testée dans une population pilote au moment des biopsies et présente des performances diagnostique pour sélectionner les lésions à biopsier. Ce score d'entropie participe de la stratification du cancer en corrélant positivement avec le score de Gleason et la longueur de cancer biopsique.

La troisième partie explore le rôle de l'IRM dans le suivi d'une thérapie émergente, dite focale, du cancer. Il s'agit d'un travail de recalage non-rigide longitudinal sur une cohorte de patients traités par thérapie focale en vue de compenser les déformation focalement induites. Il apparaît que ce type de recalage peut permettre un suivi objectif des résultats d'ablation et potentiellement élaborer une cible biopsique et radiologique dans le suivi oncologique.

Titre en anglais

Modelling prostate cancer using MRI: detection, risk stratification, 3D therapeutic planning and follow up of focal therapy based on image processing and co-registration

Résumé en anglais :

Conventional prostate MRI, enhanced by diffusion and perfusion sequences, and then named multiparametric, showed high performances for detection of prostate cancer using visual scoring. Indications in stratification, prognosis, treatment planning and follow up are currently under investigations.

First part of this work attached itself to describe, elaborate and use a non-rigid image fusion method in 3D between gold standard histology of radical prostatectomy and MRI. Investigations captured the significant differences in shape and volume of *in vivo* and *ex vivo* prostate using MRI. The developed multimodality fusion method was applied to a cohort of patients who underwent MRI prior surgery. Results showed a stratified underestimation of cancer volume by MRI. Clinical output resides in detection, stratification and surgical planning.

The second part proposed some texture analysis of sequences and quantitative maps. As a multiparametric approach, the Entropy Score is applied in a pilot cohort at time of biopsy and showed some potential usefulness to select MRI targets without compromising detection of significant cancer. By positively correlating with the Gleason Score and the maximal core length of cancer, Entropy Score participates of stratification of cancer.

The third part explored application of image registration in the longitudinal follow up of an emergent therapy, said focal (FT). As a conservative approach, FT induces very local deformation of the gland which appears to be appropriately modelled by non-rigid registration, then opening possibilities to guide further control biopsy and radiologic assessment.

Mots clés proposés : Cancer de prostate, Diagnostic, Imagerie, Résonance magnétique nucléaire, Biopsie, Pronostic, traitement d'image, recalage